THE SIGNIFICANCE OF MATERIAL DUCTILITY TO THE RELIABILITY AND LOAD CARRYING CAPACITY OF PEAK PERFORMANCE STRUCTURES

Volker Weiss, et al

Syracuse University

Prepared for:

Naval Air Systems Command

January 1973

Unclassified

Security Classification

DOCUMENT CONTROL DATA - R & D

(Security classification of title, body of abstract and indexing annotation must be entered when the overall report is classified)

1. ORIGINATING ACTIVITY (Corporate author)

Syracuse University, Office of Sponsored Programs
Department of Chemical Engineering and Materials Science, Syracuse, New York 13210

2a. REPORT SECURITY CLASSIFICATION

Unclassified

2b. GROUP

3. REPORT TITLE

THE SIGNIFICANCE OF MATERIAL DUCTILITY TO THE RELIABILITY AND LOAD CARRYING CAPACITY OF PEAK PERFORMANCE STRUCTURES (U)

4. DESCRIPTIVE NOTES (Type of report and inclusive dates)

Final Report (1 January 1972 to 31 December 1972)

5. AUTHOR(S) (First name, middle initial, last name)

Volker Weiss
M. Sengupta
W. Sanford

6. REPORT DATE	7a. TOTAL NO. OF PAGES	7b. NO. OF REFS
January 1973	110	26

8a. CONTRACT OR GRANT NO.	9a. ORIGINATOR'S REPORT NUMBER(S)
N00019-72-C-0214	MS-VW-1705-F173
b. PROJECT, TASK, AND WORK UNIT NO.	
c. DOD ELEMENT	9b. OTHER REPORT NO(S) (Any other numbers that may be assigned this report)
d. DOD SUBELEMENT	

10. DISTRIBUTION STATEMENT

This document has been approved for public release and sale, its distribution is unlimited.

11. SUPPLEMENTARY NOTES	12. SPONSORING MILITARY ACTIVITY
	NAVAL AIR SYSTEMS COMMAND Department of the Navy Washington, D.C.

13. ABSTRACT

The relationships between fracture toughness, flow stress and material ductility were studied for the high strength steels, D6AC and 300M, each heat treated to 3 strength levels. In addition to the experimental part of the study which included biaxial ductility test, notch-tensile test and fracture toughness test the theoretical studies, to develop an analytical basi. for correlations between fracture toughness and flow properties of solids, were continued.

The fracture ductility was found to decrease significantly on going from the uniaxial stress state to the plane strain stress state to the balanced biaxial condition. A strong influence of the surface finish was noted. This gave rise to some scatter, particularly for the bulge tests. More experimentation is planned in the continuing program to clarify this point. The notch sensitivity decreases with increasing tempering temperature for both materials, with a reduction being somewhat greater for 300M steel. The values of the Neuber micro support effect const ρ*, were determined and found to lie between 0.0002 to 0.0014 inches.

The analytical studies suggested that the correlation between fracture toughness and ductility should have the general form $K_{Ic}=A_{\varepsilon i}E\sqrt{s\rho^*}\varepsilon_i$ where E is the modulus of elasticity, s the shape factor for the plastic zone, ε_i the effective fracture strain corresponding t· the stress state i and $A_{\varepsilon i}$ a corresponding constant. The experimental results were found to be in good agreement with the bulge ductility correlation. The analytical correlations were also extended to the plane stress fracture condition.

DD FORM 1 NOV 68 1473

Unclassified

Security Classification

14 KEY WORDS	LINK A		LINK B		LINK C	
	ROLE	WT	ROLE	WT	ROLE	WT
fracture; flow stress; fracture toughness; multiaxial fracture strain $\bar{\varepsilon}_{F_{\alpha\beta}}$;notch sensitivity stress ratios α and β; stress strain relation exponent, "n"; Neuber's micro-support effect constant 'ρ^*'; plastic zone shape factor 's'; ultra-high strength materials; D6AC steel (R_c 50, R_c 46.5, R_c 42.5); 300M steel (R_c 51.5, R_c 47.5, R_c 39.0).						

ia

THE SIGNIFICANCE OF MATERIAL DUCTILITY TO THE RELIABILITY AND LOAD CARRYING CAPACITY OF PEAK PERFORMANCE STRUCTURES (U)

Final Report

(1 January 1972 to 31 December 1972)

January 1973

By

Volker Weiss
M. Sengupta
W. Sanford

Prepared under Contract No. N00019-72-C-0214
for
Naval Air Systems Command
Department of the Navy

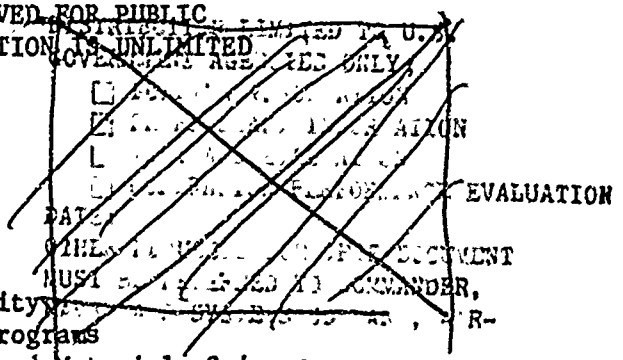

Syracuse University
Office of Sponsored Programs
Department of Chemical Engineering and Materials Science
Syracuse, New York
MS-VW-1705-F173

ABSTRACT

The relationships between fracture toughness, flow stress and material ductility were studied for the high strength steels, D6AC and 300M, each heat treated to three strength levels. The experimental part of the study was conducted in three phases: 1. Study of the effect of stress state on fracture ductility; 2. Study of the notch strength and ductility characteristics of the materials involved; 3. Determination of the fracture toughness of the materials. In addition, the theoretical studies, to develop an analytical basis for correlations between fracture toughness and flow properties of solids, were continued.

The fracture ductility was found to decrease significantly on going from the uniaxial stress state (tension test) to the plane strain stress state (bend test or Clausing-type tension test) to the balanced biaxial condition (bulge test or plunger bulge test). The effective fracture strain is generally reduced to a value of less than half the value of the tensile fracture strain and sometimes to a value of only 12% of the tensile fracture ductility. A strong influence of the surface finish was noted. This gave rise to some scatter, particularly for the bulge tests. More experimentation is planned in the continuing program to clarify this point.

The notch sensitivity decreases with increasing tempering temperature for both materials, with a reduction being somewhat greater for 300M steel. The values of the Neuber micro support effect constant, ρ^*, were determined and found to lie between 0.0002 to 0.0014 inches.

Measurements of the effective fracture strain at the notch root showed a general trend of decreasing notch root fracture strain with increasing stress concentration factor. In general the minimum values of a notch root effective fracture strain lie close to the plunger ductility for 300M steel (hardness R_c 51.5 and R_c 47.5), higher for D6AC (hardness R_c 50) and between the bend and plunger ductility for D6AC steel (hardness R_c 46.5 and R_c 42.5). For 300M steel (R_c 39), the scatter in the data was too large to identify a trend.

Fracture toughness values were determined for all materials with compact tension specimens. The values determined for 1.0 inch thick specimens met the requirements for plane strain fracture toughness, K_{Ic}.

The analytical studies suggest that the correlation between fracture toughness and ductility should have the general form $K_{Ic} = A_{\varepsilon_i} E\sqrt{s\rho^*}\varepsilon_i$ where E is the modulus of elasticity, s the shape factor for the plastic zone (approximately 0.54 for n = 1) ρ^* the Neuber micro support effect constant, ε_i the effective fracture strain corresponding to the stress state i and A_{ε_i} a corresponding constant. The table below gives the values of A_{ε_i} for various fracture ductility values and failure criteria.

Fracture Ductility Used for Correlation	Value of A_{ε_i}	
	Vol. Strain Fracture Criterion	Max. Normal Stress Fracture Criterion
Balanced Biaxial tension ductility $\bar{\varepsilon}_{F_{\alpha=1,\beta=0}}$	0.32	0.39
Plane Strain Ductility $\bar{\varepsilon}_{F_{\alpha=\frac{1}{2},\beta=0}}$	0.28	0.45

The experimental results were found to be in good agreement with the bulge ductility correlation but in somewhat poor agreement with the bend ductility correlation. Surface finish effects in the measurements of the bend ductility could be partly responsible for this discrepancy. The analytical correlations were also extended to the plane stress fracture condition. However, reliable estimates of the fracture strain corresponding to the plane stress condition ahead of a crack could not be made. Furthermore an experimental determination of the true plane stress fracture toughness is difficult. Nevertheless, it is anticipated that similar correlations can be established for plane stress conditions or mixed mode fracture.

INTRODUCTION

The development of a procedure for the reliable determination of the load carrying capacity of peak performance structures requires the study of fundamental properties of material that influences its resistance to fracture. Since it is generally accepted that all the structural components have in them at least some flaws it is necessary to base the design against failure in terms of fracture toughness of the material. Fracture toughness, defined as the work required to produce a unit area crack extension, is given by

$$G_c = 2(\gamma_s + \gamma_p) \tag{1}$$

where γ_s = surface energy

γ_p = plastic work associated with crack extension.

For most of the technical metals and alloys in structural applications, the plastic energy associated with crack extension is much higher than the surface energy ($\gamma_p \approx 10^4 \gamma_s$). Cottrell[1] suggested that the plastic work can be calculated from

$$2\gamma_p = 2 \int_0^\infty \sigma_{YY}\, dv \tag{2}$$

where dv is the displacement associated with crack extension of da.

Accurate experimental determination of the fracture toughness of a material requires that the stress state in the specimen at the instance

INTRODUCTION

The development of a procedure for the reliable determination of the load carrying capacity of peak performance structures requires the study of fundamental properties of material that influences its resistance to fracture. Since it is generally accepted that all the structural components have in them at least some flaws it is necessary to base the design against failure in terms of fracture toughness of the material. Fracture toughness, defined as the work required to produce a unit area crack extension, is given by

$$G_c = 2(\gamma_s + \gamma_p) \tag{1}$$

where γ_s = surface energy

γ_p = plastic work associated with crack extension.

For most of the technical metals and alloys in structural applications, the plastic energy associated with crack extension is much higher than the surface energy ($\gamma_p \approx 10^4 \gamma_s$). Cottrell[1] suggested that the plastic work can be calculated from

$$2\gamma_p = 2 \int_0^\infty \sigma_{YY}\, dv \tag{2}$$

where dv is the displacement associated with crack extension of da.

Accurate experimental determination of the fracture toughness of a material requires that the stress state in the specimen at the instance

of failure, be fairly well represented by the linear elastic stress field equations. Thus, it is quite feasible for brittle materials but leads to difficulties and rather expensive procedures for tougher materials. It is therefore desirable to develop other, conceivably indirect methods to determine the fracture toughness of typical structural engineering materials. As an interim step to the development of accurate indirect methods, it was the immediate goal of the present study to work towards the development of reliable and useful correlations between readily obtainable mechanical properties and fracture toughness. It is hoped that such correlations would also be able to serve as the basis for materials selection, design and quality control specifications.

Studies to-date by various investigators suggest the existence of some functional relationship between fracture toughness and material's flow stress and ductility.

Wells[2] analyzed the crack opening stretch at the onset of fracture, δ, and could show that the fracture toughness G_{Ic} is given by

$$G_{Ic} = \delta_{Ic}\, \sigma_Y \qquad (3)$$

where $\delta_{Ic} = 2v_{Ic}$ at fracture. The fracture toughness is clearly a function of the materials flow stress and its ductility, where σ_Y is a measure of the flow stress and δ_{Ic} is a measure of its ductility.

Beeuwkes[3] conducted a detailed plasticity analysis for parabolic cracks from which he obtained a relationship for the fracture toughness, assuming that crack propagation occurs under a constant stable root radius ρ_o.

His fracture criterion is a maximum stress criterion where $\sigma_{max} = \sigma_Y (1 + \phi)$, ϕ being the angle change of the slip line. Accordingly the fracture toughness is given by

$$K_{IC} = \sigma_Y \sqrt{\pi\rho} \cdot \frac{1}{L}$$

$$L = f(\phi) = g(E, \nu, \sigma_Y, \sigma_N, \rho_o) \qquad (4)$$

where L defines the boundary having a strain equal to the yield strain ε_Y.

Krafft[4] has made an estimate of the fracture toughness from the assumption that fractures initiate in a small ligament adjacent to the crack surface of size d_T, when that ligament is subjected to a strain which is equal to tensile instability strain, ε_{TI}, or n, for exponential strain hardening of the type $\sigma = k \cdot \varepsilon^n$. Assuming a strain distribution adjacent to the crack tip which varies as $(1/r)^{0.5}$ Krafft obtains

$$K_{IC} = E.n \sqrt{2\pi d_T} \qquad (5)$$

Several precise tests by Krafft on steel are in agreement with the proposed relationship. Yoder[5] studied the fracture surfaces in maraging steel specimens with scanning electron fractography, and noted lines of constant spacing which he interpreted as the "process zone size," d_T of Krafft's tensile ligament instability theory of fracture toughness. From measurements of d_T and the instability strains he calculated K_{IC} values and found agreement within 30 percent of the values determined from fracture tests.

Hahn and Rosenfield[6] experimentally determined the strain distributions in the vicinity of a crack and proposed a relationship for the fracture toughness, K_{IC}, by relating the critical strain at fracture to the critical crack opening displacement. Their relationship is

$$K_{IC} \simeq n\sqrt{(2/3) \cdot E \cdot \sigma_Y \cdot \varepsilon_F} \qquad (6)$$

where ε_F is the tensile fracture strain. They suggest that the actual fracture strain is (1/3) ε_F for plane strain and (1/2) ε_F for plane stress. Yoder's calculations of K_{IC} from Equation (6) showed poorer correlations than those from Equation (5).

Barsom[7] also proposed an expression for the fracture toughness which is based on the relationship between crack opening displacement, δ, and the strain distribution. He assumed that $\delta = (\varepsilon/\alpha)^{1/m}$ hence,

$$K_{IC} = A\sqrt{\sigma_Y} \cdot (\varepsilon_{F,p.s})^{1/2m} \qquad (7)$$

($m \simeq 1/4$, and α is a proportionality constant) where A is an adjustable constant, $\varepsilon_{F,p.s.}$ is the plane strain fracture ductility and m is a material characteristic to be determined experimentally. Crucial to his model is that plane strain fracture occurs when the strain reaches a critical value, which he terms the critical plane strain fracture ductility. This value is determined experimentally from tests on a specimen proposed by Clausing[8,9] (cf. Figure 3).

All these efforts and correlations clearly indicate that it should

be possible to determine a valid relationship between material ductility, material flow stress, and fracture toughness for technical materials. It is also quite evident that one must select those values of the flow stress and of the fracture ductility which are characteristic for the critically stressed zone ahead of the tip of the crack. In this region, the stress state is biaxial and triaxial, depending on the geometry of the specimen, and the flow stress is elevated due to the plastic constraint. Thus the multiaxiality of the stress state will affect both the flow stress and the fracture strain .

The elevation of flow stress, commonly referred to as the plastic constraint factor, can be readily obtained from either the Tresca or the Hencky-von Mises yield criteria. The effect of stress state on the ductility value was studied[10] for Aluminum alloys (2024-T4 and 7075-T6), Titanium alloys Ti6AL-4v annealed, Ti-6Al-6v-2Sn annealed and Ti-2.5 Al-16v (solution treated) and steels (4340 steel R_c 39 and R_c 53; 250 grade maraging R_c 48). The results[10] show that the effective fracture strain, $\bar{\varepsilon}_{F_{\alpha\beta}}$ was found to decrease as the stress state changes from the uniaxial to the biaxial case and the minimum was observed in all materials for the balanced biaxial case ($\alpha = \sigma_2/\sigma_1 = 1$, $\beta = \sigma_3/\sigma_1 = 0$). The experimental results agree well with a critical volume strain fracture criterion[10,11] proposed by Weiss. According to this theory, the fracture strain ratio is written

$$\frac{\bar{\varepsilon}_{F_{\alpha\beta}}}{\bar{\varepsilon}_{TF}} = (wm)^{1/n} \qquad (8)$$

where

$\bar{\varepsilon}_{TF}$ = uniaxial tensile fracture strain

$$w = \frac{1}{1+\alpha+\beta}$$

$$m = [(1 + \alpha + \beta)^2 - 3(\alpha + \beta + \alpha\beta)]^{1/2}$$

n = strain hardening exponent in $\bar{\sigma} = K\bar{\varepsilon}^{n}$

$\bar{\sigma}$ and $\bar{\varepsilon}$ are the von Mises effective stress and strain respectively. It has to be noted that the value of "n" must represent the entire stress strain diagram and not the plastic portion only.

Studies of notch-tensile tests showed that the minimum effective fracture strains at the notch root were in general close to the minimum fracture strains under balanced biaxial tension ($\alpha = 1$, $\beta = 0$) obtained in the bulge test though in some cases (e.g. 250 maraging steel) the notch root fracture ductility was found to be somewhat higher.

With this better understanding of the relationship between fracture ductility and stress states analytical relationships for fracture toughness were developed[10,11].

$$K_c^2 = \pi\sigma_Y^2\rho^* \left[\left(\frac{\bar{\varepsilon}_{F_{\alpha\beta}}}{\bar{\varepsilon}_Y}\right)^{n+1} - 1\right] \tag{9}$$

$$K_c^2 = \frac{\pi\sigma_Y^2}{n}\rho^* \left[\left(\frac{\bar{\varepsilon}_{F_{\alpha\beta}}}{\bar{\varepsilon}_Y}\right)^{n+1} - 1\right] \tag{10}$$

Equation (9) was developed from Irwin's plastic zone size definition and notch analysis of fracture[12]. Equation (10) was obtained from fundamental

energy approach and using notch analysis of fracture. The above correlations were applied[10] in the case of Al 2014 T6 alloy with indifferent success.

The principal objective of this year's program was concerned with the development of a design system for definitely identifiable design situations, namely (a) the plane strain fracture toughness of ultra high strength materials, (b) the plane strain fracture toughness for medium strength structural materials requiring inordinately large test specimens to obtain valid K_{Ic} values, (c) the fracture toughness under non-plane strain conditions and (d) the load carrying capacity of parts containing finite stress concentration such as notches, grooves, fillets etc. This required further refinement of the analytical formula developed in the last year and performing a number of tests on some selected materials to check the proposed analysis.

Research experience in the past[13] has clearly indicated that the sharp crack fracture mechanics is well suited for the case of ultra high strength materials and therefore, can provide an important bench mark for any correlations between K_{Ic} and the materials strength and deformation characteristics. Our experimental investigations this year were, therefore, concerned mainly with ultra high strength materials namely 300M steel and D6AC steel. To obtain a range of strength levels 3 different tempers on each of these alloys were carried out and the predictive power and accuracy of K_c and K_{Ic} values from the proposed analysis was checked by comparing with the experimental values. It is also intended to perform

tests on Ti and Al alloys. But the special alloys chosen were not available until last month. These are expected to be received this month and the results of the tests on these alloys will be furnished in the next report.

The proposed analysis requires a precise determination of the ductility value under balanced biaxial tension ($\alpha = 1$, $\beta = 0$). To achieve this a bulge test fixture was designed to replace the simple indentation plunger test. To check the thickness effect, on the balanced biaxial ductility, bulge tests were performed on 2 different thicknesses for both D6AC and 300M steel specimens. Tensile tests on double-edge notched specimens with various root radii including a fatigue crack were performed to obtain the value of Neuber's micro support effect constant ρ^*. The determination of the value of ρ^* and its variations, if any, with thickness, temper etc. is also an important consideration in the application and extension of the proposed fracture toughness correlation. Finally fracture toughness tests were performed on three different thicknesses to obtain a range of fracture toughness values on each temper including the plane strain fracture toughness values, if possible.

The theoretical analysis of last year was further refined and a more accurate correlation obtained. Predictions of the plane strain fracture toughness (K_{Ic}) values from this relationship were compared with the experimentally obtained values of plane strain fracture toughness, for ultra high strength steels. Similar estimates for plane stress fracture toughness (K_c) were also made for the ultra high strength steels. For medium strength tough structural materials additional work is required,

especially accurate determinations of ρ^*. Bulge ductility test was performed on HY-80 steel and the literature value of its fracture toughness reported. This report contains the results of the experimental and analytical studies conducted during the reporting year.

EXPERIMENTAL PROCEDURES

The ultra high strength materials selected for this year's study were D6AC steel and 300M steel. The chemical composition of these two alloys are given in Table I and II respectively. Three different strength levels of each of these alloys were obtained by varying the tempering temperature after quenching and they were:

1. D6AC Steel (500°F (260°C) temper, 2 hours; R_c = 50)
2. D6AC Steel (800°F (427°C) temper, 2 hours; R_c = 46.5)
3. D6AC Steel (1100°F (593°C) temper, 2 hours; R_c = 42.5)
4. 300M Steel (500°F (260°C) temper, 2 hours; R_c = 51.5)
5. 300M Steel (800°F (427°C) temper, 2 hours; R_c = 47.5)
6. 300M Steel (1100°F (593°C) temper, 2 hours, R_c = 39).

The heat treatment performed on the D6AC steel was as follows:

1. Normalize at 1675°F (913°C) for 40 minutes
2. Austenitize at 1575°F (857°C) for 40 minutes
3. Oil quench at 75°F (22°C)
4. Initial temper at 400°F (205°C) for 2 hours immediately after quenching.
5. Final temper at the required temperature for 2 hours.

The heat treatment followed for the 300M steel was:

1. Normalize at 1675°F (913°C) for 40 minutes
2. Austenitize at 1575°F (857°C) for 40 minutes
3. Oil quench at 75°F (22°C)
4. Tempering at the required temperature for 2 hours immediately after quenching.

The specimens were approximately 0.145 inch (3.69 mm) thick except in some cases where thickness of the specimens were varied to observe the thickness effect. All tests were conducted at room temperature.

A. Biaxial Ductility Tests:

Five types of tests were performed to determine the fracture ductilities under biaxial stress conditions. They are:

1) Uniaxial Tensile Test ($\sigma_2/\sigma_1 = \alpha = 0$ and ∞)

2) Plane Strain Bend Test ($\sigma_2/\sigma_1 = \alpha = 1/2$ and 2)

3) Plane Strain Tensile Test ($\sigma_2/\sigma_1 = \alpha = 1/2$ and 2) (Clausing specimen)

4) Indentation Plunger Bulge Tests ($\sigma_2/\sigma_1 = \alpha = 1$)

5) Hydraulic Bulge Tests ($\sigma_2/\sigma_1 = \alpha = 1$)

All these tests were performed in both longitudinal and transverse directions of the sheet specimens. The stress ratios, α, of 0, 1/2 and 1 correspond to longitudinal tests and those of ∞, 2 and 1 correspond to transverse tests.

The uniaxial tensile test, the plane strain bend test, the plane strain tensile test, the plunger indentation bulge test and the hyraulic bulge test were conducted on all tempers of both materials.

For each test the principal strains at the onset of visible cracking, ε_{1F}, ε_{2F}, and ε_{3F} were determined. The results are given in terms of effective fracture strains:

$$\bar{\varepsilon}_F = 1/3\sqrt{2[(\varepsilon_{1F} - \varepsilon_{2F})^2 + (\varepsilon_{2F} - \varepsilon_{3F})^2 + (\varepsilon_{3F} - \varepsilon_{1F})^2]} \qquad (11)$$

or, for volume constancy, $\varepsilon_{1F} + \varepsilon_{2F} + \varepsilon_{3F} = 0$,

$$\bar{\varepsilon}_F = [\tfrac{2}{3}(\varepsilon_{1F}^2 + \varepsilon_{2F}^2 + \varepsilon_{3F}^2)]^{1/2} \tag{12}$$

Uniaxial Tensile Tests: Uniaxial tests were conducted on sheet specimens of geometry as shown in Figure 1. Care was taken to design these sheet specimens so that the strains in the width and thickness directions were comparable. The effective fracture strain, $\bar{\varepsilon}_F$, was calculated using:

$$\bar{\varepsilon}_F = \varepsilon_{1F} = \ln \frac{A_o}{A_F} \tag{13}$$

where A_o is the initial cross sectional area and A_F is the final cross sectional area.

Plane Strain Biaxial Tests: Two series of plane strain biaxial tests were performed.

a. Plane Strain Bend Test: Bending of wide specimens over a cylindrical die was used to determine the plane strain fracture ductility values, ($\sigma_2/\sigma_1 = 1/2$, $\sigma_3 = 0$). It has been demonstrated[14-15] that plane strain conditions are obtained at the center section of the top and bottom surfaces of a bend specimen, for width to thickness ratios in excess of 8. For the present test series, a specimen geometry having a width to thickness ratio of greater than 15 was chosen. The experimental setup is shown in Figure 2. The test is essentially a three point bend test with a side clearance of approximately one sheet thickness once the specimen has achieved a "U" bend over the cylindrical mandrel (indentor). To minimize friction, teflon tape was inserted under the mandrel and between the edge

supports and the specimen. The fracture strain was designated as that strain which caused surface cracking of the sheet. To determine the critical bend radius, specimens were bent around a set of cylinders having diameters in 1/8 inch intervals. The effective strain in this case is given by:

$$\bar{\varepsilon}_F = \frac{2}{\sqrt{3}} \varepsilon_{1F}, \text{ since } \varepsilon_{3F} = 0 \text{ and } \varepsilon_{1F} = -\varepsilon_{2F} \tag{14}$$

If the sheet specimen is bent over a cylinder of diameter D, ε_1 is

$$\varepsilon_1 = \ln\left(1 + \frac{t}{D+t}\right) \tag{15}$$

where t is the specimen thickness. In the center of the outer surface of the bend specimen, $\varepsilon_3 = 0$, $\varepsilon_2 = -\varepsilon_1$.

b. Plane Strain Tensile Test: Another set of plane strain biaxial tests were conducted using a grooved tensile specimen[8,9]. The specimen design is shown in Figure 3. Plane strain biaxiality is obtained at the center section of the groove. In this case the fracture strain is given by:

$$\bar{\varepsilon}_F = \frac{2}{\sqrt{3}} \varepsilon_{1F}, \ \varepsilon_{2F} = 0 \text{ and } \varepsilon_{1F} = -\varepsilon_{3F} = -\ln \frac{t_F}{t_o} \tag{16}$$

where t_o is the initial thickness and t_F the final thickness.

Balanced Biaxial Tension Tests: To obtain the fracture ductilities under balanced biaxial tension two types of tests were performed: Plunger identation bulge test and hydraulic bulge test.

a. Plunger Indentation Bulge Test: The experimental setup for this test is shown in Figure 4. Instead of using a hydraulic medium to apply the stress, a plunger with a hemispherical end was pressed through a cushion against a circularly clamped flat disk specimen. The cushion consisted of a laminate made up of a layer of teflon tape, an aluminum sheet (t = 0.040 in.), a silicone rubber sheet (t = 0.0625 in.) and another layer of teflon sheet. The effective fracture strain for this case is determined from thickness measurements, i.e.

$$\bar{\varepsilon}_F = -\varepsilon_{3F} = \ln \frac{t_o}{t_F} \tag{17}$$

since $\varepsilon_1 = \varepsilon_2 = -\varepsilon_3/2$ (using volume constancy); ε_{3F} is the thickness strain at crack initiation.

B. Hydraulic Bulge Test: Figure 5 shows the basic components of the bulge fixture developed during the current year. This essentially consists of the pressure cylinder with hydraulic oil, a piston and the top support. The specimen along with the cylinder and the top support is held in position between two flanges. In order to prevent leakage of oil during testing an O-ring is provided between the specimen and the pressure cylinder. To pressurize the cylinder the piston is connected with the moving platen of the Riehle Testing machine (300,000 lbs. capacity). Two different thicknesses of specimens namely 0.050 inch (1.27mm), 0.075 inch (1.91mm) were tested to determine the effect of thickness variation in bulge ductility. The effective fracture strain for this case is also determined from Equation (17).

B. Notch Tensile Tests:

Notch tensile tests have been completed on D6AC steel (R_c 50, 46.5 and 42.5) and 300M steel (R_c 51.5, 47.5, 39.0). The test specimen geometry is shown in Figure 6. The specimens were double-edge notched with a 30% notch depth. The variation in stress concentration factor was achieved by varying the notch root radius (ρ). The stress concentration factors, K_t, were determined from Peterson's tables[16] and ranged from 1.54 (ρ = .655 mm) to as high as that of a crack ($\rho \simeq 0$, obtained by a fatigue crack). In addition, tensile specimens (Figure 7) were tested in the same series. These specimens had the same net cross sectional area as the notched specimens.

The notch strength, σ_{NF}, was calculated from the maximum load by dividing it through the original net cross sectional area. The longitudinal strain and the thickness strain at the notch root at fracture was measured on the broken specimens. The longitudinal strain was determined from

$$\varepsilon_{LF} = \ln \left(\frac{\rho_f}{\rho_i}\right)^{1/2} \tag{18}$$

where ρ_i is the initial and ρ_f is the final root radius. This relationship has been shown to be a good approximation of the longitudinal root radius strain[17]. The thickness strain at fracture was determined in the usual way from the initial and final thickness values near the notch root, t_i and t_f, from

$$\varepsilon_{TF} = \ln \frac{t_f}{t_i} \tag{19}$$

Assuming volume constancy, $\varepsilon_W = -(\varepsilon_L + \varepsilon_T)$ and effective fracture strain in the region just ahead of the notch root is thus given by

$$\bar{\varepsilon}_F = [\frac{2}{3} (\varepsilon_{LF}^2 + \varepsilon_{WF}^2 + \varepsilon_{TF}^2)]^{1/2} \tag{20}$$

C. Fracture Toughness Testing

Fracture toughness tests on compact tension specimens (Figure 8) were performed following the ASTM procedure[18] on D6AC steel (R_c 50, 46.5 and 42.5) and 300M steel (R_c 51.5, 47.5, 39.0). Tests were performed on three different thicknesses, namely 0.145 inch (3.69 mm), 0.500 inch (12.7 mm) and 1.00 inch (25.4 mm). The thicknesses of 0.145 inch and 0.50 inch of the materials tested were not adequate to qualify them as valid K_{Ic} tests. Instead they provide the apparent fracture toughness value K_Q. The plane strain fracture toughness value (K_{Ic}) was obtained from the tests on 1 inch (25.4 mm) thick specimens.

For evaluating the apparent fracture toughness (K_Q) or the plane strain fracture toughness (K_{Ic}) values from the compact tensile specimens the displacement at the edge was measured by a 1 inch (25.4 mm) gauge length extensometer instead of the usual clip-on gauge. The fracture toughness values were calculated according to[18]

$$K_Q = \frac{P_Q}{t\sqrt{w}} f\left(\frac{a}{w}\right) \tag{21}$$

$$K_{Ic} = \frac{P_{Ic}}{t\sqrt{w}} f\left(\frac{a}{w}\right)$$

where P_Q represents the load for 5% secant offset, P_{Ic} is the load at pop-in, t = thickness, w = width and a is the crack length of the specimen. The value of the function, f(a/w) was obtained from the listed table[18] for the ratio a/w.

Also from the double edge notched specimens (with a fatigue crack), K_c values were calculated using the formula[19]

$$K_c = \frac{P\sqrt{a}}{tw}\left[1.98 + 0.36\,\frac{2a}{w} - 2.12\,\left(\frac{2a}{w}\right)^2 + 3.42\,\left(\frac{2a}{w}\right)^3\right] \qquad (22)$$

where P is the maximum load for the pre-cracked specimen of gross width w, thickness t and 2a is the total crack length.

RESULTS AND DISCUSSIONS

Biaxial Ductility Tests The experimental results of the effect of stress biaxiality on fracture ductility are presented in Tables III and IV and plotted in Figures 9 - 14. To supplement the balanced biaxial ductility values obtained by the plunger indentation bulge test, hydraulic bulge tests were performed on two different thicknesses, 0.05 and 0.076 in. The results of the hydraulic bulge tests are presented in Table V and also plotted in Figures 9 - 14.

Figures 9 - 14 indicate that there is a significant loss in ductility on going from the uniaxial stress state to the plane strain state ($\alpha = 1/2$, $\beta = 0$). Considering the plunger indentation bulge ductility, the observed effects of the stress state on material ductility are similar to those obtained by similar tests on other materials[10] namely a minimum fracture ductility for the balanced biaxial condition for all materials except 300M steel (39 R_c) where the plane strain ductility measured from the bend test was slightly lower than the balanced biaxial tension ductility (Figure 14).

It is noted that the hydraulic bulge ductility values are consistently higher than the previously determined ductility values for balanced biaxial tension by the plunger test, as indicated in Figures 9 - 14. A difference in the surface condition between the plunger bulge test specimens and the hydraulic bulge test specimens is the principal cause for this discrepancy. The final grinding on the former as well as the tension and Clausing specimens resulted in a surface roughness of an RMS value between 18 and 20 micro-inches. The surface roughness of the hydraulic bulge test specimens was RMS 9 to 12 micro-inches. A comparison

hydraulic bulge test on 300M steel (R_c 39) clearly showed this effect. For a fine surface finish, RMS 9-12, the bulge ductility was 0.45, for a coarse finish, RMS 50 micro-inches, the bulge ductility was only 0.27. Different grinding methods could also cause different residual stress patterns and thereby affect the ductility. Moreover, it was noted that the hydraulic bulge specimens were frequently in the lower hardness range for a given heat treatment - possibly due to a higher thickness of the blanks as prepared for heat treating. Some typical values are:

Material and temper	Average hardness of the biaxial ductility specimens	Average hardness of the hydraulic bulge specimens
D6AC, 500°F, 2 hours	R_c 50	R_c 46
D6AC, 800°F, 2 hours	R_c 46.5	R_c 40
D6AC, 1100°F, 2 hours	R_c 42.5	R_c 39
300M, 500°F, 2 hours	R_c 51.5	R_c 51.5
300M, 800°F, 2 hours	R_c 47.5	R_c 45
300M, 1100°F, 2 hours	R_c 39	R_c 40

An attempt will be made soon to resolve all these questions which bear on the applicability of the fracture postulate.

The recent findings of Azrin and Backofen[20] as a result of careful experiments performed to verify the Marciniak and Kuczynski's[21] theory of instability of a sheet under plane stress in the range of $1/2 < \alpha(= \sigma_2/\sigma_1) < 1$ may also suggest an explanation of the discrepancy

between the balanced biaxial ductility values obtained by hydraulic bulge test and plunger indentation bulge test. Their principal observation is the development of a plane strain instability region in a balanced biaxial tension test due to the pressure of a material inhomogeneity. According to these findings one might expect little difference between the plane strain (Clausing or bend test) ductility and the bulge ductility, especially as determined by the plunger bulge test.

Values of fracture ductility obtained in the transverse region are generally lower than those obtained in the longitudinal region. This difference is attributed to the mechanical anisotropy of the sheet materials tested.

Notch Tensile Tests The results of the notch tensile tests are presented in Table VI - XI and plotted in Figures 15 - 38. The individual fracture strains, i.e. the longitudinal thickness and the width strains, vary greatly with the original specimen geometry as indicated in Figure 15, 19, 23, 27, 31 and 35. The effective fracture strains calculated in accordance with Equation (20) show a decrease (Figures 16, 20, 24, 28 and 32) with increasing stress concentration factor to a plateau, though there is some scatter observed at higher stress concentration factors. The effective fracture strain values obtained with the lower strength (R_c 39.0) 300M steel show large amounts of scatter (Figure 36) in the results and do not seem to decrease to a plateau.

For the sake of comparison the minimum fracture ductility values obtained from the biaxial ductility tests are also plotted in Figure 16, 20, 24, 28, 32 and 36. The minimum notch root effective fracture

strains lie between the plane strain ductility value and the plunger indentation bulge ductility (Figures 20 and 24) for D6AC steel (R_c 46.5 and 42.5) and are very close (Figure 28 and 32) to the plunger indentation ductility values for 300M steel (R_c 51.5 and 47.5). The notch root minimum strain for D6AC steel (R_c 50) is higher (Figure 16) than the minimum biaxial ductility value. The results for the 300M steel (R_c 39.0) show too much scatter to identify any particular trend (Figure 36).

The variation of notch strength with increasing stress concentration factors are shown in Figures 17, 21, 25, 29, 33 and 37. All of them show an initial notch strengthening followed by a decrease in notch strength with increasing stress concentration factors. The notch sensitivity, in general, tends to decrease with increasing tempering temperature for both materials, though this is more predominant in 300M steel. For high K_t values the curves reach a plateau. From the transition point between the decreasing and the flat portion of the curve K_t^* can be obtained and using the formula[12]

$$K_t^* = 1 + 2\sqrt{c/2\rho^*} \qquad (23)$$

where c is the crack length (in this case, the length of the fatigue crack, $\rho \approx 0$), the appropriate values of the Neuber's micro support effect constant ρ^* are determined for the materials tested. The values of ρ^* obtained are 0.0007 inch or 0.0178 mm ($K_t^* = 39$), 0.0012 inch or 0.0305 mm ($K_t^* = 26$), and 0.0014 inch or 0.0356 mm ($K_t^* = 24$) for D6AC steel having

hardness values of R_c = 50, R_c = 46.5 and R_c = 42.5 respectively and are 0.0002 inch or 0.005 mm (K_t^* = 57), 0.0003 inch or 0.008 mm (K_t^* = 51), and 0.0004 inch or 0.010 mm (K_t^* = 45) for 300M steel having hardness values of R_c = 51.5, R_c = 47.5 and R_c = 39.0 respectively.

The notch root thickness contraction, ε_t, in the sheet thickness direction, is plotted as a function of root radius to thickness ratio (ρ/t) in Figures 18, 22, 26, 30, 34 and 38. The data follow the general trend postulated by Yoder, Weiss and Liu[22].

The values of the fracture toughness, K_c, is calculated from Equation (22) from the notch tensile test data with fatigue cracks and the results are:

Material	Fracture Toughness
D6AC Steel (R_c 50)	42.6 Ksi$\sqrt{in}$ (1483 N. mm$^{-3/2}$)
D6AC Steel (R_c 46.5)	78.6 Ksi$\sqrt{in}$ (2735 N. mm$^{-3/2}$)
D6AC Steel (R_c 42.5)	76.9 Ksi$\sqrt{in}$ (2676 N. mm$^{-3/2}$)
300M Steel (R_c 51.5)	62.6 Ksi$\sqrt{in}$ (2179 N. mm$^{-3/2}$)
300M Steel (R_c 47.5)	60.3 Ksi$\sqrt{in}$ (2098 N. mm$^{-3/2}$)
300M Steel (R_c 39.0)	129.3 Ksi$\sqrt{in}$ (4500 N. mm$^{-3/2}$)

Fracture Toughness Test and the Correlations Between Fracture Toughness and Material Ductility: The results of fracture toughness test performed on 3 different thicknesses, namely 0.15 inch (3.82 mm) 0.50 inch

(12.2 mm) and 1.0 inch (25.4 mm), of D6AC steel and 300M steel are summarized in Tables XII - XVI. The dimensional requirements satisfying the plane strain fracture criterion, namely both the thickness, t, and crack length, a, should be greater than 2.5 $(K_{Ic}/\sigma_Y)^2$, are fulfilled for all materials in 1 inch thickness. The above conditions are also fulfilled in 0.146 inch thick and 0.50 inch thick specimens of D6AC steel (R_c = 50 and R_c = 46.5) and 300M steels (R_c = 51.5 and R_c = 47.5); but the other dimension of importance, i.e. the width, w, is not in strict accordance with the ASTM design of plane strain fracture toughness. Therefore, these results are designated as apparent plane strain fracture toughness (K_Q).

Fracture Toughness Correlations Two theoretical correlations have been obtained in this study, as presented earlier

$$K_c^2 = \pi \sigma_y^2 \rho^* \left[\left(\frac{\bar{\varepsilon}_{F_{\alpha\beta}}}{\bar{\varepsilon}_Y}\right)^{n+1} - 1\right] \qquad (9)$$

and

$$K_c^2 = \frac{s\sigma_Y^2}{n} \rho^* \left[\left(\frac{\bar{\varepsilon}_{F_{\alpha\beta}}}{\bar{\varepsilon}_Y}\right)^{n+1} - 1\right] \qquad (10)$$

The former equation is derived from Irwin's plastic zone size definition and the latter is based on the fundamental definition of fracture, $G = dW/dA$, and represents the corrected form of similarly derived expression reported[10] previously. The two equations are identical except for constant multipliers. The symbols used are:

σ_Y - yield strength (uniaxial)

ρ^* - Neuber Micro Support Effect Constant[12]

$\bar{\varepsilon}_{F_{\alpha\beta}}$ - effective fracture strain for stress state ahead of crack, $\alpha = \frac{\sigma_2}{\sigma_1}$ $\beta = \frac{\sigma_3}{\sigma_1}$

$\bar{\varepsilon}_Y$ - effective strain at $\bar{\sigma} = \sigma_Y$

n - strain hardening exponent from $\bar{\sigma} = k\bar{\varepsilon}_t^n$ (ε_t = total strain)

s - shape factor for plastic zone

A very simple approximate and intuitively useful relationship is obtained for n = 1, which is reasonable since most measurements[23] of the strain distribution within the plastic zone are well represented with n = 1, namely:

$$K_c = E\sqrt{s\rho^*}\,\bar{\varepsilon}_{F_{\alpha\beta}} \qquad (24)$$

This equation predicts a linear relationship between K_c and the multiaxial fracture ductility associated with the stress state ahead of the crack. It also suggests that it should be possible to estimate K_c values from plane stress to plane strain, using the appropriate values of $\bar{\varepsilon}_{F_{\alpha\beta}}$, if s does not vary too much or if its variation with the change of stress state is known.

To use Equation (24) for plane strain fracture toughness correlations it is necessary to obtain $\bar{\varepsilon}_{F_{\alpha\beta}}$. This is a difficult task; however, estimates of $\bar{\varepsilon}_{F_{\alpha\beta}}$ characteristic of the zone in front of a crack at the

instant of plane strain fracture can be made from measurements of bulge ductility or the bend ductility.

From slip line field theory[24], the stress state ahead of a notch can be determined. The basic equation

$$\sigma_m \pm 2k\phi = \text{constant} \tag{25}$$

where σ_m is the mean stress, k the yield strength in pure shear and ϕ the angle change of a slip line, yields, for a sharp notch

$$\sigma_1 = \sigma_{max} = 2k(1 + \pi/2)$$

$$\sigma_2 = \sigma_{mean} = k(1 + \pi) \tag{26}$$

$$\sigma_3 \quad \sigma_{min} = k\pi$$

and hence $\alpha = (1+\pi)/(2+\pi) = 0.906$ and $\beta = \pi/(2+\pi) = 0.611$. Therefore $w = 0.414$, $m = 0.337$ and $wm = 0.14 = 1/(7.17)$ for plane strain conditions inside the plastic zone. Furthermore from the definition of the effective stress

$$\bar{\sigma} = 3\sigma_m \; 3m \tag{27}$$

Anywhere inside the plastic zone the effective stress equals the uniaxial yield stress, σ_Y, and therefore

$$\sigma_Y = 3\sigma_m \quad wm \tag{28}$$

also

$$\sigma_m = k(1 + \pi) \tag{29}$$

For the Hencky-von Mises yield criterion $\sigma_Y = \sqrt{3}k$. Putting the value in Equation (28) and substituting in Equation (29) one also obtains $2m = 1/(7.17)$, as already shown above. For the ratio of fracture ductilities for different stress states one obtains

$$\frac{\bar{\varepsilon}_{F_2}}{\bar{\varepsilon}_{F_1}} = \left(\frac{w_2 m_2}{w_1 m_1}\right)^{1/n} \tag{30}$$

for the mean stress (volume strain) failure postulate, and

$$\frac{\bar{\varepsilon}_{F_2}}{\bar{\varepsilon}_{F_1}} = \left(\frac{m_2}{m_1}\right)^{1/2} \tag{31}$$

for a maximum normal stress failure postulate. For $n = 1$ the ratio between bulge ductility and plane strain fracture ductility is

$(\bar{\varepsilon}_{F_{ps}} / \bar{\varepsilon}_{F_{\alpha=1,\beta=0}}) = 0.28$ for the volume strain fracture postulate; and

$(\bar{\varepsilon}_{F_{ps}} / \bar{\varepsilon}_{F_{\alpha=1,\beta=0}}) = 0.34$ for the maximum normal stress failure criterion.

Similarly, the relationship for the bend ductilities, $\bar{\varepsilon}_{\alpha=1,\beta=0}$, are

$(\bar{\varepsilon}_{F_{ps}} / \bar{\varepsilon}_{F_{\alpha=1/2,\beta=0}}) = 0.24$ for the volume strain fracture postulate, and

$(\bar{\varepsilon}_{F_{ps}} / \bar{\varepsilon}_{F_{\alpha=1/2,\beta=0}}) = 0.39$ for the maximum normal stress failure concept.

Equation (24) can be rewritten for the plane strain fracture condition as:

$$K_{Ic} = \frac{E\sqrt{s\rho^*}}{\sqrt{1-\nu^2}} \cdot \bar{\varepsilon}_{F_{ps}} \tag{32}$$

Correlating K_{Ic} with the bulge ductility one obtains, for $\nu = 1/2$,

$$K_{Ic} = 0.32\ E\sqrt{s\rho^*} \cdot \bar{\varepsilon}_{F_{\alpha=1,\beta=0}} \quad \text{(vol. strain frac.)} \tag{33}$$

$$K_{Ic} = 0.39\ E\sqrt{s\rho^*} \cdot \bar{\varepsilon}_{F_{\alpha=1,\beta=0}} \quad \text{(maxm. normal stress frac.)} \tag{34}$$

Figure 39 shows the plot of K_{Ic} values obtained on 1 inch (25.4 mm) WOL specimens vs. the hydraulic bulge ductility on smoothly ground (10 micro-inches RMS) specimens of thickness = 0.050 inch (1.27 mm). It shows a very good correlation with

$$K_{Ic} = 169\ \bar{\varepsilon}_{F_{\alpha=1,\beta=0}} \tag{35}$$

A rough calculation of the shape factor s yields the value of 0.54 for n = 1. Taking the Young's modulus $E = 28.5 \times 10^3$ ksi, Equation (35) and (37) yields a value of $\rho^* = 6.4 \times 10^{-4}$ inch (0.016 mm) with the volume strain fracture criterion and Equation (36) and (37) yields a

value of $\rho^* = 4.28 \times 10^{-4}$ inch (0.0109 mm) for the critical normal stress failure postulate. This value of ρ^* calculated from the slope of the line is very close to the average value of ρ^* for these steels obtained from the notch tensile test; approximately 7.0×10^{-4} inch (0.0178 mm).

Similar correlations between plane strain fracture toughness and the bend ductility may be obtained by expressing the plane strain fracture ductility ahead of the crack tip region in terms of $\bar{\varepsilon}_{F_{\alpha=1/2,\beta=0}}$. Thus one obtains

$$K_{Ic} = 0.28\, E\sqrt{s\rho^*}\cdot\bar{\varepsilon}_{F_{\alpha=1/2,\beta=0}} \quad \text{(vol. strain frac.)} \tag{36}$$

$$K_{Ic} = 0.45\, E\sqrt{s\rho^*}\cdot\bar{\varepsilon}_{F_{\alpha=1/2,\beta=0}} \quad \text{(maxm. normal stress frac.)} \tag{37}$$

Figure 40 shows the plot of K_{Ic} values obtained on 1 inch (25.4 mm) WOL specimens against the bend ductility values obtained on coarsely ground (RMS = 19) specimens of average thickness 0.15 inch (3.81 mm). Here again the data fall on a straight line with

$$K_{Ic} = 622\ \bar{\varepsilon}_{F_{\alpha=1/2,\beta=0}} \tag{38}$$

The calculated ρ^* values do not agree with those obtained from the notch data, namely 7×10^{-4} inch (0.0178 mm). This could be attributed to the poor surface finish of the bend specimens. Also the plastic zone shape factor s could be different.

To obtain the value of fracture toughness for non-plane strain conditions, it is necessary to know the $\bar{\varepsilon}_{F_{\alpha\beta}}$ corresponding to the stress state ahead of the crack. The elastic solution[25] of the stress field ahead of a crack suggests a stress state $\alpha = \sigma_2/\sigma_1 = 1$, $\beta = \sigma_3/\sigma_1 = 0$ for the plane stress condition. Thus the balanced biaxial ductility can directly be used to obtain the plane stress fracture toughness as

$$K_c = E\sqrt{s\rho^*}\cdot\bar{\varepsilon}_{F_{\alpha=1,\beta=0}} \tag{39}$$

Comparing Equation (39) with Equations (33) and (34) we find that the plane stress fracture toughness is given by a line through the origin with a slope which is approximately 3.13 times steeper than that for the K_{Ic}- correlation line for the volume strain fracture concept and 2.57 times steeper than that for the K_{Ic}-correlation line for the critical normal stress fracture criterion. Accordingly from Equation (37) the predicted plane stress fracture toughness values for these steels are given by

$$K_c = 529\ \bar{\varepsilon}_{F_{\alpha=1,\beta=0}} \quad \text{(vol. strain frac.)} \tag{40}$$

$$K_c = 434\ \bar{\varepsilon}_{F_{\alpha=1,\beta=0}} \quad \text{(maxm. normal stress frac.)} \tag{41}$$

It was not possible to obtain true plane stress fracture toughness value K_c experimentally. However, all the apparent fracture toughness (K_Q)

values obtained in thinner specimens lie within the above limit when based on the hydraulic bulge ductility (Figure 41). The figure also shows the plot of the data for annealed HY-80 steel, a medium strength tough structural material. The hydraulic bulge ductility was measured to be 0.92 and the literature[23] value of fracture toughness was 800 ksi $\sqrt{in}$ (27840 N. $mm^{-3/2}$). Since the value of ρ^* for this steel is not known it is difficult to comment on this particular point; however, if the suggested correlation can be extended for these materials, it seems that ρ^* value for this steel should be about 4 times the value obtained for ultra high strength steels, i.e. approximately 3×10^{-3} inch compared to 7×10^{-4} inch obtained as the average ρ^* value for D6AC and 300M steel. If the plunger indentation ductility correlation is made, the data seem to lie on a line having slope 870 ksi $\sqrt{in}$ (Figure 42), i.e.,

$$K_Q = 870\ \bar{\varepsilon}_{F_{\alpha=1,\beta=0}} \tag{41}$$

This slope is higher than that predicted by the upper limit given by Equation (40).

Although the elastic solutions suggest a balanced biaxial stress state in the region ahead of a crack, direct measurements[26] of strain in the vicinity of a crack showed that a stress state producing $\varepsilon_x \approx 0$ exists where x is the direction in the crack plane along the width. Thus for the plane stress case this leads to a stress state corresponding to the biaxial bend test and therefore the plane stress fracture toughness (K_c) can be correlated with bend ductility, i.e.

$$K_c = E\sqrt{s\rho^*}\cdot \bar{\varepsilon}_{F_{\alpha=1/2,\beta=0}} \tag{42}$$

Equation (42) when compared with Equations (36) and (37) suggests that the K_c vs. $\bar{\varepsilon}_{F_{\alpha=1/2,\beta=0}}$ line will have a slope which is 3.57 times greater than the slope of K_{Ic} vs. $\bar{\varepsilon}_{F_{\alpha=1/2,\beta=0}}$ line for the volume strain fracture criterion and is 2.22 times greater than the slope of the K_{Ic} vs. $\bar{\varepsilon}_{F_{\alpha=1/2,\beta=0}}$ line for the maximum normal stress failure criterion. Thus for the materials tested, Equation (42) predicts

$$\begin{aligned} K_c &= 2220\ \bar{\varepsilon}_{F_{\alpha=1/2,\beta=0}} \quad \text{(vol. strain frac.)} \\ K_c &= 1380\ \bar{\varepsilon}_{F_{\alpha=1/2,\beta=0}} \quad \text{(maxm. normal stress frac.)} \end{aligned} \tag{43}$$

Figure 43 shows a plot of apparent fracture toughness (K_Q) values obtained on 0.150 inch (3.81 mm) thick WOL specimens against bend ductility ($\varepsilon_{F_{\alpha=1/2,\beta=0}}$) obtained on coarsely ground specimens (19 micro-inches RMS). The data can be represented by a straigth line as

$$K_Q = 815\ \bar{\varepsilon}_{F_{\alpha=1/2,\beta=0}} \tag{44}$$

This slope 815 ksi$\sqrt{\text{in}}$ lies within the limit predicted by Equation (43).

SUMMARY AND CONCLUSION

The relationships between fracture toughness and material ductility were studied for high strength steels, D6AC and 300M, each heat treated to three strength levels. The results are summarized as follows:

1. Biaxial ductility tests on D6AC steel (hardness R_c 50, R_c 46.5 and R_c 42.5) and 300M steel (hardness R_c 51.5, R_c 47.5 and R_c 39.0) showed that the fracture ductility decreased significantly on going from the uniaxial stress state (tension test) to the plane strain stress state (bend test or Clausing type tension test) to the balanced biaxial condition (bulge test or plunger bulge test). The effective fracture strain is generally reduced to a value of less than half the value of the tensile fracture strain and sometimes to a value as low as 12% of the tensile fracture ductility. A strong influence of the surface finish was noted. This gave rise to some scatter, particularly for the bulge tests.

2. Notch tensile tests on D6AC steel (hardness R_c 50, R_c 46.5 and R_c 42.5) and 300M steel (R_c 51.5, R_c 47.5 and R_c 39.0) showed that the notch sensitivity decreases with increasing tempering temperature for both materials, with the reduction being somewhat greater for 300M steel. The values of the Neuber micro support effect constant, ρ^*, were determined and found to vary from 0.0002 inches (0.005 mm) (300M steel hardness R_c 51.5) to 0.0014 inches

(0.035 mm) D6AC steel, hardness R_c 42.5). Measurement of the effective fracture strain at the notch root showed a general trend of decreasing notch root fracture strain with increasing stress concentration factor. In general the minimum values of the notch root effective fracture strain lie close to the plunger ductility for 300M steel (hardness R_c 51.5 and R_c 47.5), higher for D6AC steel (hardness R_c 50) and between the bend and plunger ductility for D6AC steel (hardness R_c 46.5 and R_c 42.5). For 300M steel (hardness R_c 39), the scatter in the data was too large to identify a trend.

3. The analytical studies yield a correlation between fracture toughness and ductility which assume a simple form for negligible plasticity, namely, $K_c = E\sqrt{s\rho^*}\,\bar{\varepsilon}_{F_{\alpha\beta}}$, where E is the modulus of elasticity, s the shape factor for the plastic zone (approximately 0.54 for n = 1), ρ^* the Neuber micro support effect constant, $\bar{\varepsilon}_{F_{\alpha\beta}}$ the effective fracture strain corresponding to the stress state α,β representing the condition ahead of a crack.

4. To estimate the plane strain fracture toughness, K_{Ic}, from easily measureable ductility values, ε: the relationship $K_{Ic} = A_{\varepsilon_i} E\sqrt{s\rho^*} \cdot \bar{\varepsilon}_i$ is suggested, where A_{ε_i} is a constant corresponding to the stress state for which the ductility ε_i was measured. The table below gives the value of A_{ε_i} for various fracture ductility correlations and failure criteria .

Fracture Ductility Used For Correlation	Value of A_{ε_1} Vol. Strain Fracture Criterion	Maximum Normal Stress Fracture Criterion
Balanced biaxial tension ductility $\bar{\varepsilon}_{F_{\alpha=1,\beta=0}}$	0.32	0.39
Plane strain ductility $\bar{\varepsilon}_{F_{\alpha=\frac{1}{2},\beta=0}}$	0.28	0.45

Fracture toughness values were determined for all materials with compact tension specimens. The values obtained in 1 inch (25.4 mm) thick specimens met the requirements of plane strain fracture toughness, K_{Ic}. The experimental results were found to be in good agreement with the bulge ductility correlation but in somewhat poorer agreement with the bend ductility correlation. Surface finish effects on the bend ductility could be partly responsible for this discrepancy.

5. The analytical correlations were also extended to near plane stress fracture conditions. However, reliable estimates of the fracture strain corresponding to the plane stress condition ahead of a crack could not be made. Furthermore an experimental determination of the true plane stress fracture toughness is difficult. Nevertheless, it is anticipated that similar correlations can be established for plane stress conditions or mixed mode fracture.

6. Finally, since both the bulge and band ductility values were very sensitive to the surface preparation, it is necessary to resolve the effects of such factors as surface finish, residual stresses, metallurgical variations on the surface etc. before the analytical correlations developed can be effectively utilized as a basis for the development of materials selection and acceptance standards.

REFERENCES

1. Cottrell, A.H., Proc. Roy. Soc., v. 282, No. 1388 (1964), p. 2.

2. Wells, A. A., Brit. Weld. Journal, v. 10, (1963), p. 563.

3. Beeuwkes, R., Jr., Surfaces and Interfaces II, Syracuse University Press, (1968), p. 277.

4. Krafft, J.M., "Fracture Toughness of Metals, Report of NRL Progress, November (1963), also: Applied Materials Research, v. 1, (1964), p. 38.

5. Yoder, G.R., "Macrofractographic Lines in Maraging Steel: Correlations with Fracture Toughness," Personal Communication - to be published.

6. Hahn, G.T. and Rosenfield, A.R., Applications Related Phenomena in Titanium Alloys, ASTM STP No. 432, p. 5, Am. Soc. Testing Materials, (1968).

7. Barsom, J.M., "Relationship Between Plane-Strain Ductility and K_{IC} For Various Steels," First Natl. Congress for Pressure Vessels and Piping, San Francisco, Calif., May (1971).

8. Corrigan, D.A., Travis, R.E., Ardito, V.P., and Adams, C.M., Jr., "Biaxial Strengths of Welds in Heat Treated Steel Sheet," Welding Research Supplement, March (1962), p. 123.

9. Clausing, D.P., "Effect of Plastic Strain Rate in Ductility and Toughness," International Journal of Fracture Mechanics, vol. 6, (1970), p. 71-85.

10. Weiss, V., Sengupta, M. and Lal, D., "The Significance of Material Ductility to the Reliability and Load Carrying Capacity of Peak Performance Structures," Syracuse University Final Report to the Naval Air System Command, #MS-VW-1915-F-172.

11. Weiss, V., "Material Ductility and Fracture Toughness of Metals," Paper, Kyoto, Japan (1971), International Conference on Mechanical Behavior of Materials.

12. Weiss, V., Fracture - Treatise on Fracture, editor, H. Liebowitz, Academic Press, vol. 3, (1971), p. 245.

REFERENCES (CONT.)

13. Weiss, V., "Fracture Mechanics for Design and Failure Analysis," Interim Technical Report, August (1970), Submitted to U.S. Navy Air Systems Command under Contract # N00019-70-C-0044.

14. Weiss, V. and Sessler, J.G., "Analysis of the Effects of Test Temperature on the Notch Strength of High Strength Sheet Alloys," Symposium on Evaluation of Metallic Materials in Design for Low Temperature Service ASTM STP No. 302, Am. Soc. Testing Mats., (1962), p. 3.

15. Sangdahl, G.S., Aul, E.L., and Sachs, G., "An Investigation of the Stress and Strain States Occurring in Bending Rectangular Bars," Proc. Soc. Exp. Stress Analy., vol. 6, no. 1, (1941), p. 1.

16. Peterson, R.E., "Stress Concentration Design Factors," John Wiley and Sons, Inc. (1953).

17. Ogasawara, Masao, "Crack Initiation at Notches in Low Cycle Fatigue - Master's thesis, Syracuse Univeristy, June (1969).

18. 1970 Annual Book of ASTM Standards, Part 31, July, Page 911, ASTM Designation E399-70T.

19. Srawley, J.E. and Brown, W.E., Jr., "Fracture Toughness Testing Methods," ASTM, STP #410, pp. 1-129.

20. Azrin, M. and Backofen, W.A., "Deformation and Failure of a Biaxially Stretched Sheet," in Metallurgical Transactions, vol. 1, October 1970, p. 2857-2865.

21. Marciniak, Z. and Kuczniski, K., "Limit Strains in the Processes of Stretch-Forming Sheet Metal," in Journal of Mechanical Sciences, vol. 9, 1967, p. 609-620.

22. Yoder, G., Weiss, V., and Liu, H.W., "Notch Properties of Some Low and Medium Strength Constructional Steels," ASME Metals Engineering Conference, Houston, Texas, Welding Research Council Bulletin #120, p. 21-28, February (1967).

REFERENCES (CONT.)

23. Ke, J.S., and Liu, H.W., "International Journal of Fracture Mechanics," Vol. 7 (1971), p. 487.

24. Hill, R., "Mathematical Theory of Plasticity," Clarendon Press, Oxford 1950.

25. Westergaard, H.M., "Bearing Pressures and Cracks," in Transactions, American Society of Mechanical Engineers, Journal of Applied Mechanics, 1939.

26. Liu, H.W., Gavigan, W.J., and Ke, J.S., "Crack Tip Deformation in Metallic Plates Beyond General Yielding With Application to Ductile Fracture," Technical Report, Syracuse University Research Institute, Dept. of Chemical Engg. & Metallurgy, MET-HWL-123-0470 (May 1970).

TABLE I

Actual Composition of D6AC Steel

Alloying Element	Percentage
C	0.48
Mn	0.83
P	0.010
S	0.005
Si	0.28
Cu	0.15
Ni	0.58
Cr	1.06
Mo	1.01
V	0.10

TABLE II

Actual Composition of 300M Steel

Alloying Element	Percentage by weight
C	0.39
Mn	0.85
P	0.008
S	0.005
Si	1.61
Ni	1.80
Cr	0.89
Mo	0.40
V	0.08

TABLE III. FRACTURE DUCTILITIES AND FRACTURE STRAIN RATIOS AS A FUNCTION OF STRESS STATE FOR D6AC STEEL.

Longitudinal			Transverse		
Stress State (σ_2/σ_1)	Fracture Strain Ratio $(\bar{\varepsilon}_F/\bar{\varepsilon}_{TF})$	Effective Fracture Strain $(\bar{\varepsilon}_F)$	Stress State (σ_2/σ_1)	Fracture Strain Ratio $(\bar{\varepsilon}_F/\bar{\varepsilon}_{TF})$	Effective Fracture Strain $(\bar{\varepsilon}_F)$
500°F temper, 2 hours, R_c 50					
0	1.0	0.372	∞	1.0	0.30
1/2	0.55*	0.205*	2	0.68*	0.205*
	0.14	0.052		0.16	0.048
1	0.116**	0.043**	1	0.143**	0.043**
800°F temper, 2 hours, R_c 46.5					
0	1.0	0.467	∞	1.0	0.308
1/2	0.456*	0.212*	2	0.607*	0.187*
	0.180	0.082		0.20	0.063
1	0.12**	0.055**	1	0.179**	0.055**
1100°F temper, 2 hours, R_c 42.5					
0	1.0	0.557	∞	1.0	0.49
1/2	0.259*	0.144*	2	0.30*	0.148*
	0.259	0.144		0.255	0.125
1	0.169**	0.094**	1	0.192**	0.094**

* Indicates the values obtained from tensile test on Clausing specimen (Figure 3).

** Indicates the values obtained from the plunger bulge test (Figure 4).

TABLE IV. FRACTURE DUCTILITIES AND FRACTURE STRAIN RATIOS AS A FUNCTION OF STRESS STATE FOR 300M STEEL.

Longitudinal			Transverse		
Stress State (σ_2/σ_1)	Fracture Strain Ratio $(\bar{\varepsilon}_F/\bar{\varepsilon}_{TF})$	Effective Fracture Strain $(\bar{\varepsilon}_F)$	Stress State (σ_2/σ_1)	Fracture Strain Ratio $(\bar{\varepsilon}_F/\bar{\varepsilon}_{TF})$	Effective Fracture Strain $(\bar{\varepsilon}_F)$
500°F temper, 2 hours R_c 51.5					
0	1.0	0.446	∞	1.0	0.387
1/2	0.222*	0.099*	2.0	0.297*	0.115*
	0.285	0.127		0.269	0.104
1.0	0.224**	0.10**	1.0	0.258**	0.10**
800°F temper, 2 hours R_c 47.5					
0	1.0	0.412	∞	1.0	0.371
1/2	0.260*	0.107*	2.0	0.35*	0.130*
	0.192	0.079		0.213	0.079
1.0	0.199**	0.082**	1.0	0.221**	0.082**
1100°F temper, 2hours R_c 39.0					
0	1.0	0.568	∞	1.0	0.519
1/2	0.287*	0.163*	2.0	0.44*	0.23*
	0.194	0.110		0.272	0.141
1.0	0.222**	0.126**	1.0	0.243**	0.126**

* Indicates the values obtained from tensile test on Clausing specimen (Figure 3).

** Indicates the values obtained in the plunger bulge test (Figure 4).

TABLE V. HYDRAULIC BULGE TEST ($\sigma_2/\sigma_1 \approx 1$) DATA ON TWO DIFFERENT THICKNESSES OF D6AC AND 300M STEEL.

Material		Initial Thickness (t_i) inch	Final Thickness (t_f) inch	Thickness Strain $\varepsilon_3 = \ln(\frac{t_f}{t_i})$	Effective Fracture Strain $\bar{\varepsilon}_F = \varepsilon_3$
Alloy Specification	Temper and Hardness				
D6AC Steel	500°F, 2 hours R_c 50	0.0515	0.040	-0.253	0.253
	800°F, 2 hours R_c 46.5	0.0515	0.035	-0.385	0.385
	1100°F, 2 hours R_c 42.5	0.052	0.033	-0.454	0.454
300M Steel	500°F, 2 hours R_c 51.5	0.0513	0.040	-0.249	0.249
	800°F, 2 hours R_c 47.5	0.0518	0.0405	-0.247	0.247
	1100°F, 2 hours R_c 39.0	0.0515	*	*	*
D6AC Steel	500°F, 2 hours R_c 50	0.0765	*	*	*
	800°F, 2 hours R_c 46.5	0.0765	0.051	-0.405	0.405
	1100°F, 2 hours R_c 42.5	0.0765	0.045	-0.530	0.530
300M Steel	500°F, 2 hours R_c 51.5	0.0755	0.0575	-0.252	0.252
	800°F, 2 hours R_c 47.5	0.0765	*	*	*
	1100°F, 2 hours R_c 39.0	0.0765	0.046	-0.507	0.507

*Specimen did not fail at the bulge but failed around the edge of the grip.

TABLE VI

NOTCH TENSILE TEST DATA FOR D6AC STEEL

(R_c 50), Thickness=0.159±0.004"

ρ (inch)	K_t	ε_L	ε_t	ε_w	$\bar{\varepsilon}_F$	σ_{NF} ksi	ρ/t
Smooth	1.00	0.227	-0.157	-0.07	0.233	250.90	∞
		0.172	-0.122	-0.05	0.177	255.19	∞
0.650	1.54	0.035	-0.157	+0.122	0.165	320.60	4.15
0.650	1.54	0.035	-0.157	+0.122	0.165	328.95	4.0
0.110	2.8	0.04	-0.131	+0.091	0.134	336.56	0.676
0.109	2.8	0.06	-0.137	+0.077	0.138	336.56	0.668
0.028	5.2	0.131	-0.057	-0.074	0.132	246.71	0.177
0.027	5.2	0.14	-0.066	-0.074	0.140	251.62	0.173
0.010	8.3	0.168	-0.02	-0.148	0.184	152.73	0.063
0.010	8.3	0.168	-0.03	-0.138	0.185	149.10	0.063
0.0040	12.8	0.178	-0.035	-0.143	0.188	117.54	0.026
0.0028	15.0	0.113	-0.03	-0.083	0.131	101.85	0.018
0.0	length, a=0.533 in.		-0.0064			42.5	0.0
0.0	length, a=0.399 in.		-0.0065			56.0	0.0

TABLE VII

NOTCH TENSILE TEST DATA FOR D6AC STEEL

(R_c 46.5), Thickness = 0.142 $\pm$ 0.010"

ρ (inch)	K_t	ε_L	ε_t	ε_w	$\bar{\varepsilon}_F$	σ_{NF} ksi	ρ/t
Smooth	1.00	0.46	-0.39	-0.07	0.460	239.85	∞
0.655	1.5	0.049	-0.28	+0.231	0.299	273.74	4.580
0.655	1.5	0.049	-0.26	+0.211	0.277	273.55	4.943
0.110	2.8	0.118	-0.22	+0.102	0.220	258.27	0.767
0.110	2.8	0.118	-0.26	+0.142	0.259	254.71	0.769
0.029	5.2	0.135	-0.086	-0.049	0.137	221.65	0.221
0.030	5.2	0.140	-0.095	-0.045	0.140	227.30	0.228
0.010	8.3	0.170	-0.095	-0.075	0.170	160.71	0.072
0.010	8.3	0.170	-0.070	-0.100	0.170	151.72	0.069
0.0027	15.2	0.157	-0.070	-0.087	0.157	133.27	0.019
0.0027	15.2	0.157	-0.058	-0.099	0.159	145.08	0.019
0.0015	19.5	-	-0.049	-	-	112.11	0.010
0.0015	19.5	-	-0.049	-	-	110.89	0.010
Crack length, a = 0.38 in.*						102.14	

*Crack didn't form in both sides of the notch.

TABLE VIII

NOTCH TENSILE TEST DATA FOR D6AC STEEL

(R_c 42.5), Thickness = 0.145" $\pm$ 0.010"

ρ (inch)	K_t	ε_L	ε_t	ε_w	$\bar{\varepsilon}_F$	σ_{NF} ksi	ρ/t
Smooth	1.0	0.47	-0.39	-0.08	0.47	184.10	∞
0.655	1.5	0.049	-0.32	+0.271	0.345	215.8	4.281
0.655	1.5	0.049	-0.25	+0.201	0.267	215.5	4.816
0.109	2.8	0.131	-0.30	+0.169	0.305	213.76	0.799
0.109	2.8	0.128	-0.29	+0.162	0.290	214.02	0.801
0.033	5.2	0.207	-0.11	-0.097	0.207	202.84	0.229
0.033	5.2	0.0207	-0.11	-0.097	0.207	209.42	0.231
0.010	8.3	0.262	-0.095	-0.167	0.264	180.99	0.070
0.010	8.3	0.235	-0.095	-0.140	0.236	170.17	0.066
0.0027	15.2	0.255	-0.053	-0.202	0.250	129.31	0.019
0.0027	15.2	0.255	-0.04	-0.215	0.254	128.31	0.019
0.0015	19.5	-	-0.03	-	-	109.85	0.010
0.0015	19.5	-	-0.035	-	-	101.78	0.010
Crack length, a = 0.385 in.						99.51	

TABLE IX

NOTCH TENSILE TEST DATA FOR 300M STEEL

(R_c 51.5), Thickness = 0.166" $\pm$ 0.006"

ρ (inch)	K_t	ε_L	ε_t	ε_w	$\bar{\varepsilon}_F$	σ_{NF} ksi	ρ/t
Smooth	1.0	0.32	-0.25	0.07	0.32	289.37	∞
	1.0	0.36	-0.25	0.11	0.36	276.82	∞
0.655	1.5	0.049	-0.210	+0.161	0.22	304.04	4.051
0.655	1.5	0.049	-0.215	+0.166	0.225	309.47	3.975
0.110	2.8	0.12	-0.235	+0.115	0.235	320.86	0.678
0.109	2.8	0.12	-0.239	+0.119	0.239	319.91	0.661
0.030	5.2	0.135	-0.104	-0.031	0.16	223.63	0.183
0.030	5.2	0.202	-0.104	-0.098	0.202	225.09	0.183
0.010	8.3	0.236	-0.039	-0.197	0.253	185.84	0.062
0.010	8.3	0.202	-0.054	-0.148	0.209	179.00	0.060
0.0027	15.2	0.197	-0.068	-0.129	0.200	155.76	0.016
0.0027	15.2	0.197	-0.058	-0.139	0.202	153.85	0.016
0.0015	19.5	-	-0.068	-	-	143.51	0.009
0.0015	19.5	-	-0.068	-	-	138.25	0.009
Crack length, a = 0.431 in.						82.28	

TABLE X

NOTCH TENSILE TEST DATA FOR 300M STEEL

(R_c 47.5), Thickness = 0.163" $\pm$ 0.007"

ρ inch)	K_t	ε_L	ε_t	ε_w	$\bar{\varepsilon}_F$	σ_{NF} ksi	ρ/t
Smooth	1.0	0.26	-0.185	-0.075	0.26	255.07	∞
Smooth	1.0	0.27	-0.193	-0.077	0.27	253.06	∞
0.655	1.5	0.035	-0.170	+0.135	0.18	279.43	4.068
0.655	1.5	0.035	-0.160	+0.125	0.168	288.52	4.081
0.109	2.8	0.086	-0.191	+0.105	0.19	279.70	0.667
0.109	2.8	0.086	-0.182	+0.096	0.182	277.73	0.639
0.030	5.2	0.202	-0.082	-0.120	0.203	208.03	0.184
0.030	5.2	0.170	-0.070	-0.100	0.170	203.80	0.183
0.010	8.3	0.202	-0.068	-0.134	0.205	151.31	0.061
0.010	8.3	0.202	-0.077	-0.125	0.204	152.78	0.060
0.0027	15.2	-	-0.077	-	-	120.65	0.017
0.0027	15.2	0.197	-0.077	-0.120	0.199	125.61	0.017
0.0015	19.5	-	-0.05	-	-	118.32	0.010
0.0015	19.5	-	-0.05	-	-	124.62	0.009
Crack length, a = 0.410 in.						78.60	

TABLE XI

NOTCH TENSILE TEST DATA FOR 300M STEEL

(R_c 39.0), Thickness = 0.161" $\pm$ 0.005"

ρ (inch)	K_t	ε_L	ε_t	ε_w	$\bar{\varepsilon}_f$	σ_{NF} ksi	ρ/t
Smooth	1.0	0.50	-0.39	-0.11	0.50	186.90	∞
Smooth	1.0	0.48	-0.37	-0.11	0.48	172.31	∞
0.655	1.5	0.049	-0.262	+0.213	0.279	221.07	3.970
0.655	1.5	0.049	-0.280	+0.231	0.30	222.46	3.960
0.109	2.8	0.122	-0.305	+0.183	0.333	216.91	0.699
0.109	2.8	0.131	-0.347	+0.216	0.351	209.63	0.679
0.030	5.2	0.254	-0.122	-0.132	0.254	199.57	0.189
0.030	5.2	0.215	-0.104	-0.111	0.212	-	0.186
0.010	8.3	0.322	-0.086	-0.236	0.333	185.53	0.064
0.010	8.3	0.348	-0.107	-0.241	0.356	182.47	0.063
0.0027	15.2	0.357	-0.100	-0.257	0.369	177.17	0.017
0.0027	15.2	0.308	-0.129	-0.179	0.309	183.77	0.016
0.0015	19.5	-	0.053	-	-	186.07	0.009
0.0015	19.5	-	0.104	-	-	183.69	0.010
Crack length, a = 0.482 in.						163.38	
Crack length, a = 0.386 in.						178.10	

TABLE XII. FRACTURE TOUGHNESS (K_Q) VALUES OF D6AC AND 300M STEELS OBTAINED ON WOL TYPE SPECIMEN (FIGURE 8) OF AVERAGE THICKNESS 0.146 INCH.

Material		Thickness t (inch)	Width w (inch)	Crack Length a (inch)	$\frac{a}{w}$	$f(\frac{a}{w})$	P_Q (lbs)	K_Q (ksi$\sqrt{in}$)	Average K_Q (ksi$\sqrt{in}$)
Alloy and Temper	Specimen Number								
D6AC Steel (R_c 50)	1	0.146	3.203	1.6225	0.507	9.81	1110	41.67	41.78
	2	0.147	3.190	1.59 82	0.501	9.65	1140	41.88	
D6AC Steel (R_c46.5)	1	0.1465	3.185	1.6145	0.507	9.81	1515	56.83	
	2	0.146	3.182	1.6535	0.520	10.21	1360	53.31	54.79
	3	0.146	3.183	1.6355	0.514	10.02	1410	54.24	
D6AC Steel (R_c42.5)	1	0.146	3.191	1.6703	0.523	10.31	2040	80.65	
	2	0.147	3.1885	1.6221	0.509	9.864	2070	77.77	81.0
	3	0.1455	3.178	1.5840	0.498	9.545	2300	84.62	
300M Steel (R_c51.5)	1	0.1465	3.190	1.6107	0.5049	9.75	1700	63.35	
	2	0.147	3.1895	1.6073	0.5039	9.72	1740	64.42	64.28
	3	0.146	3.185	1.5963	0.5011	9.64	1760	65.06	
300M Steel (R_c47.5)	1	0.1465	3.1875	1.5958	0.5006	9.62	1670	61.40	
	2	0.1467	3.193	1.6296	0.5103	9.90	1700	64.23	63.97
	3	0.147	3.1925	1.8115	0.5674	11.92	1460	66.27	
300M Steel (R_c39.0)	1	0.1465	3.1905	1.6081	0.5040	9.72	3350	124.44	
	2	0.1467	3.1890	1.6003	0.5018	9.66	3250	119.82	120.2
	3	0.147	3.193	1.6010	0.5014	9.65	3165	116.33	

$$K_Q = \frac{P_Q}{t\sqrt{w}} f(\frac{a}{w})$$

TABLE XIII. FRACTURE TOUGHNESS (K_Q) VALUES OF D6AC STEEL OBTAINED ON WOL TYPE SPECIMEN (FIG. 8) OF AVERAGE THICKNESS 0.50 INCH

Material		Thickness t (inch)	Width w (inch)	Crack Length a (inch)	$\frac{a}{w}$	$f(\frac{a}{w})$	P_Q (lbs)	K_Q (ksi $\sqrt{in}$)	Average K_Q (ksi $\sqrt{in}$)
Alloy & Temper	Specimen Number								
D6AC Steel (R_c 50)	1	0.501	1.997	1.084	0.543	11.0	2440	37.89	37.41
	2	0.501	1.999	1.064	0.532	10.62	2480	37.18	
	3	0.500	2.000	1.074	0.537	10.78	2430	37.05	
	4	0.500	1.998	1.048	0.5245	10.36	2560	37.51	
D6AC Steel (R_c 46.5)	1	0.500	1.996	1.002	0.502	9.74	3965	54.62	54.02
	2	0.5005	1.995	1.043	0.523	10.32	3680	53.65	
	3	0.501	1.997	1.064	0.533	10.64	3570	53.62	
	4	0.501	1.997	1.042	0.522	10.28	3735	54.20	
D6AC Steel (R_c 42.5)	1	0.501	1.994	1.042	0.5225	10.30	5000	72.70	75.58
	2	0.501	1.996	1.080	0.541	10.92	5000	77.08	
	3	0.5005	1.995	1.033	0.518	10.14	5380	77.09	
	4	0.5005	1.994	1.065	0.534	10.68	5000	75.46	

$$K_Q = \frac{P_Q}{t\sqrt{w}} \cdot f\left(\frac{a}{w}\right)$$

TABLE XIV. FRACTURE TOUGHNESS (K_Q) VALUES OF 300 M STEEL OBTAINED ON WOL TYPE SPECIMEN (FIG. 8) OF AVERAGE THICKNESS 0.50 INCH

Material		Thickness t (inch)	Width w (inch)	Crack Length a (inch)	$\frac{a}{w}$	$f(\frac{a}{w})$	P_Q (lbs)	K_Q (ksi $\sqrt{in}$)	Average K_Q (ksi $\sqrt{in}$)
Alloy & Temper	Specimen Number								
300M Steel (R_c 51.5)	1	0.492	1.998	1.068	0.5345	10.70	3475	53.44	52.57
	2	0.492	2.006	1.067	0.532	10.62	3400	51.90	
	3	0.4915	2.000	1.046	0.523	10.32	3570	53.01	
	4	0.4915	1.999	1.052	0.526	10.40	3470	51.93	
300 M Steel (R_c 47.5)	1	0.492	1.995	1.017	0.510	9.90	3610	51.37	52.41
	2	0.492	1.998	1.297	0.649	16.71	2100	50.44	
	3	0.492	1.997	1.019	0.510	9.90	3750	53.36	
	4	0.492	1.994	1.030	0.5165	10.08	3760	54.48	
300 M Steel (R_c 39.0)	1	0.492	1.998	1.049	0.525	10.36	6075	90.46	87.15
	2	0.492	1.991	1.087	0.546	11.11	5600	89.43	
	3	0.492	1.996	1.060	0.531	10.58	5500	83.64	
	4	0.492	1.999	1.082	0.541	10.92	5420	85.07	

$$K_Q = \frac{P_Q}{t\sqrt{w}} \cdot f\left(\frac{a}{w}\right)$$

TABLE XV. PLANE STRAIN FRACTURE TOUGHNESS (K_{Ic}) VALUES OF D6AC STEEL OBTAINED ON WOL TYPE SPECIMEN (Fig. 8) OF AVERAGE THICKNESS 1.00 INCH

Material		Thickness t (inch)	Width w (inch)	Crack Length a (inch)	$\frac{a}{w}$	$f(\frac{a}{w})$	P_{Ic} (lbs)	K_Q (ksi $\sqrt{in}$)	Average K_Q (ksi $\sqrt{in}$)
Alloy & Temper	Specimen Number								
D6AC Steel (R_c 50)	1	1.007	1.996	1.032	0.517	10.11	4940	35.08	
	2	1.007	2.001	1.031	0.515	10.04	4830	34.05	34.48
	3	1.007	1.999	1.046	0.523	10.32	4550	32.98	
	4	1.007	1.996	1.059	0.531	10.58	4820	35.81	
D6AC Steel (R_c 46.5)	1	1.006	1.995	1.139	0.571	12.06	6300	53.47	
	2	1.006	1.995	1.116	0.559	11.60	6850	55.92	53.67
	3	1.006	1.996	1.118	0.560	11.64	6480	53.06	
	4	1.006	1.992	1.097	0.551	11.30	6565	52.24	
D6AC Steel (R_c 42.5)	1	1.008	1.999	1.105	0.553	11.38	9800	78.27	
	2	1.007	1.997	1.075	0.538	10.82	10,200	77.59	77.15
	3	1.006	2.002	1.069	0.534	10.68	10,200	76.52	
	4	1.008	1.995	1.076	0.539	10.85	10,000	76.20	

$$K_{Ic} = \frac{P_{Ic}}{t\sqrt{w}} \cdot f\left(\frac{a}{w}\right)$$

TABLE XVI. PLANE STRAIN FRACTURE TOUGHNESS (K_{Ic}) VALUES OF 300 M STEEL OBTAINED ON WOL TYPE SPECIMEN (FIG. 8) OF AVERAGE THICKNESS 1.00 INCH

Material		Thickness t (inch)	Width w (inch)	Crack Length a (inch)	$\frac{a}{w}$	$f(\frac{a}{w})$	P_{Ic} (lbs)	K_Q (ksi $\sqrt{in}$)	Average K_Q (ksi $\sqrt{in}$)
Alloy & Temper	Specimen Number								
300 M Steel (R_c 51.5)	1	1.010	1.996	1.065	0.534	10.68	6930	51.83	49.12
	2	1.010	2.001	1.092	0.546	11.11	6760	52.59	
	3	1.010	1.995	1.054	0.528	10.48	6290	46.16	
	4	1.010	2.001	1.147	0.573	12.14	5400	45.90	
300 M Steel (R_c 47.5)	1	1.010	1.988	1.088	0.547	11.15	6050	47.34	49.20
	2	1.010	1.998	1.122	0.562	11.72	6100	50.06	
	3	1.010	1.994	1.068	0.537	10.74	6620	49.85	
	4	1.010	1.995	1.081	0.542	10.96	6450	49.55	
300 M Steel (R_c 39.0)	1	1.010	1.989	1.139	0.573	12.14	9960	84.85	81.37
	2	1.010	1.996	1.123	0.563	11.87	9970	82.87	
	3	1.009	2.000	1.103	0.552	11.34	9590	76.23	
	4	1.012	1.997	1.137	0.569	11.98	9740	81.54	

$$K_{Ic} = \frac{P_{Ic}}{t\sqrt{w}} \cdot f\left(\frac{a}{w}\right)$$

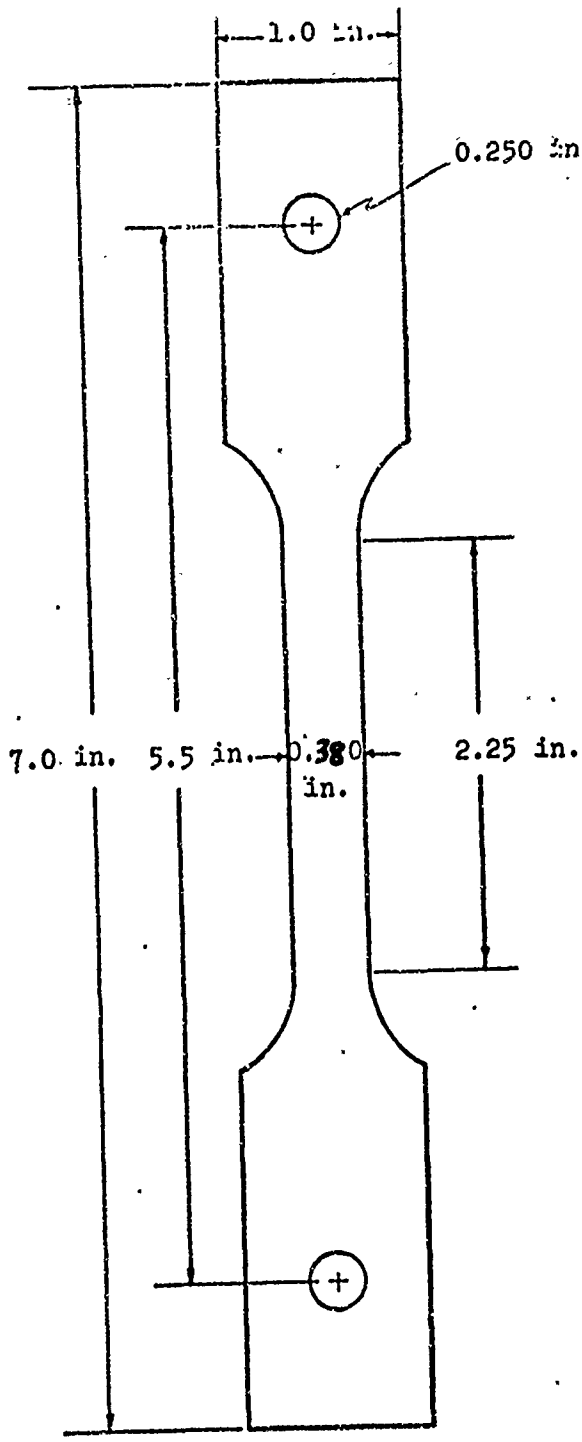

FIG. 1. UNIAXIAL TENSILE TEST SPECIMEN.

BEND TESTING

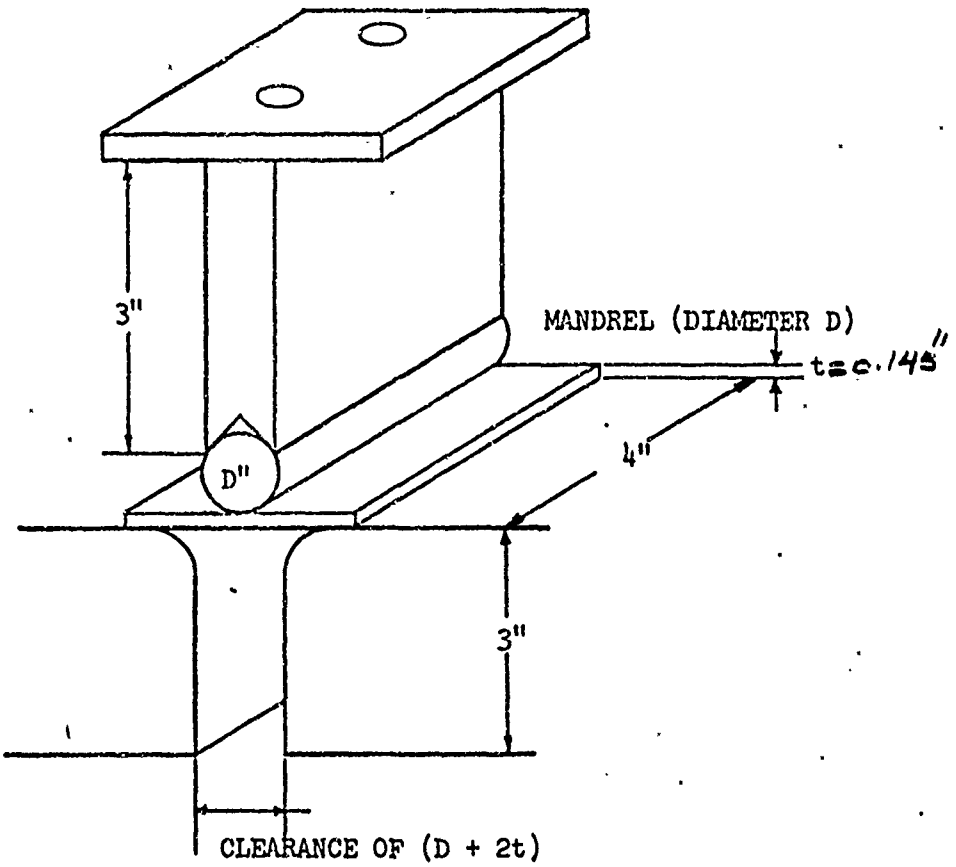

FIG. 2. EXPERIMENTAL SET-UP FOR PLANE STRAIN DUCTILITY TEST 2:1 BIAXIAL LOADING.

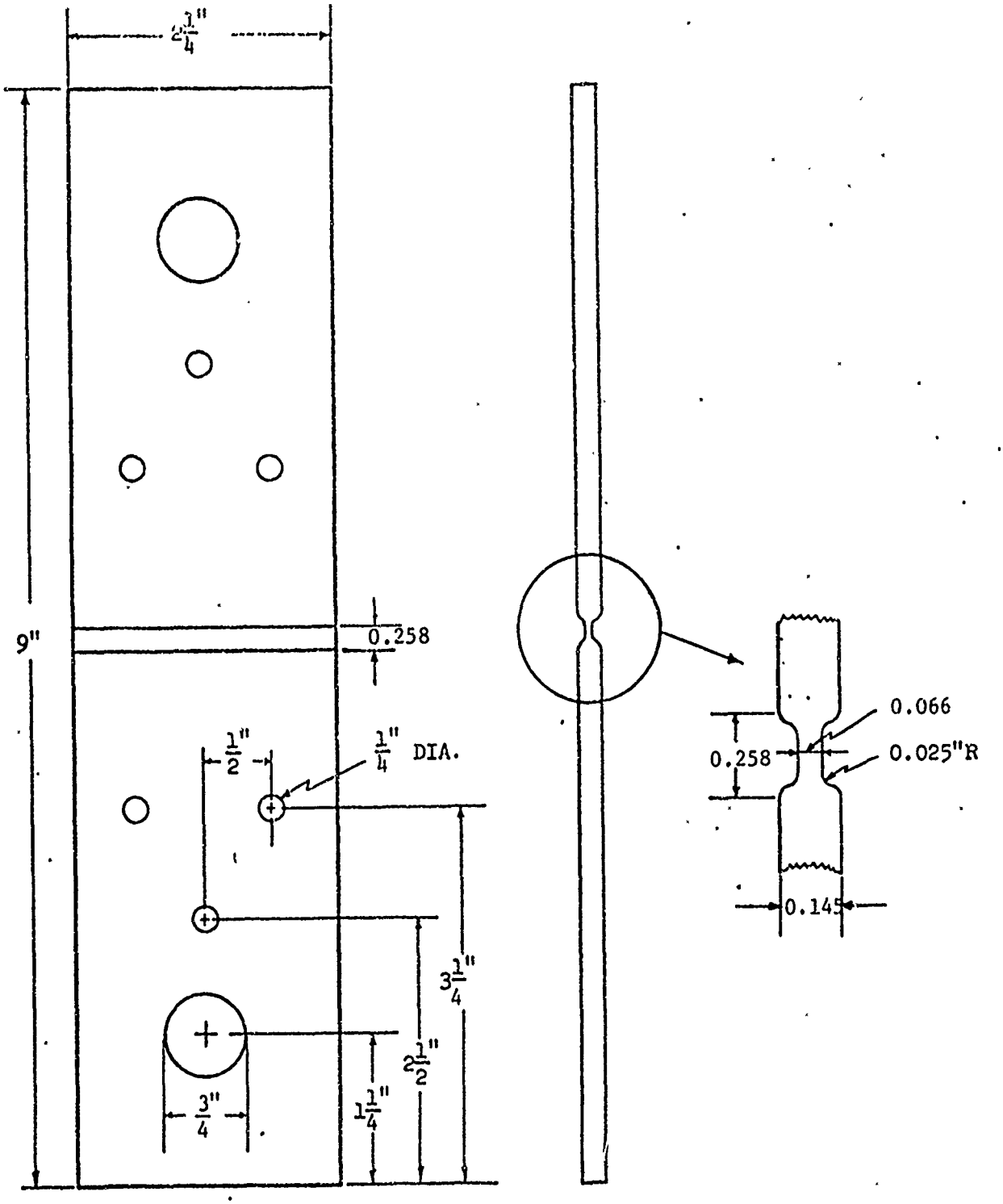

FIG. 3. PLANE STRAIN (σ_2/σ_1=2:1) TENSILE SPECIMEN DESIGN.

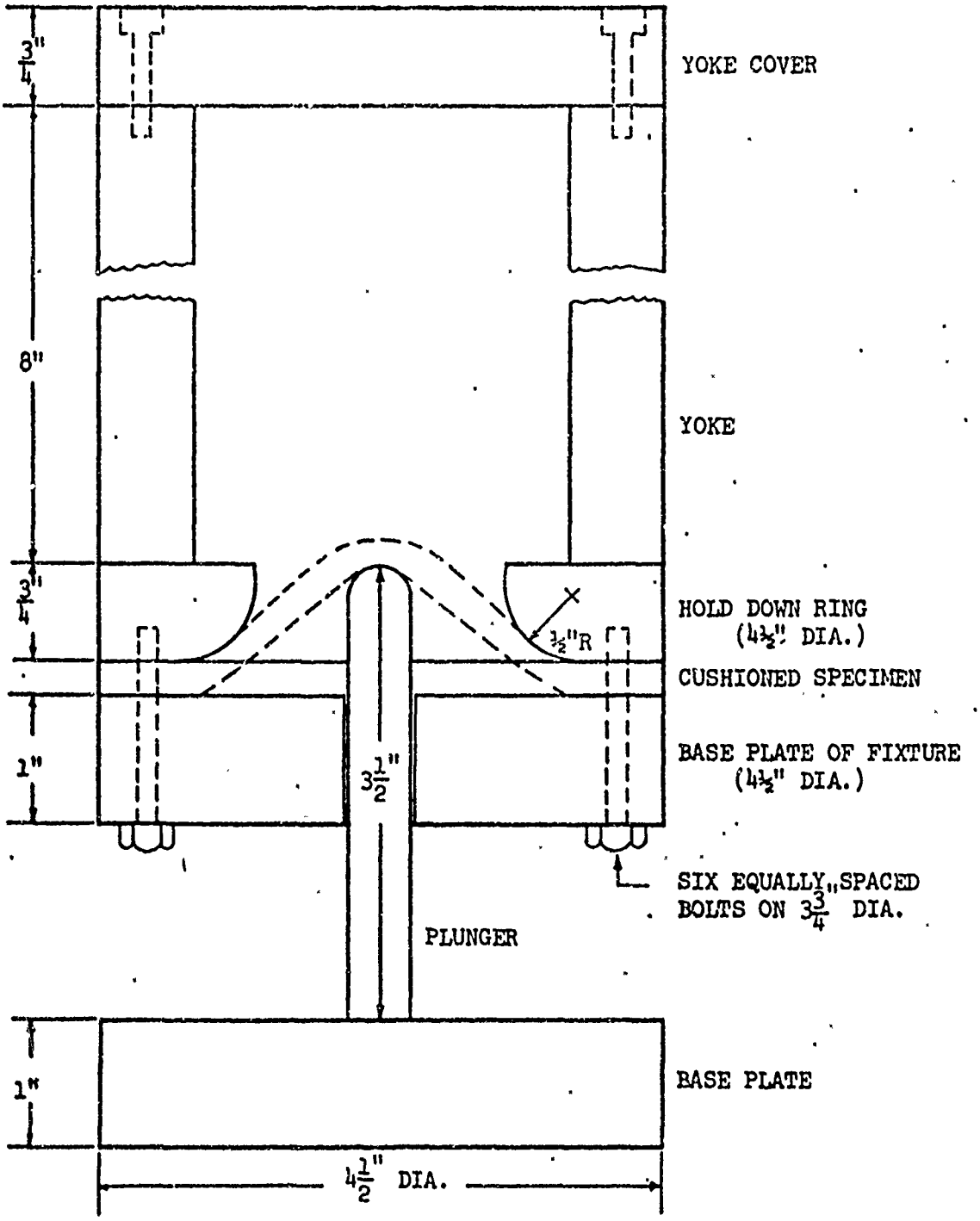

FIG. 4. MODIFIED PLUNGER BULGE TEST FIXTURE ($\sigma_2/\sigma_1 = 1$).

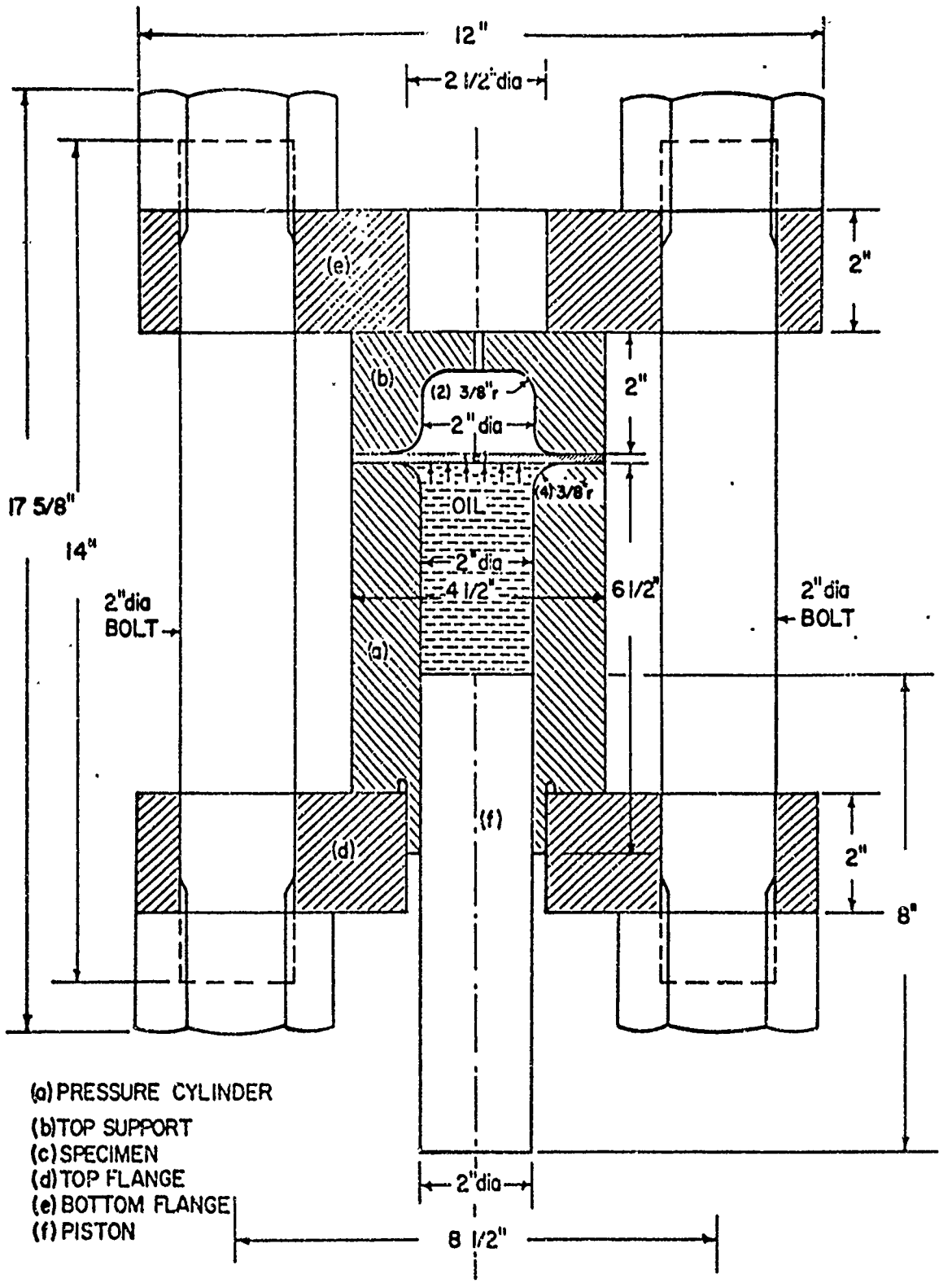

FIG. 5. HYDRAULIC BULGE FIXTURE FOR BALANCED BIAXIAL ($\sigma_2/\sigma_1 = 1$, $\sigma_3/\sigma_1 = 0$) TENSION TEST.

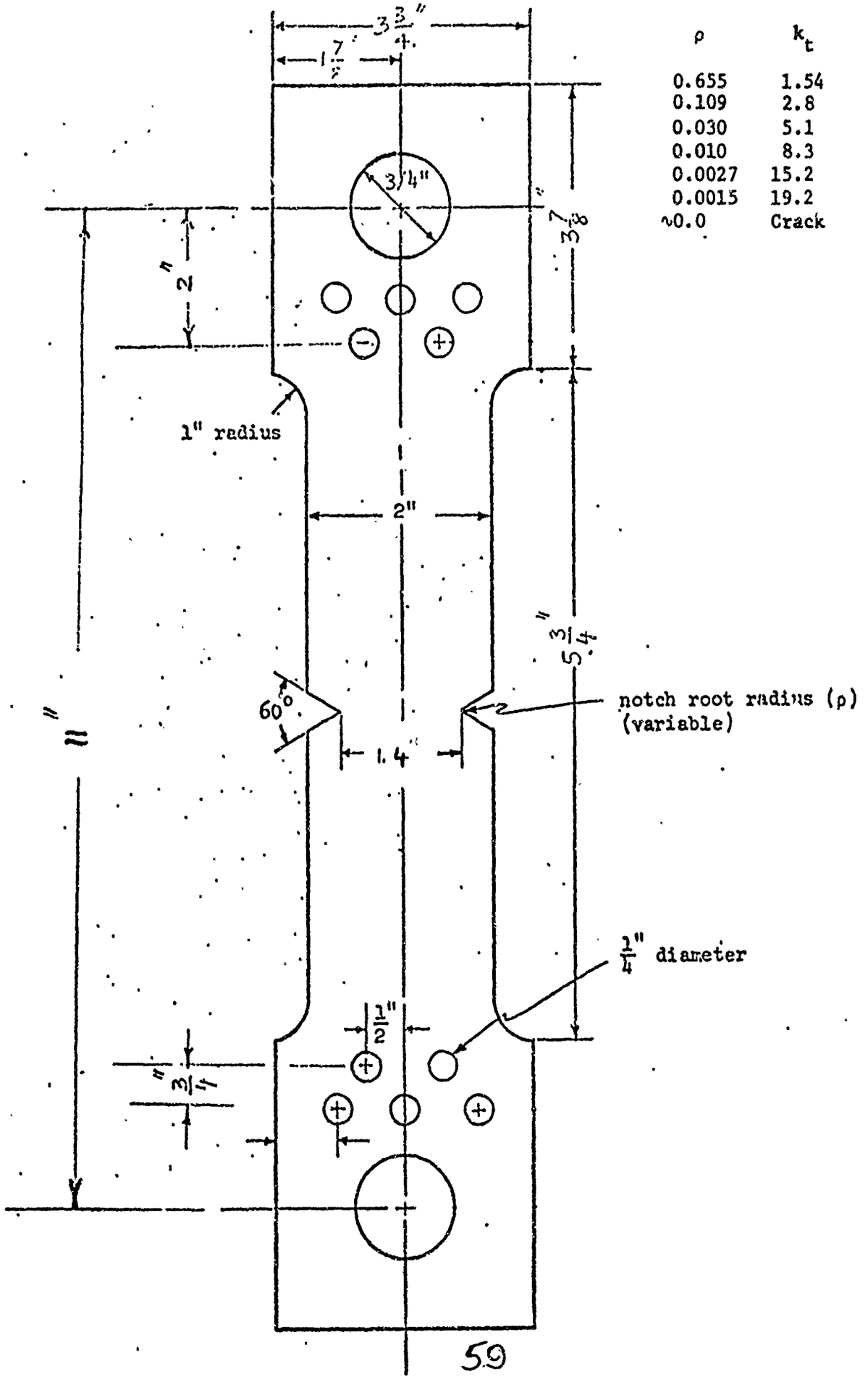

ρ	k_t
0.655	1.54
0.109	2.8
0.030	5.1
0.010	8.3
0.0027	15.2
0.0015	19.2
≈0.0	Crack

FIG. 6. NOTCH TENSILE TEST SPECIMEN.

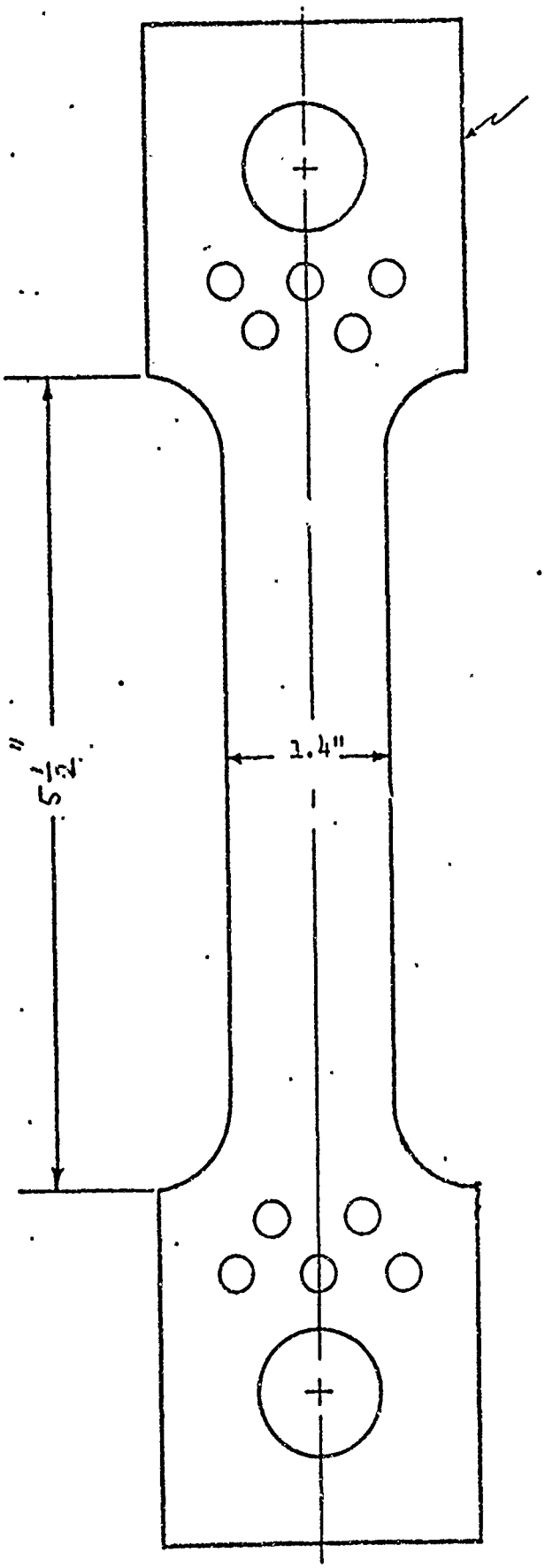

FIG. 7. . SMOOTH TENSILE SPECIMEN.

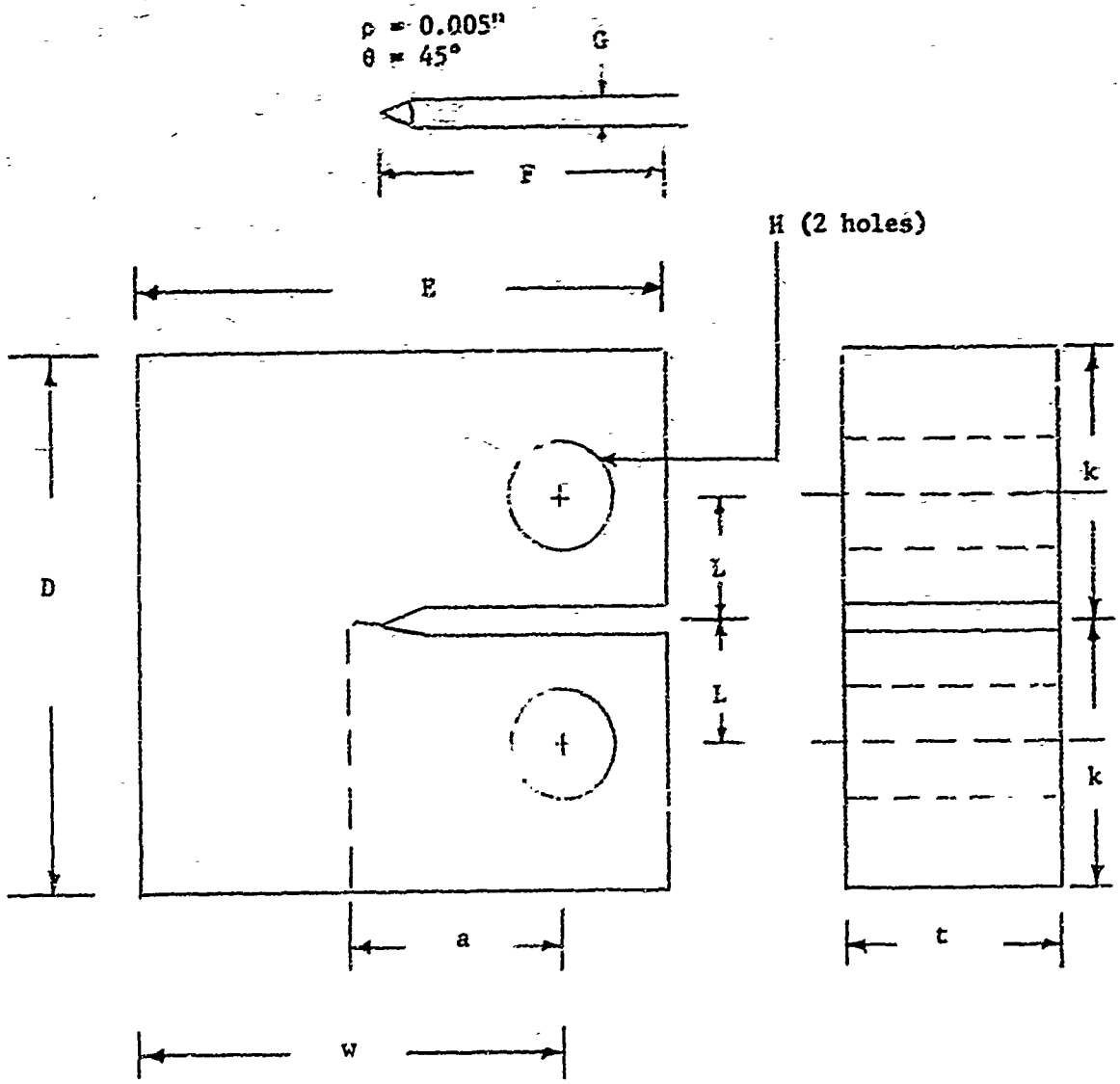

Dimensions (approx) / Thickness	w INCH	t INCH	a INCH	D INCH	E INCH	F INCH	G INCH	H INCH	K INCH	L INCH
0.150 INCH	3.2	0.150	1.6	4.0	4.0	2.075	0.125	0.750	2.0	0.875
0.50 INCH	2.0	0.50	1.0	2.5	2.5	1.3	0.062	0.500	1.25	0.55
1.00 INCH	2.0	1.0	1.0	2.5	2.5	1.3	0.062	0.500	1.25	0.55

FIGURE 8 FRACTURE TOUGHNESS SPECIMEN DESIGN

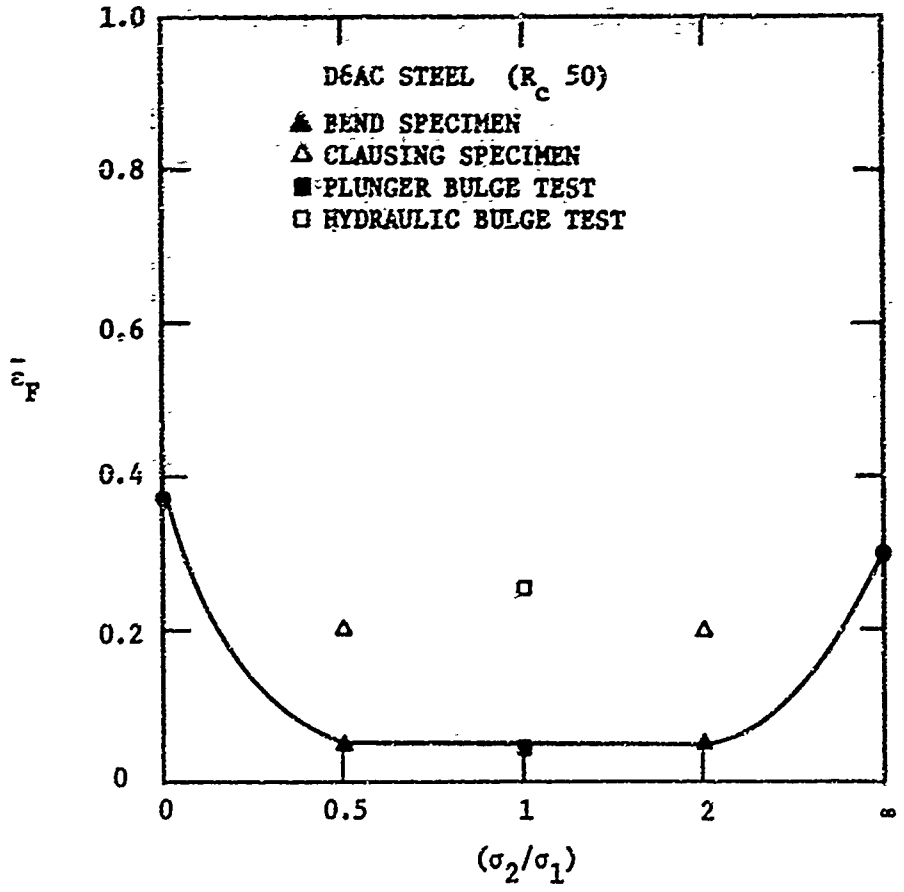

FIGURE 9 EFFECT OF STRESS STATE ON FRACTURE DUCTILITY FOR D6AC STEEL (R_c 50) SHEET (0.145" THICK).

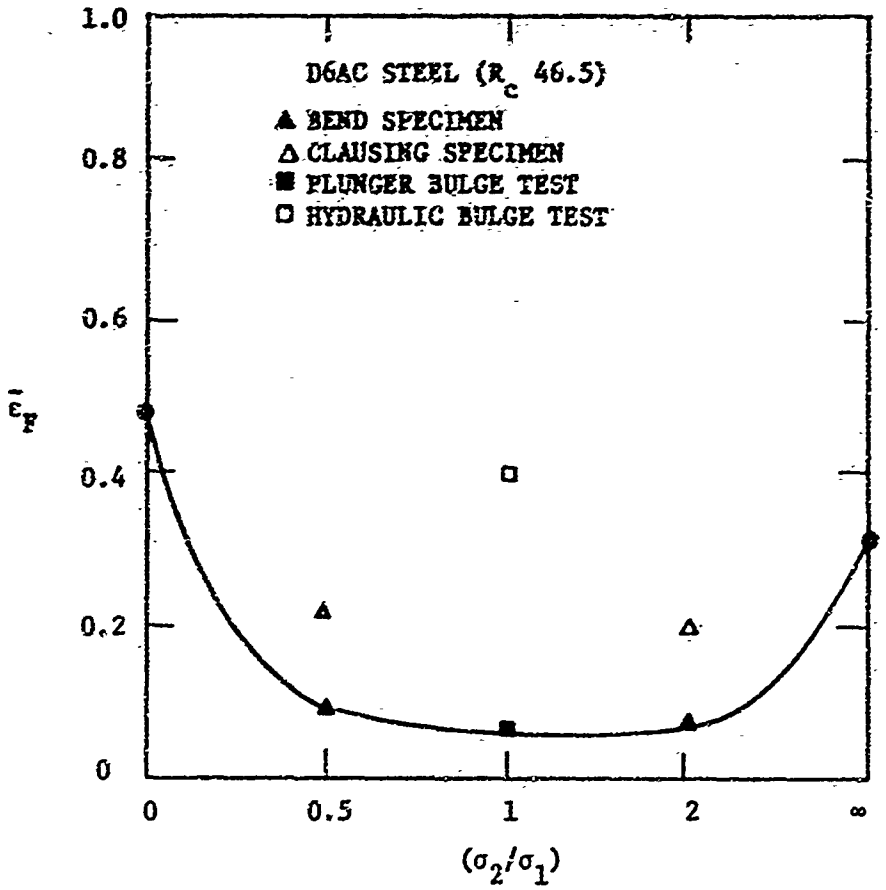

FIGURE 10 EFFECT OF STRESS STATE ON FRACTURE DUCTILITY FOR D6AC STEEL (R_c 46.5) SHEET (0.145" THICK).

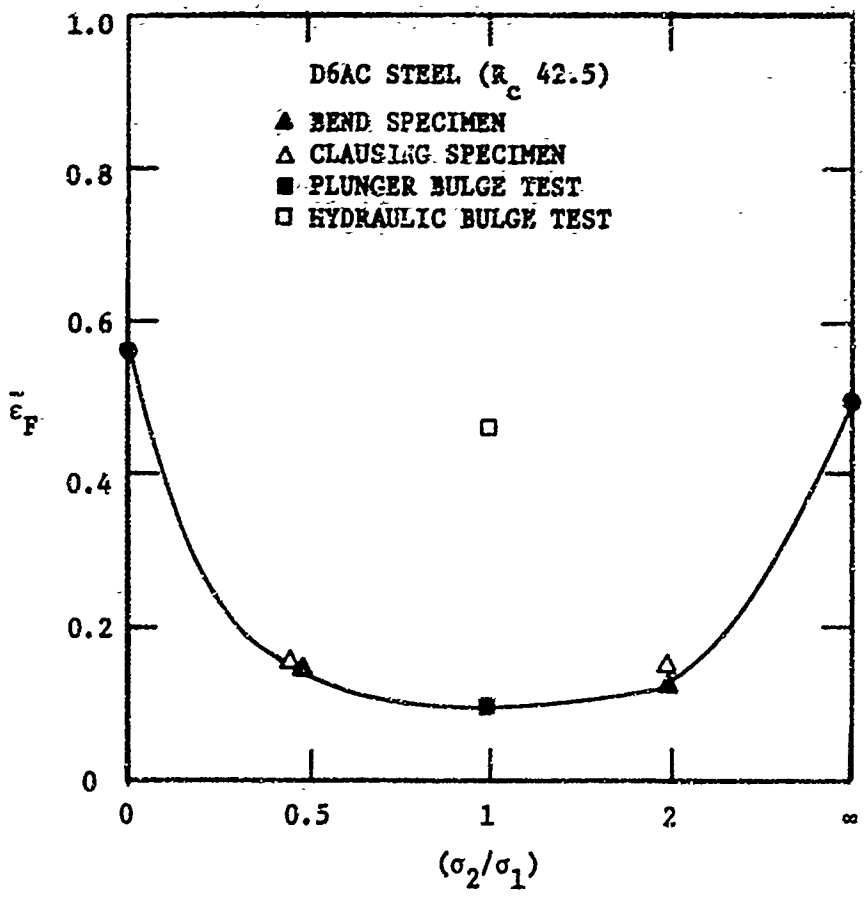

FIGURE 11 EFFECT OF STRESS STATE ON FRACTURE DUCTILITY FOR D6AC STEEL (R_c 42.5) SHEET (0.145" THICK).

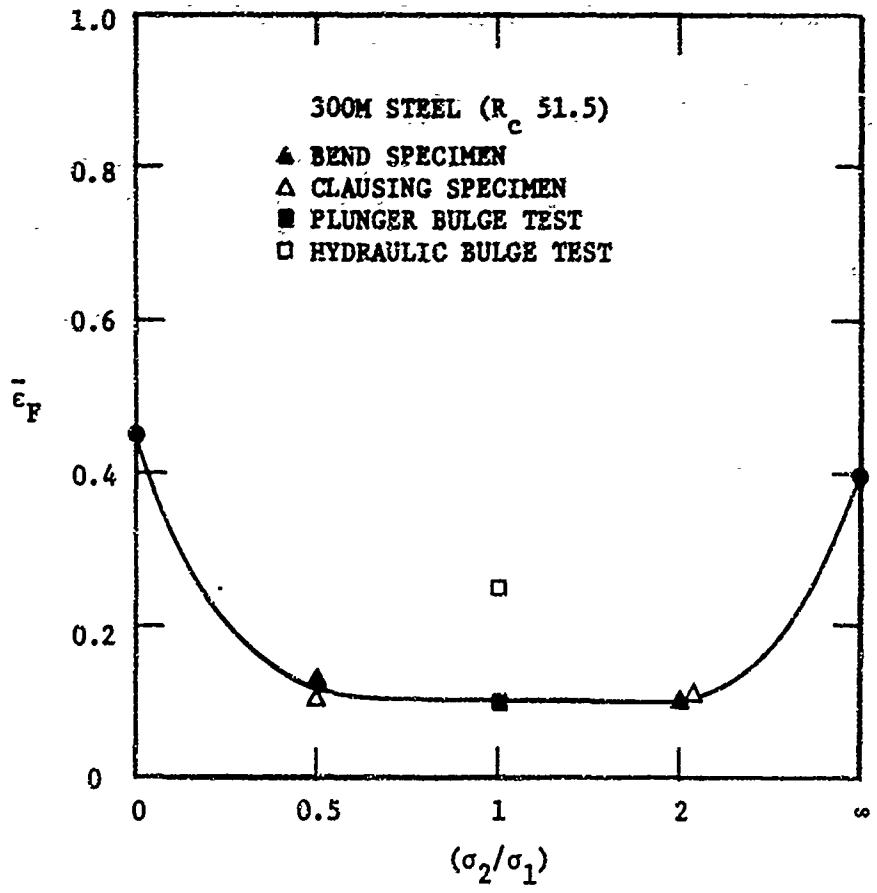

FIGURE 12 EFFECT OF STRESS STATE ON FRACTURE DUCTILITY FOR 300M STEEL (R_c 51.5) SHEET (0.145" THICK).

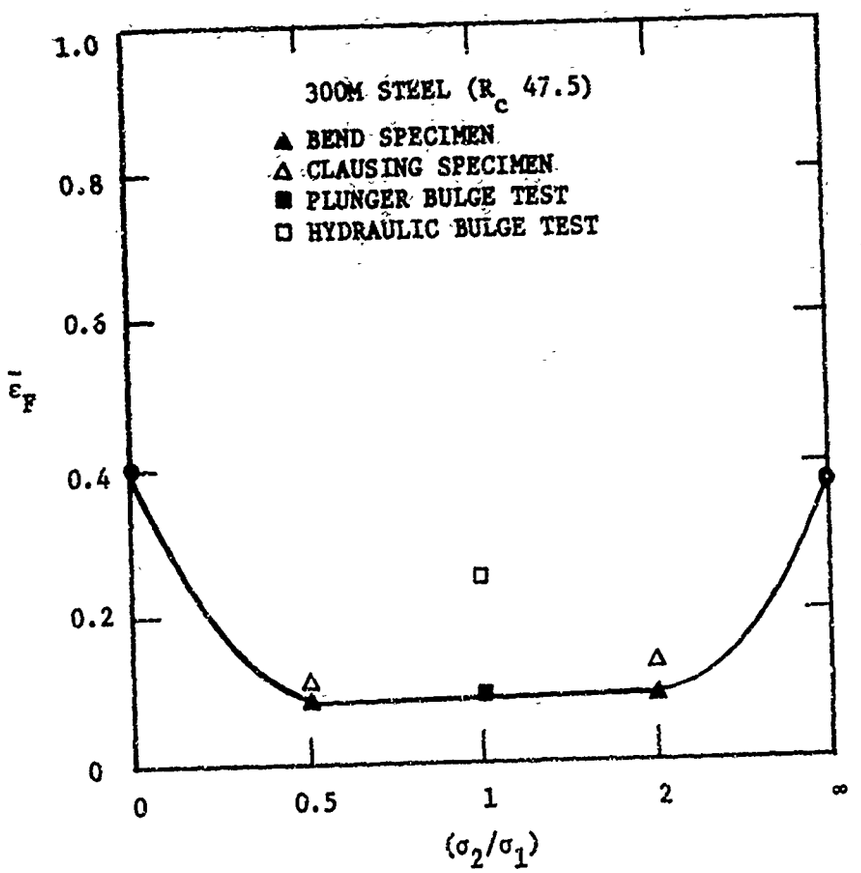

FIGURE 13 EFFECT OF STRESS STATE ON FRACTURE DUCTILITY FOR 300M STEEL (R_c 47.5) SHEET (0.145" THICK).

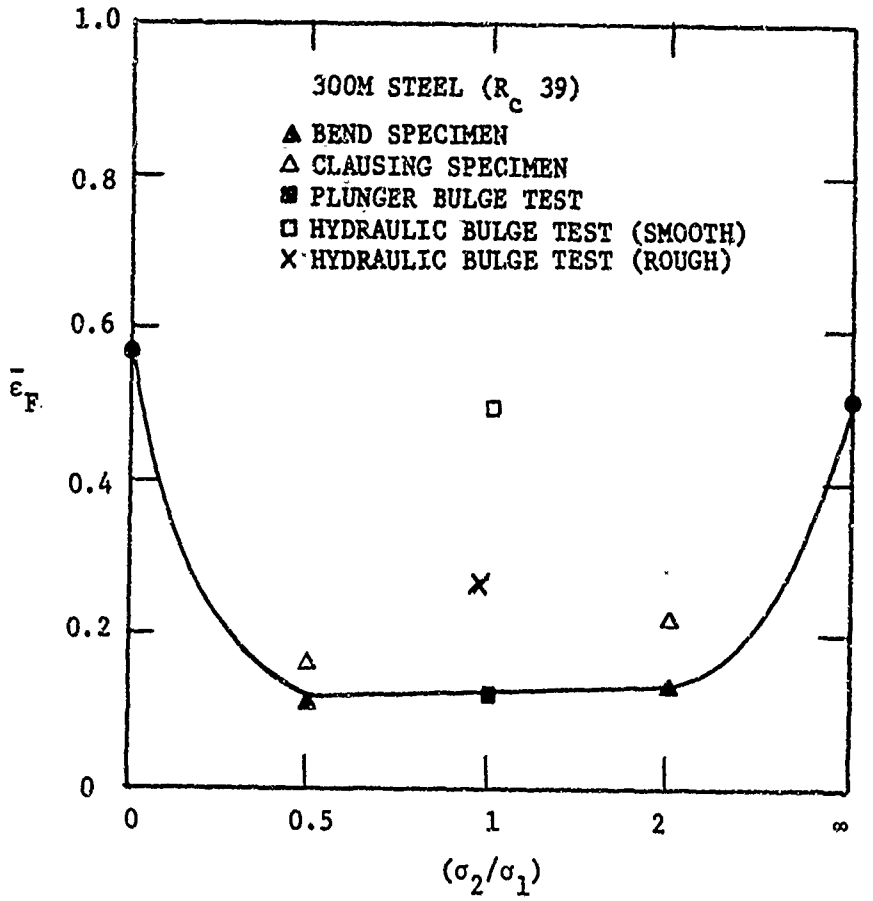

FIGURE 14 EFFECT OF STRESS STATE ON FRACTURE DUCTILITY FOR 300M STEEL (R_c 39) SHEET (0.145" THICK), SMOOTH-RMS 10 μ INCHES, ROUGH-RMS 50 μ INCHES.

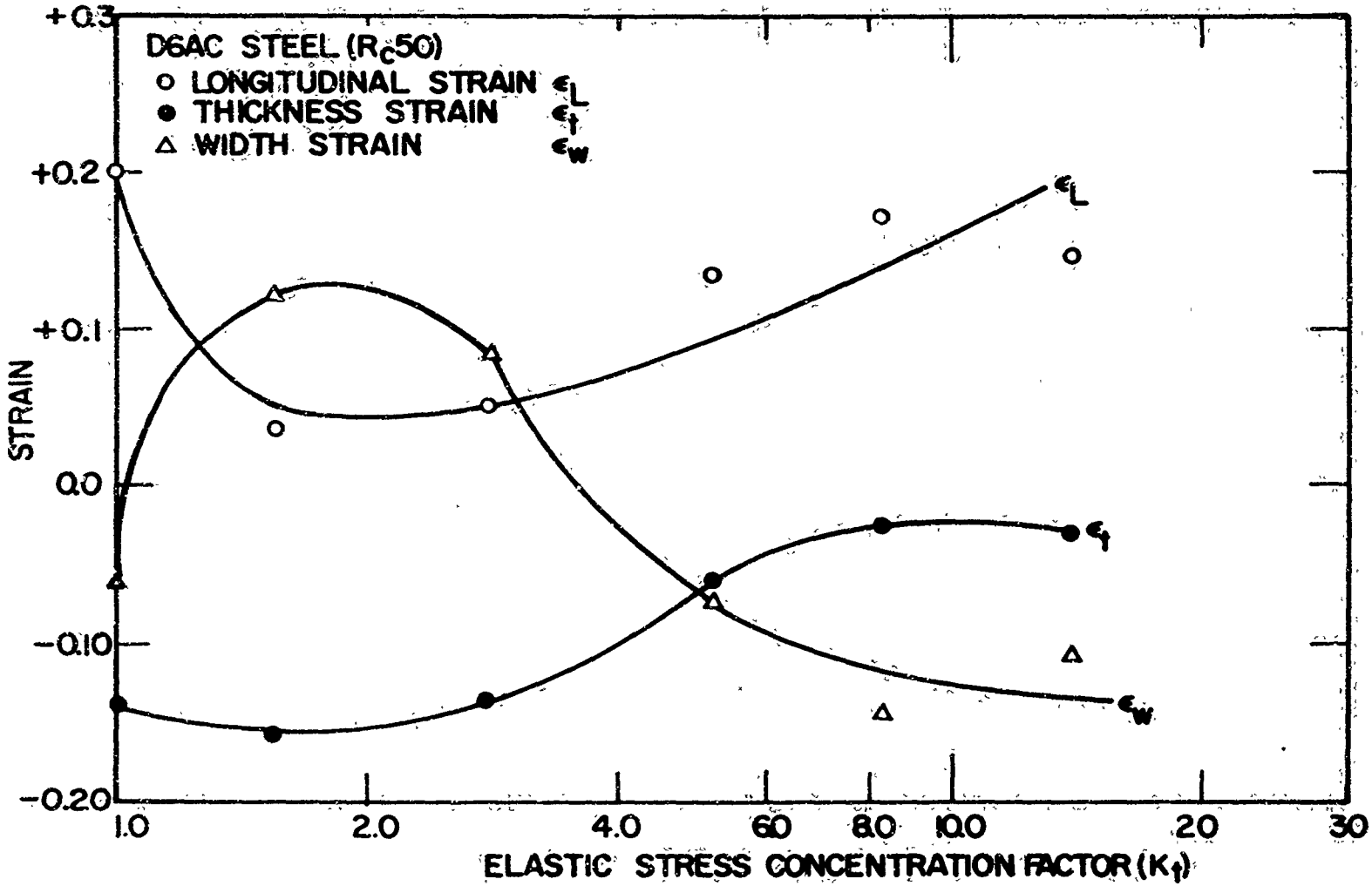

Figure 15 Fracture Strains as a Function of Elastic Stress Concentration Factor for D6AC Steel (R_c 50); thickness = 0.159 ± 0.004"

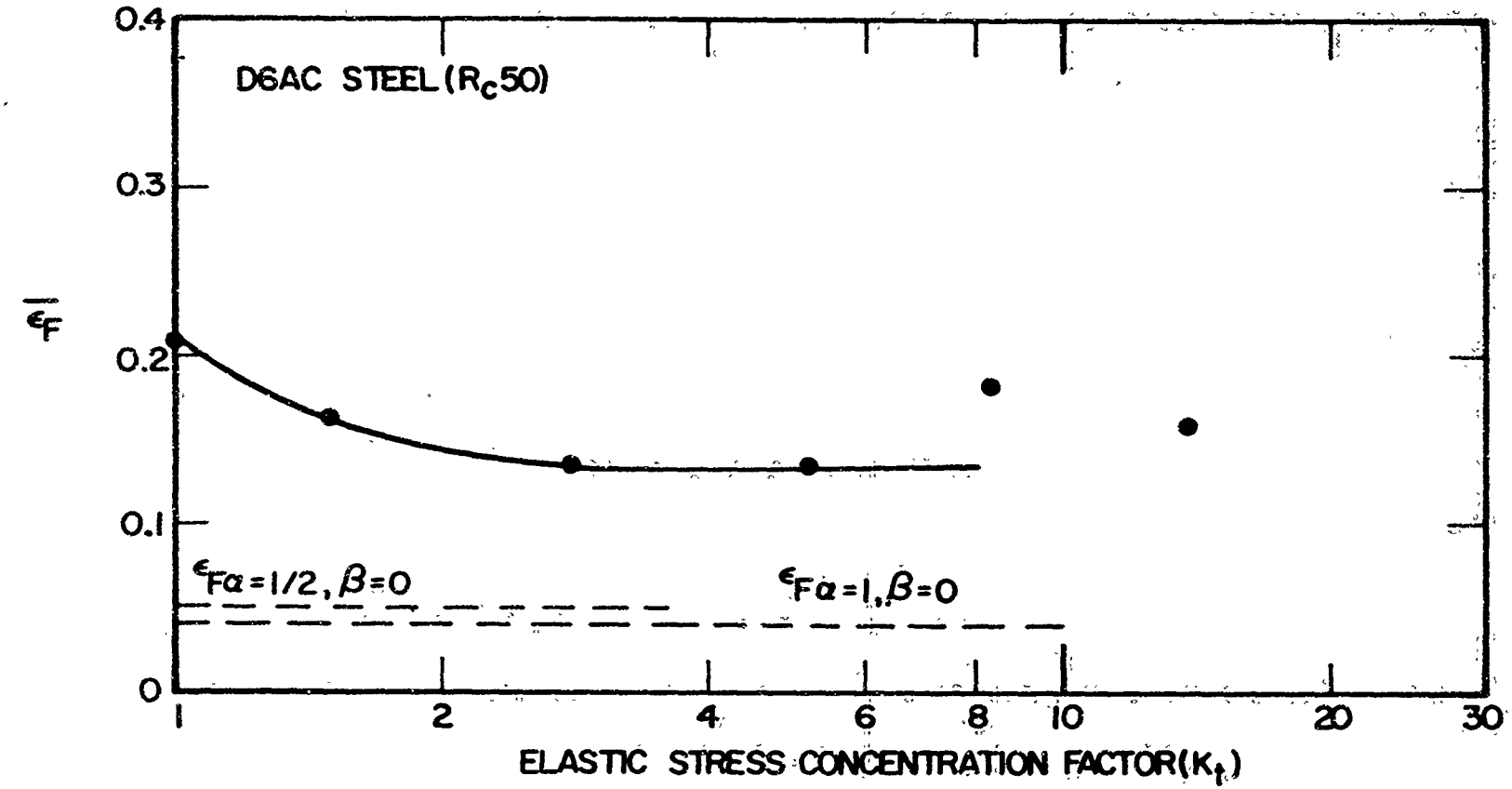

Figure 16 Effect of Initial Stress Concentration Factor on the Effective Fracture Strain for D6AC Steel (R_c 50); thickness = 0.159 ± 0.004".

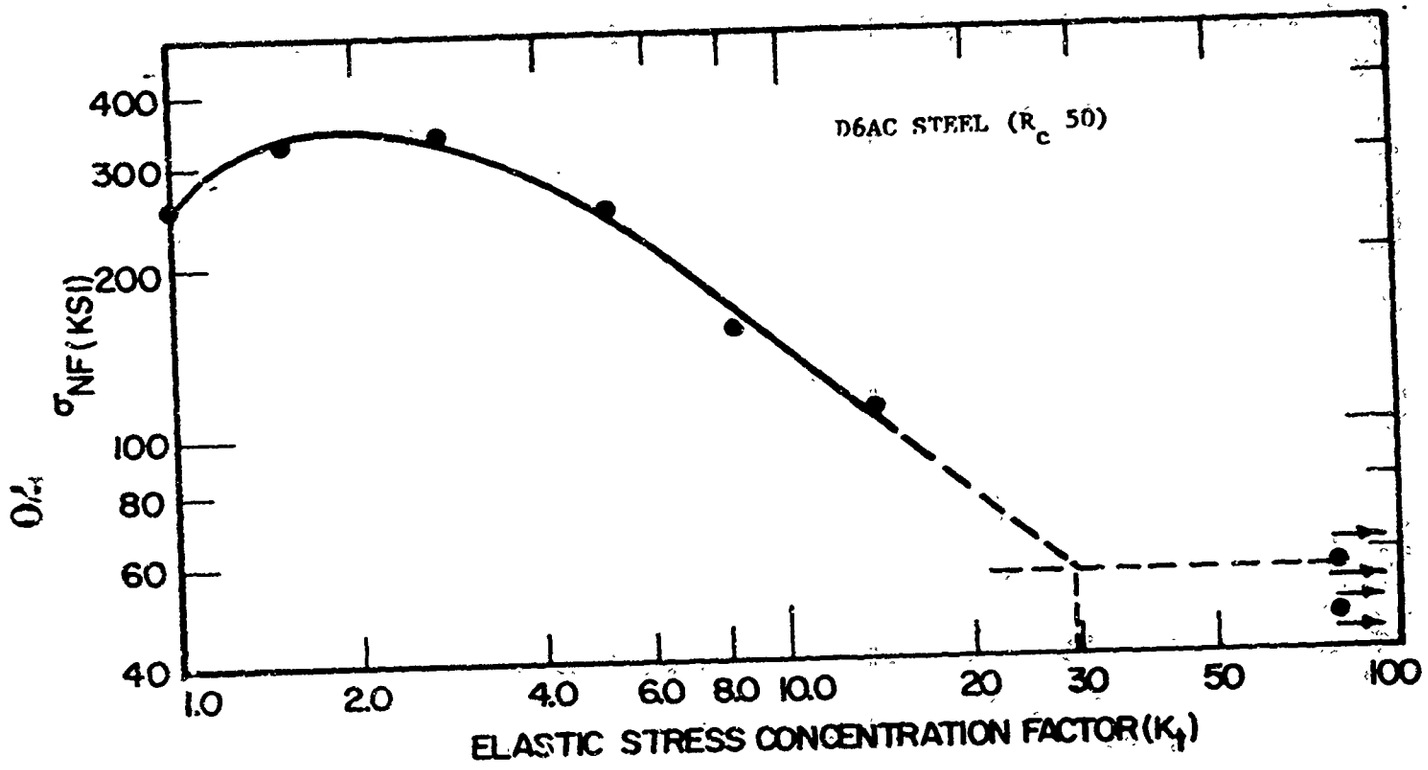

Figure 17 Effect of Initial Stress Concentration Factor on the Notch Strength for D6AC Steel (R_c 50); thickness = 0.159 ± 0.004"

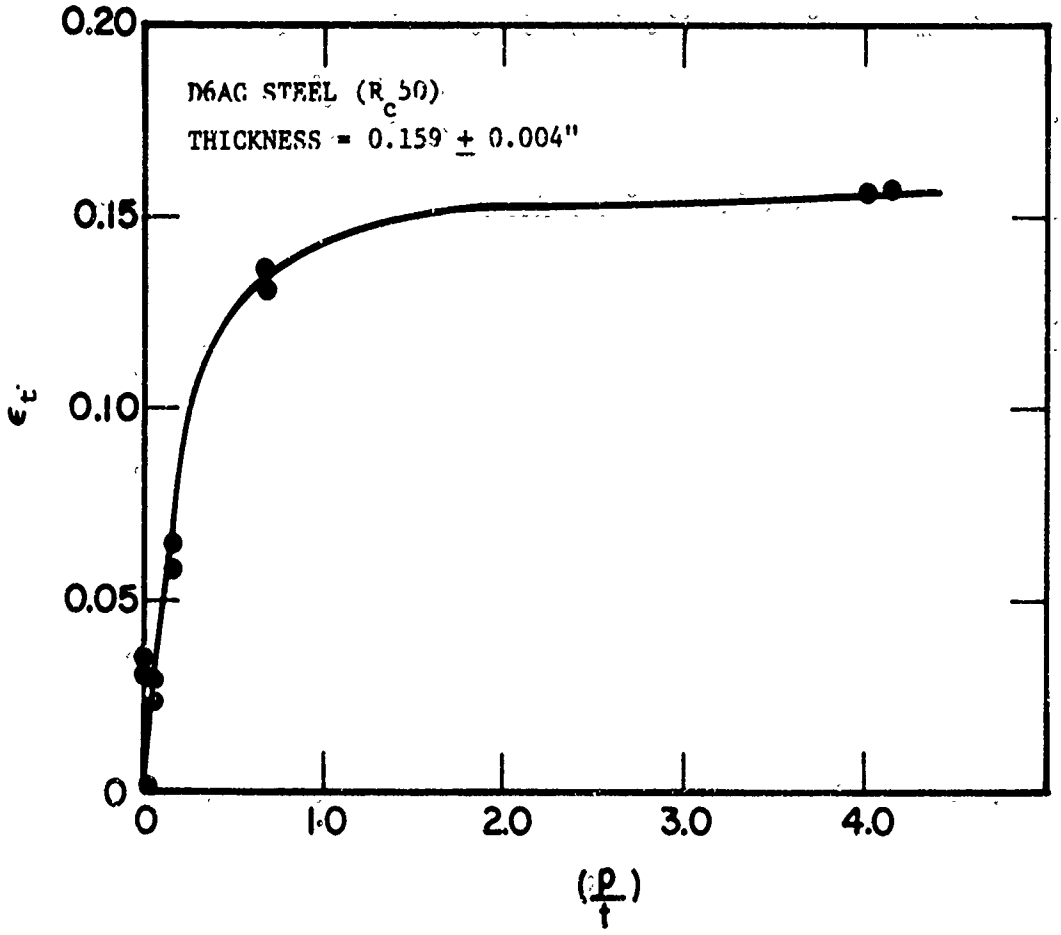

FIGURE 18 EFFECT OF ROOT RADIUS TO THICKNESS RATIO (ρ/t) ON THICKNESS STRAIN AT FRACTURE (ε_t) FOR D6AC STEEL (R_c 50).

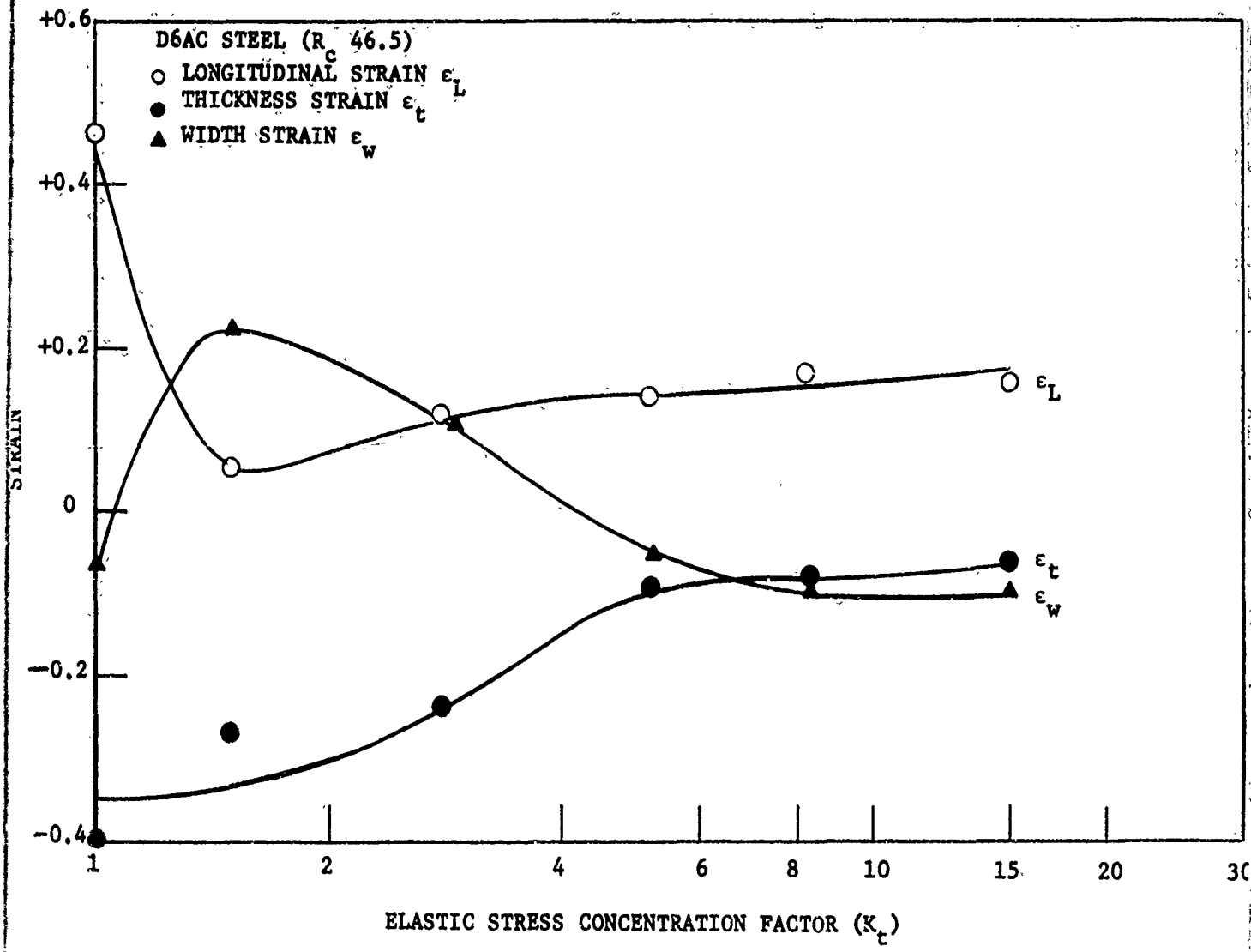

FIGURE 19 FRACTURE STRAINS AS A FUNCTION OF ELASTIC STRESS CONCENTRATION FACTOR FOR D6AC STEEL (R_c 46.5); THICKNESS = 0.142" ± 0.010".

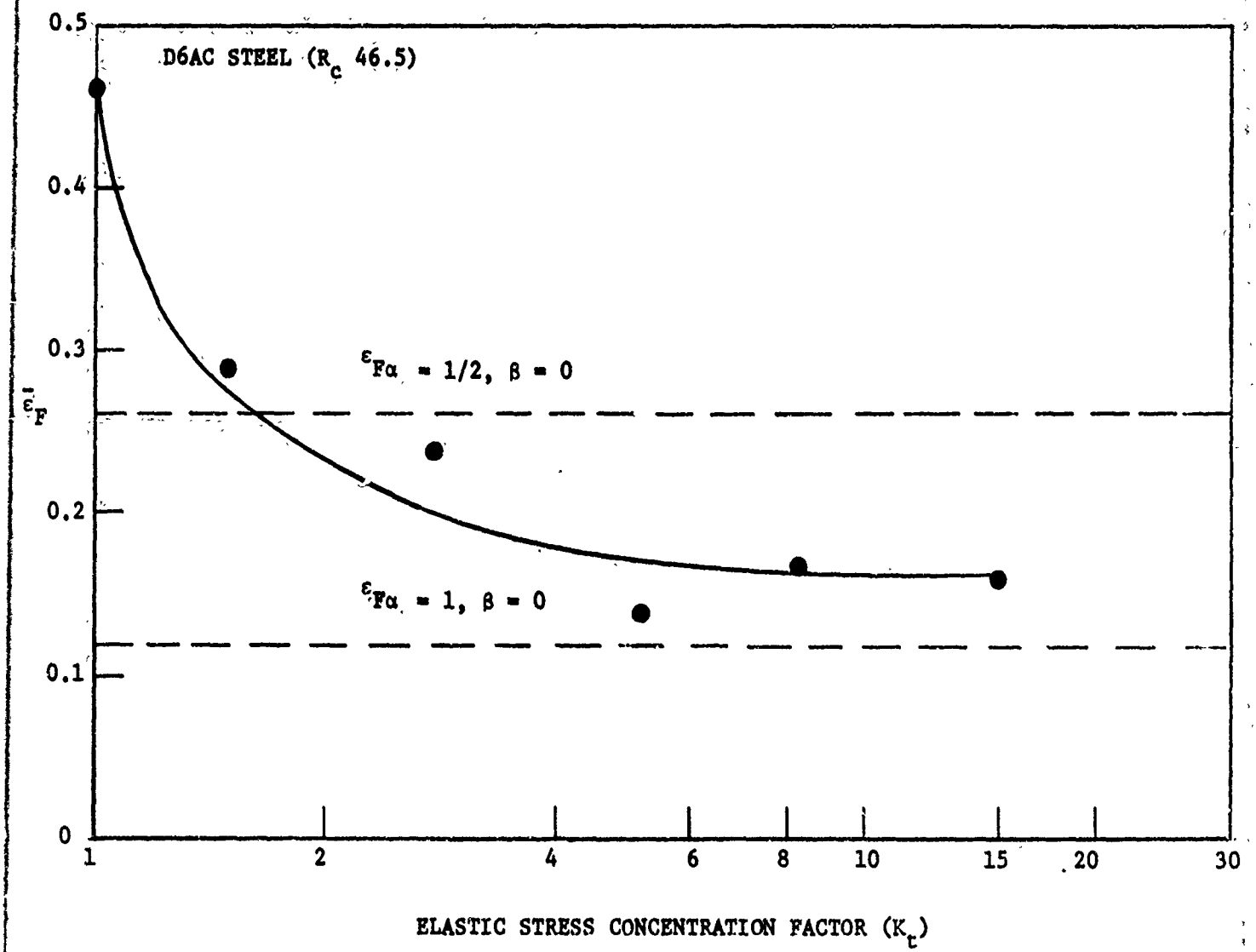

FIGURE 20 EFFECT OF INITIAL STRESS CONCENTRATION FACTOR ON THE EFFECTIVE FRACTURE STRAIN FOR D6AC STEEL (R_c 46.5); THICKNESS = 0.142" ± 0.010".

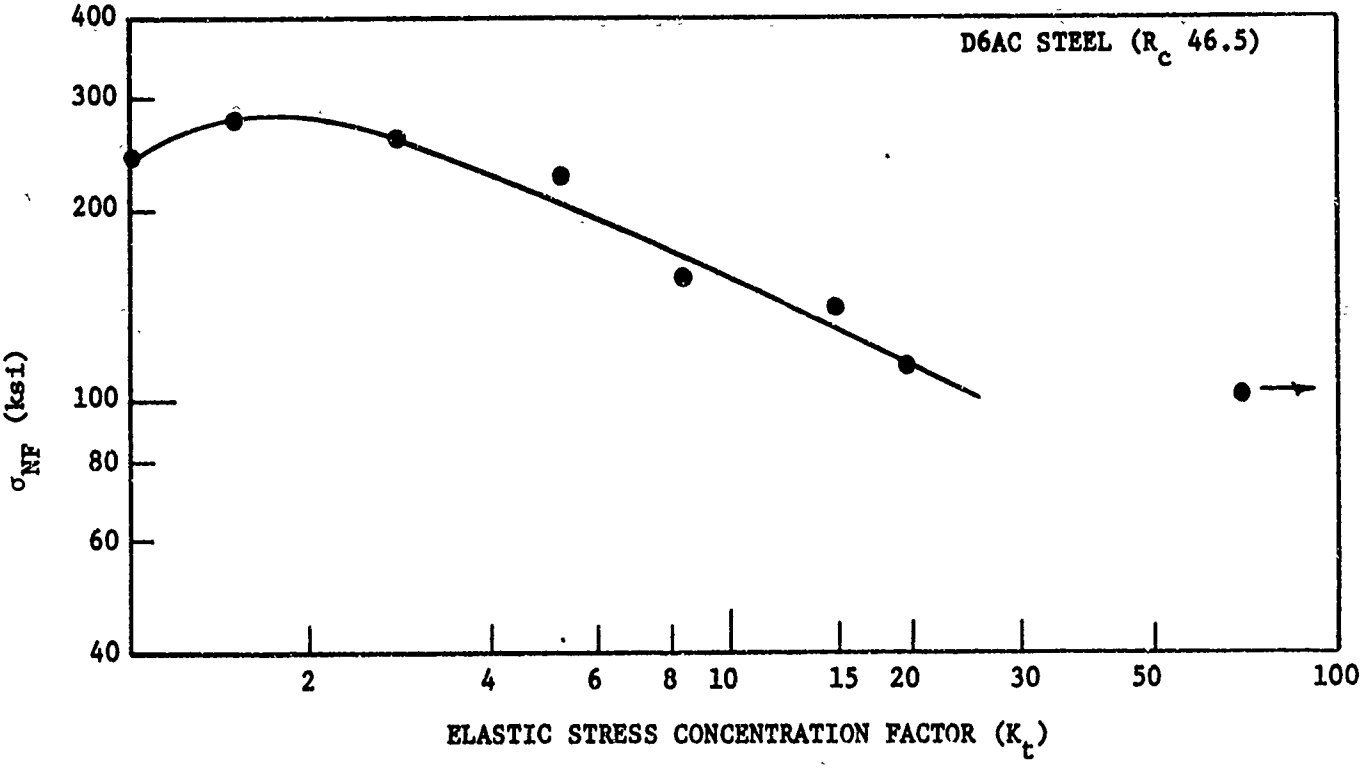

FIGURE 21 EFFECT OF INITIAL STRESS CONCENTRATION FACTOR ON THE NOTCH STRENGTH FOR D6AC STEEL (R_c 46.5); THICKNESS = 0.142" ± 0.010".

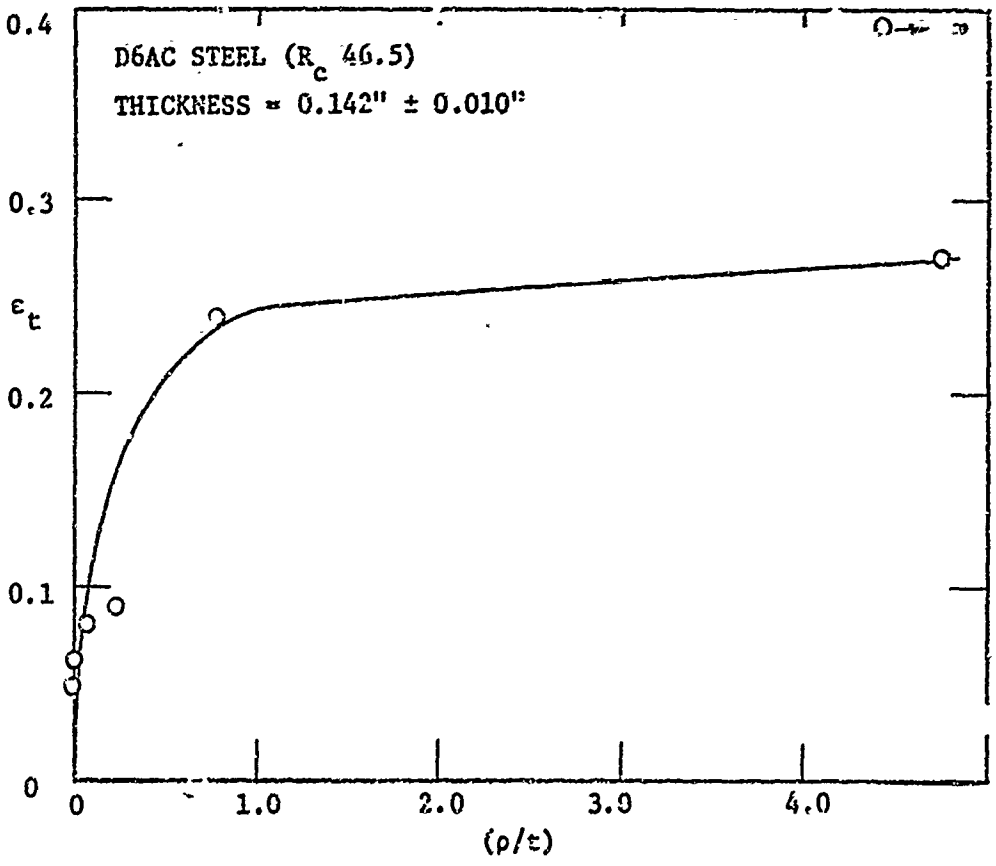

FIGURE 22 EFFECT OF ROOT RADIUS TO THICKNESS RATIO (ρ/t) ON THICKNESS STRAIN (ε_t) AT FRACTURE FOR D6AC STEEL (R_c 46.5).

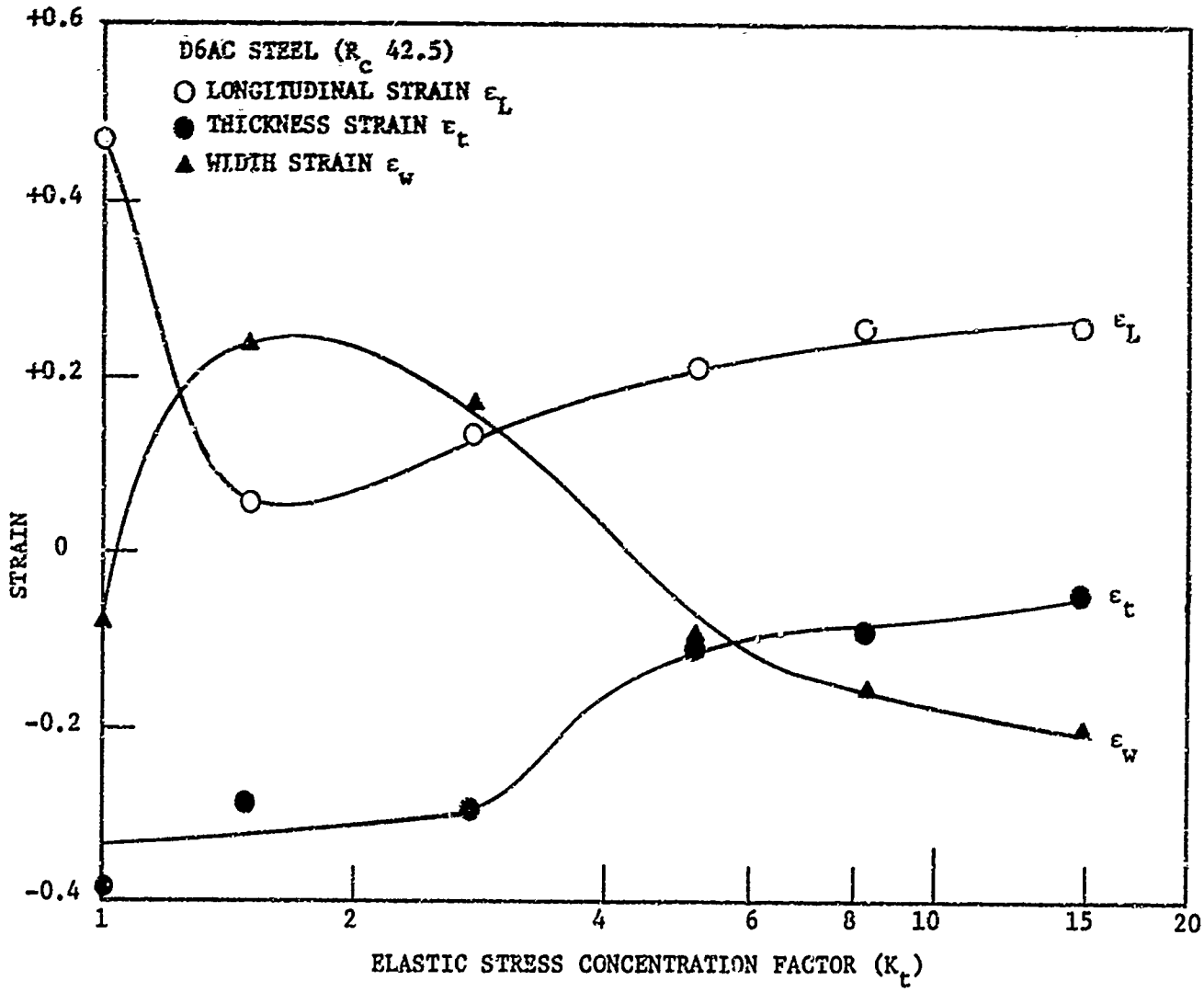

FIGURE 23 FRACTURE STRAINS AS A FUNCTION OF ELASTIC STRESS CONCENTRATION FACTOR FOR D6AC STEEL (R_c 42.5); THICKNESS = 0.145" ± 0.010".

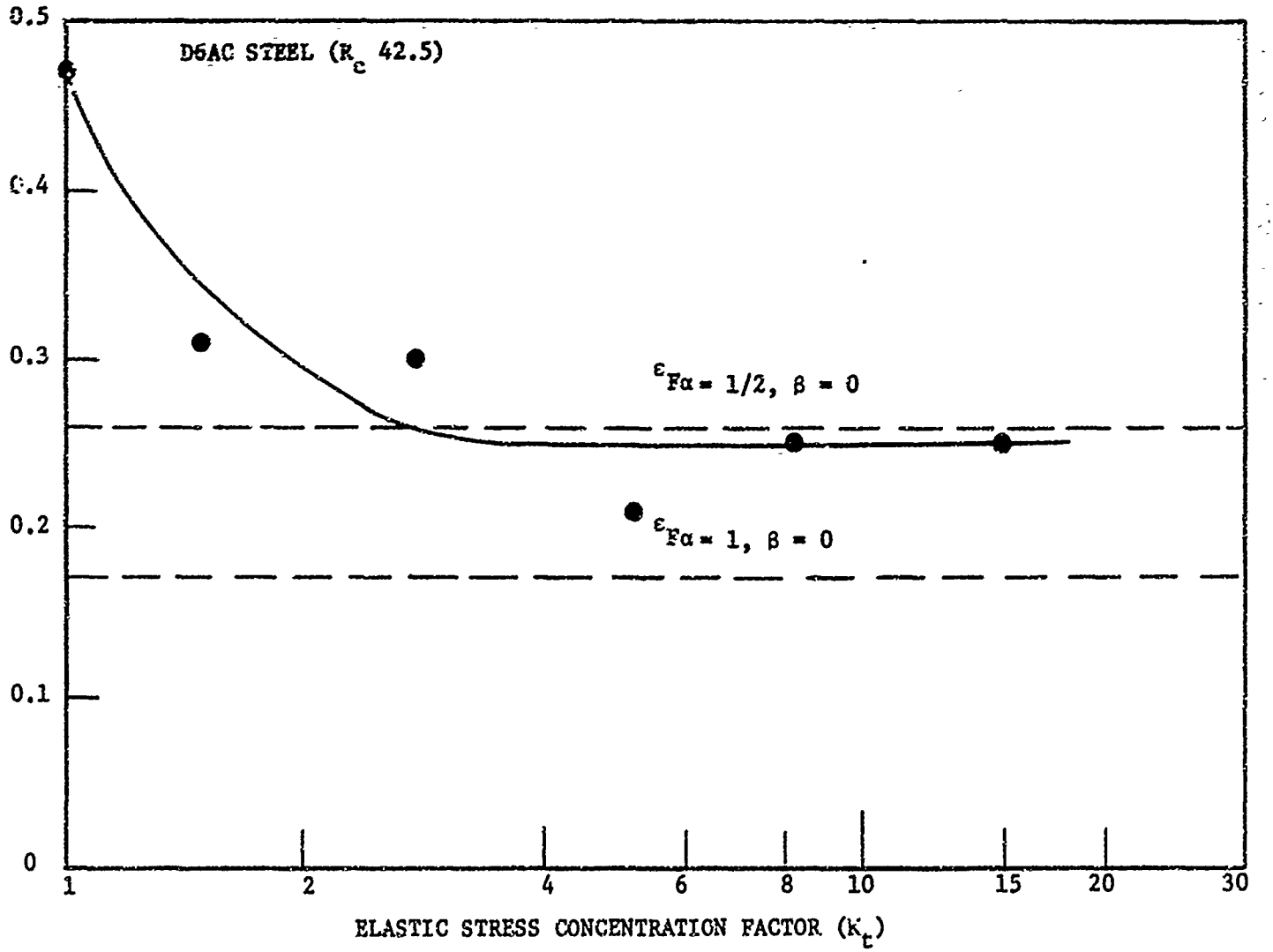

FIGURE 24 EFFECT OF INITIAL STRESS CONCENTRATION FACTOR ON THE EFFECTIVE FRACTURE STRAIN FOR D6AC STEEL (R_c 42.5); THICKNESS = 0.145 ± 0.010".

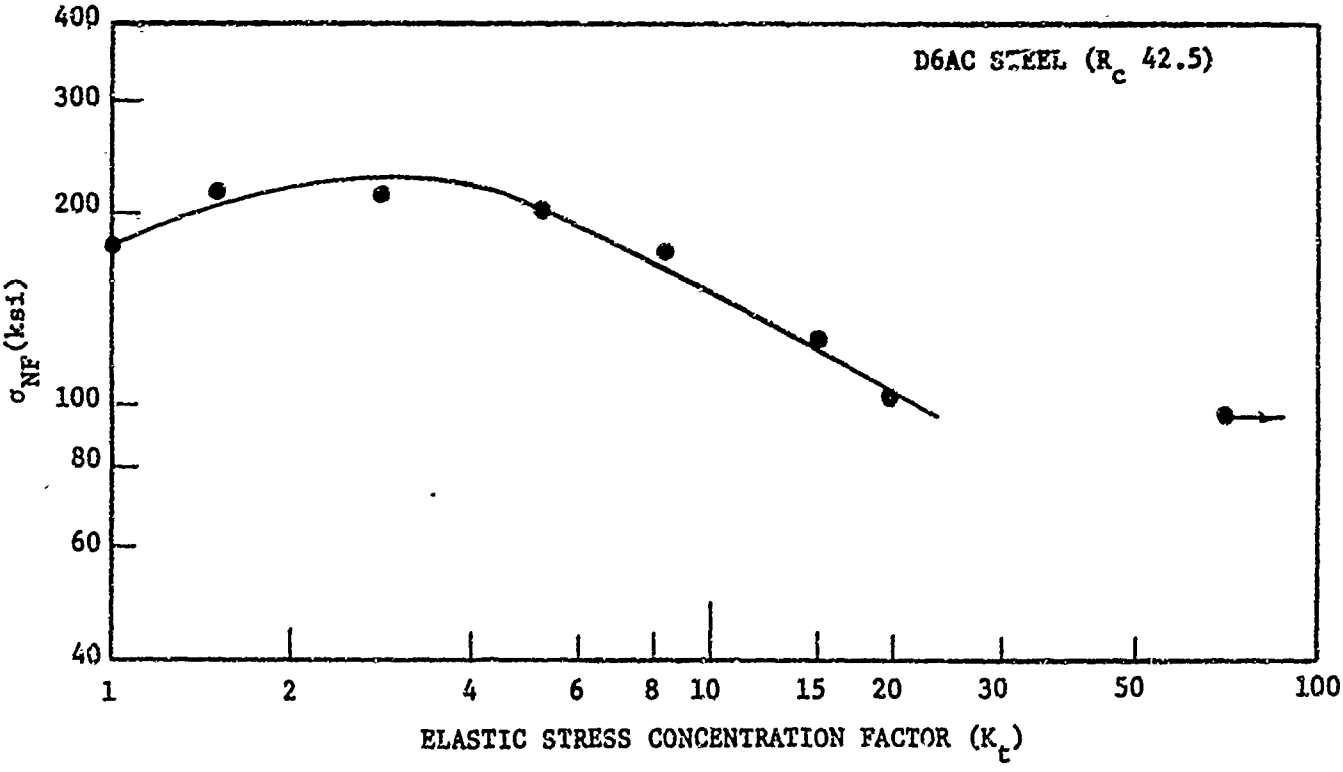

FIGURE 25 EFFECT OF INITIAL STRESS CONCENTRATION FACTOR ON THE NOTCH STRENGTH FOR D6AC STEEL (R_c 42.5); THICKNESS = 0.145 ± 0.010".

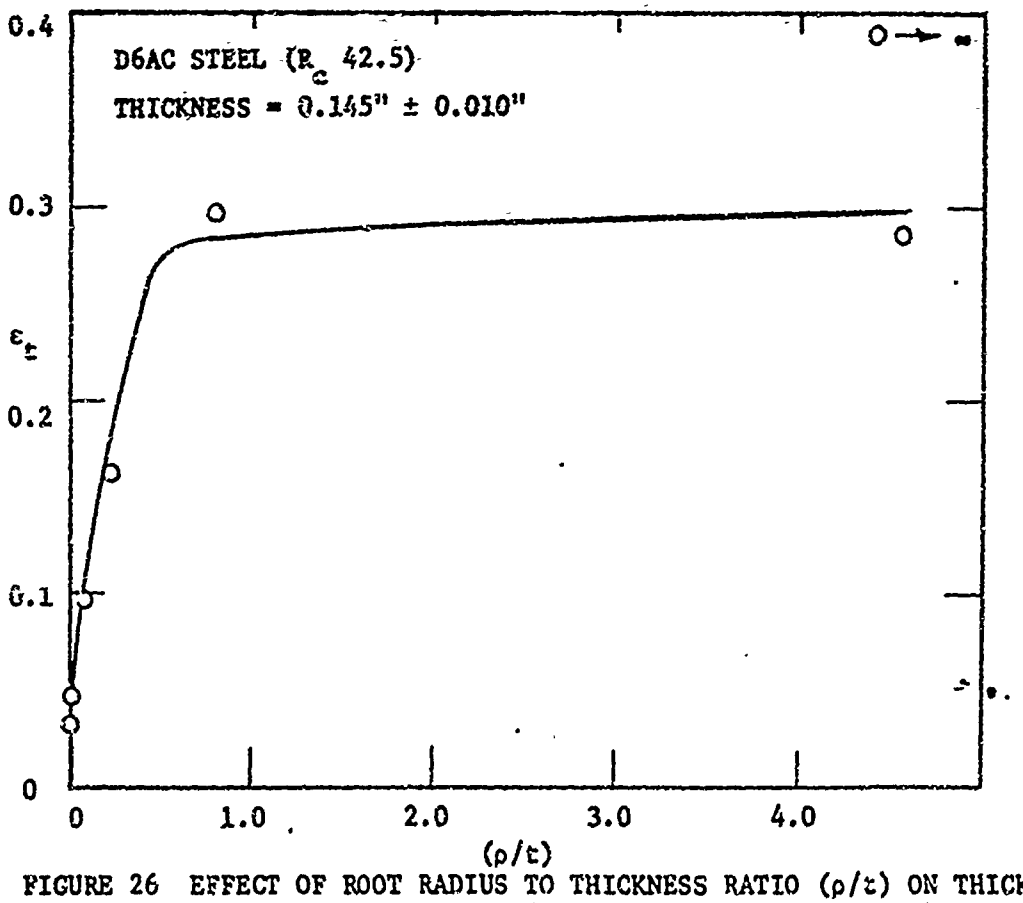

FIGURE 26 EFFECT OF ROOT RADIUS TO THICKNESS RATIO (ρ/t) ON THICKNESS STRAIN AT FRACTURE (ε_t) FOR D6AC STEEL (R_c 42.5).

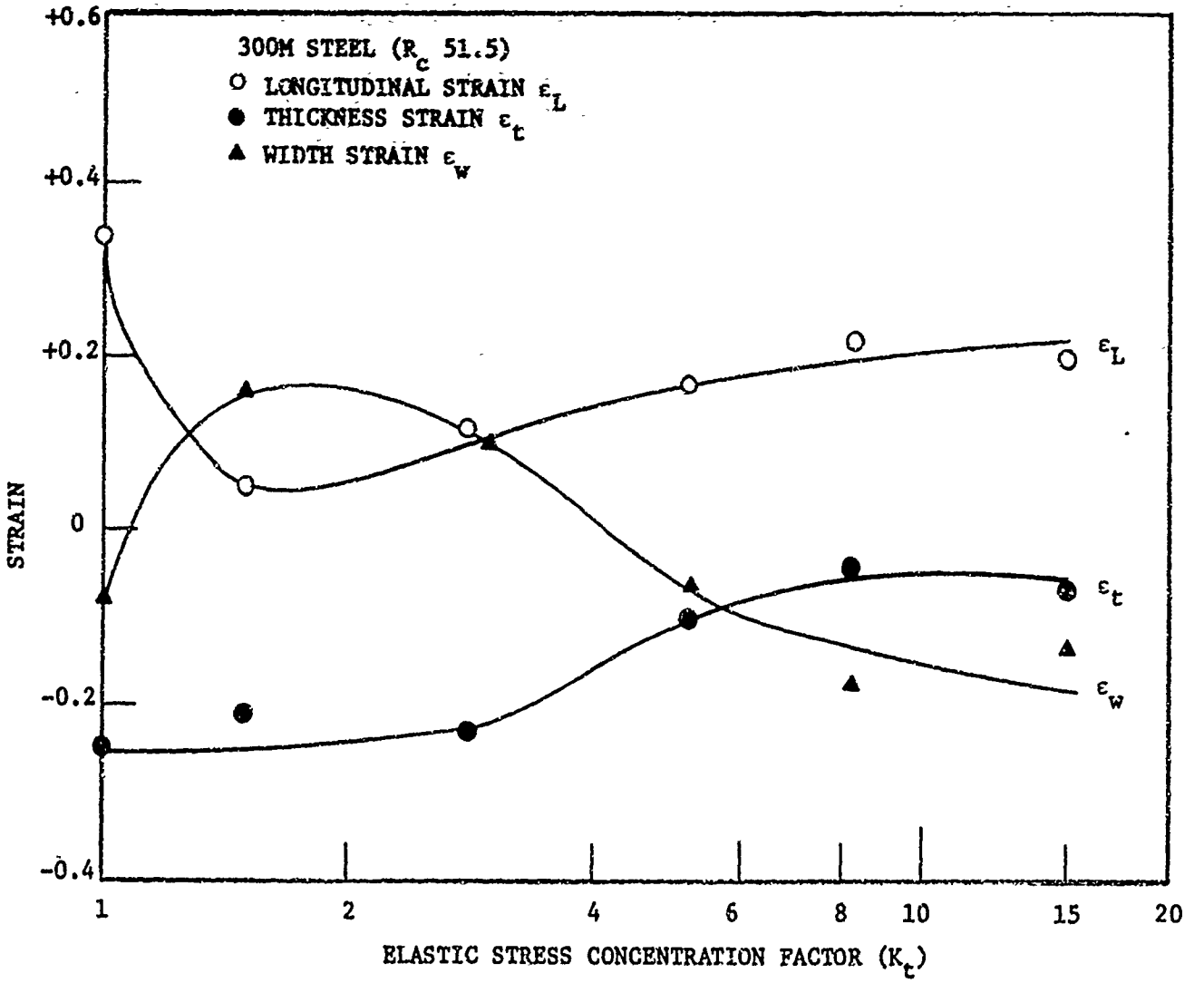

FIGURE 27 FRACTURE STRAINS AS A FUNCTION OF ELASTIC STRESS CONCENTRATION FACTOR FOR 300M STEEL (R_c 51.5); THICKNESS = 0.166" ± 0.006".

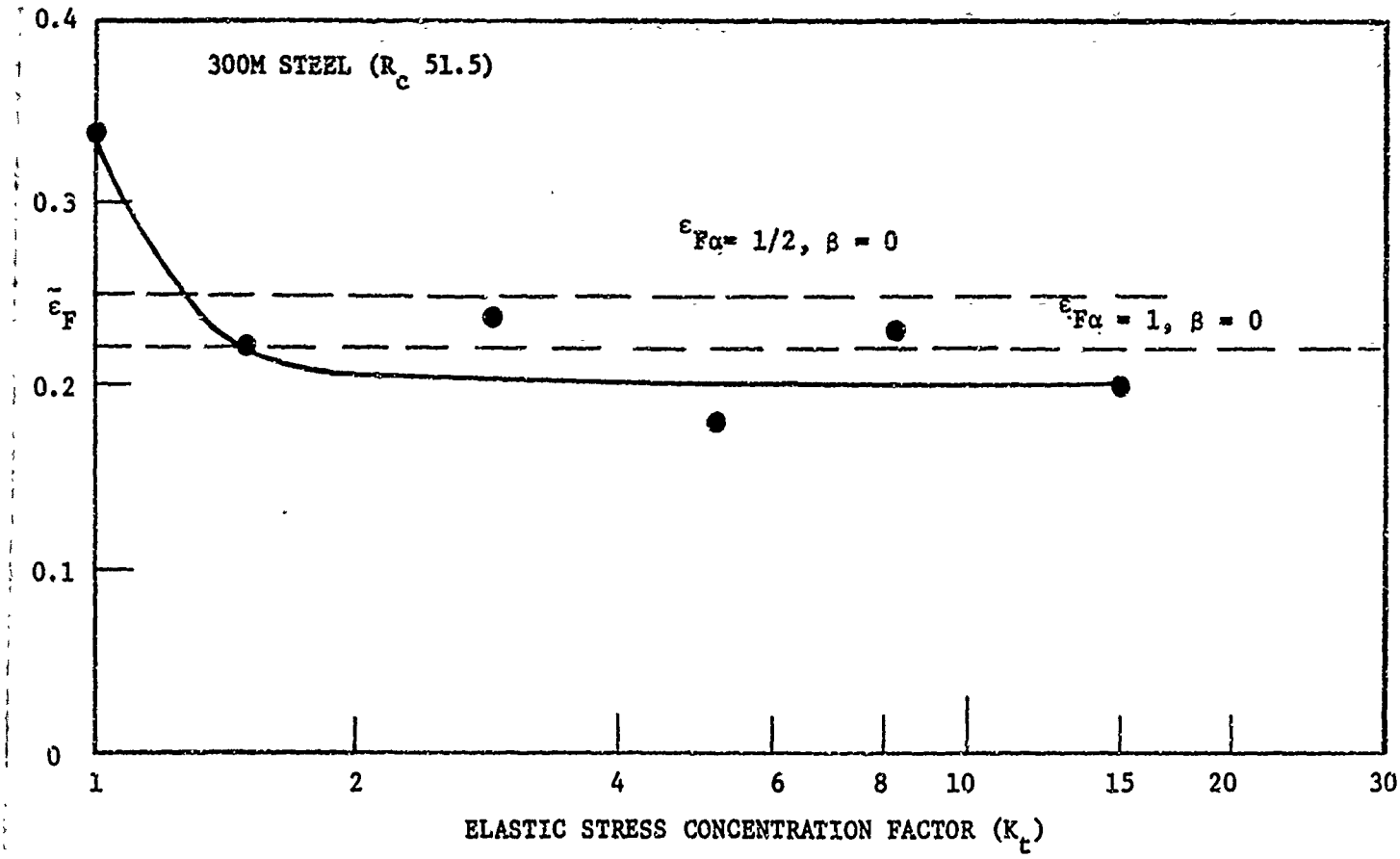

FIGURE 28 EFFECT OF INITIAL STRESS CONCENTRATION FACTOR ON THE EFFECTIVE FRACTURE STRAIN FOR 300M STEEL (R_c 51.5), THICKNESS = 0.166" ± 0.006".

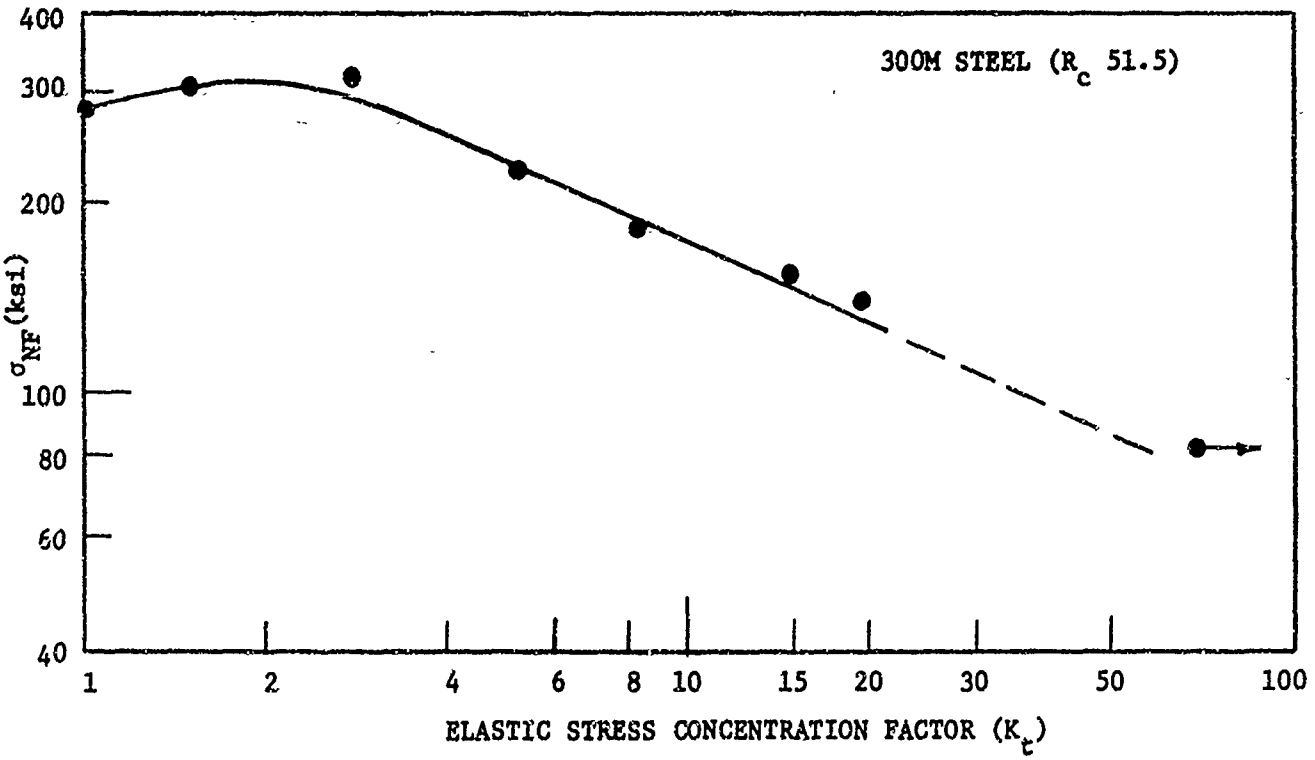

FIGURE 29 EFFECT OF INITIAL STRESS CONCENTRATION FACTOR ON THE NOTCH STRENGTH FOR 300M STEEL (R_c 51.5), THICKNESS = 0.166" ± 0.006".

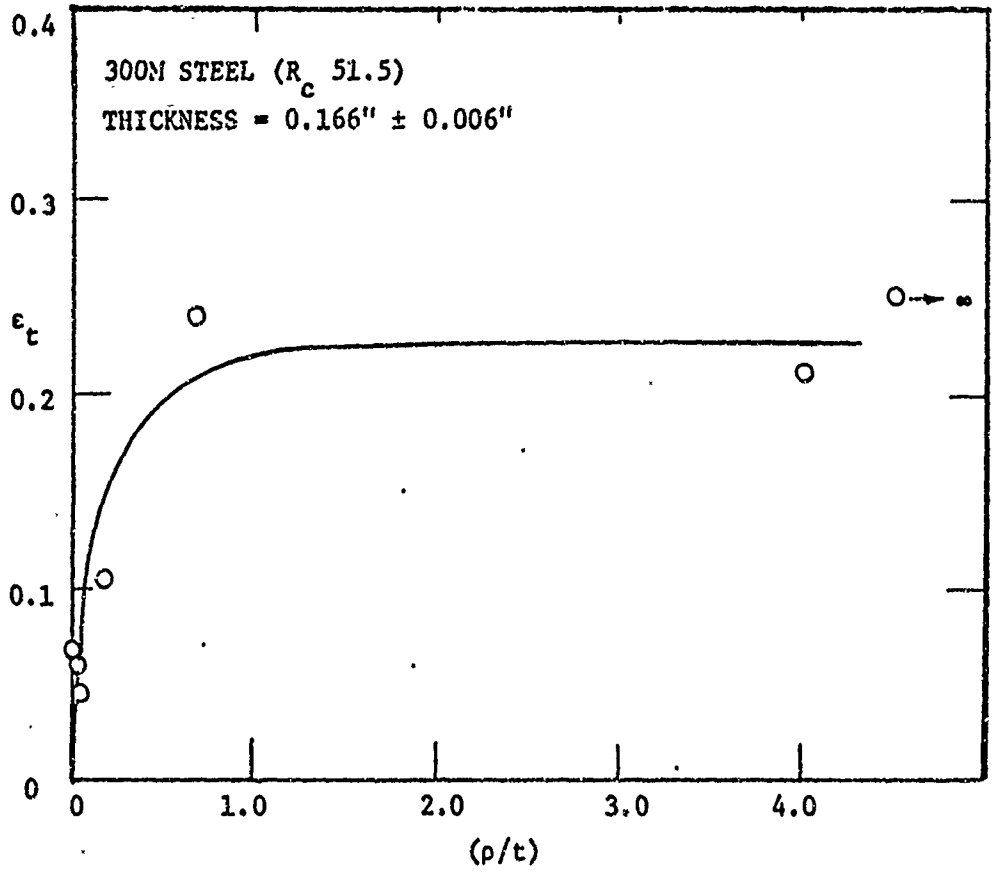

FIGURE 30 EFFECT OF ROOT RADIUS TO THICKNESS RATIO (ρ/t) ON THICKNESS STRAIN (ε_t) AT FRACTURE FOR 300M STEEL (R_c 51.5).

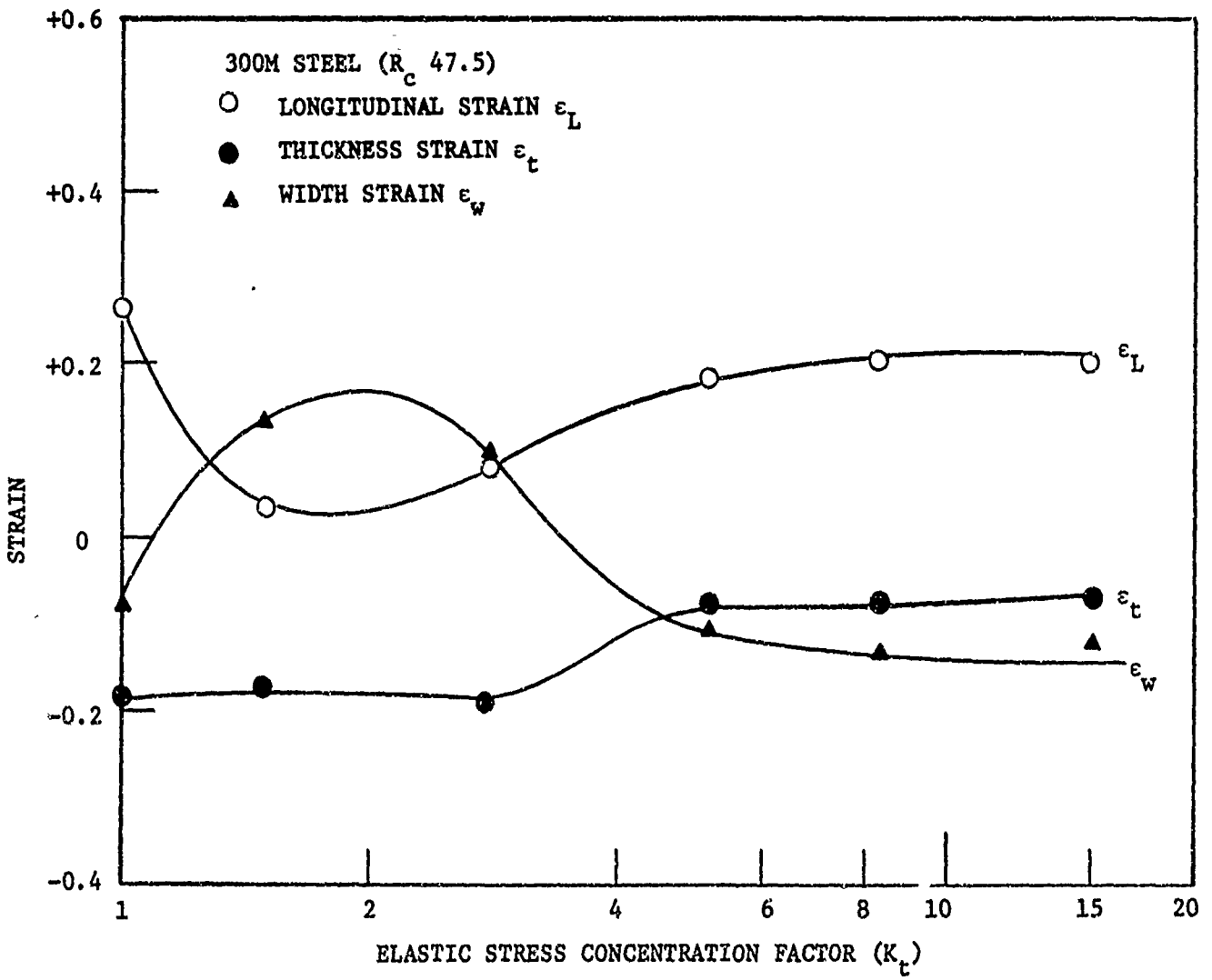

FIGURE 31 FRACTURE STRAINS AS A FUNCTION OF ELASTIC STRESS CONCENTRATION FACTOR FOR 300M STEEL (R_c 47.5), THICKNESS = 0.163" ± 0.007".

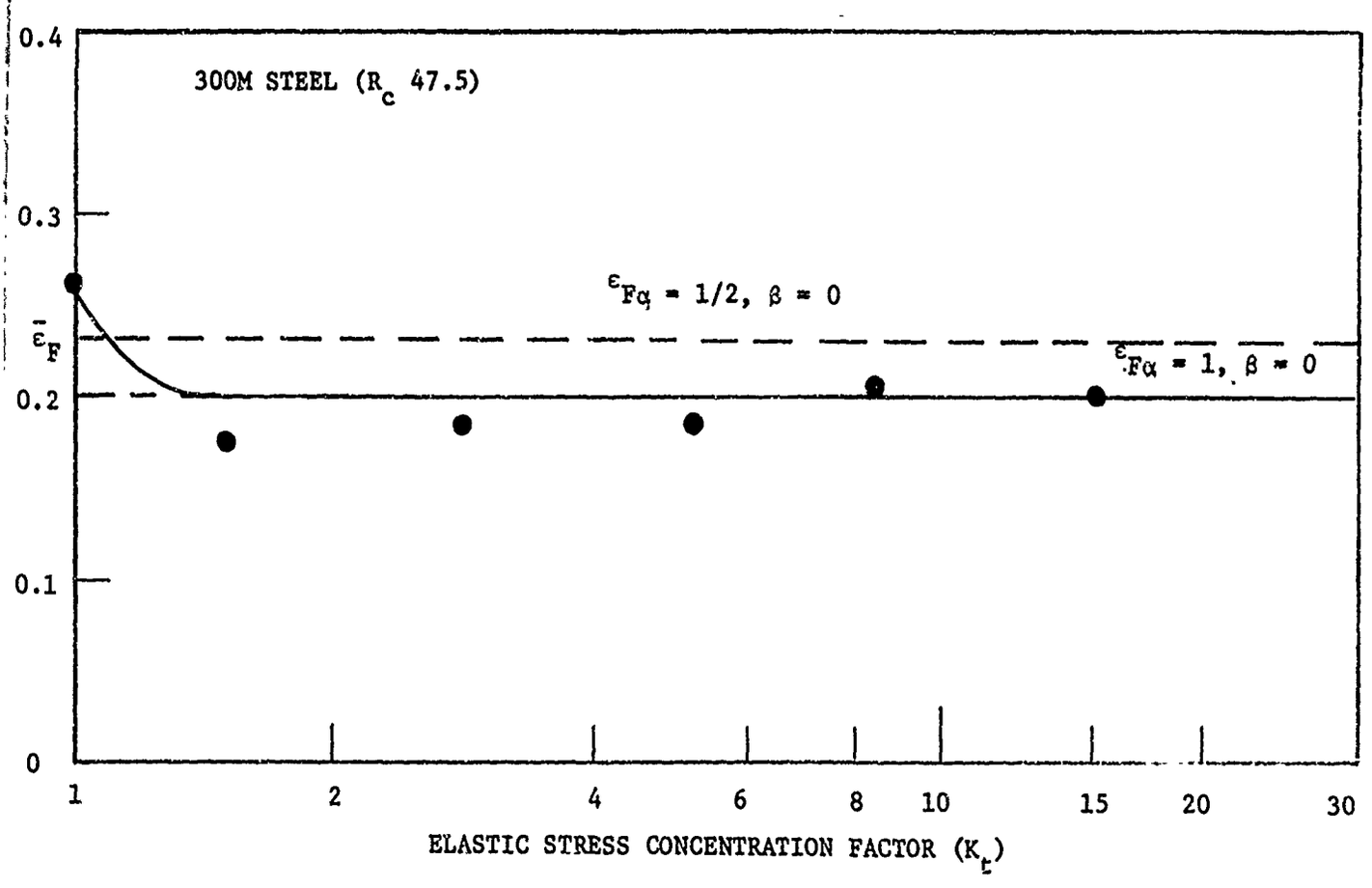

FIGURE 32 EFFECT OF INITIAL STRESS CONCENTRATION FACTOR ON THE EFFECTIVE FRACTURE STRAIN FOR 300M STEEL (R_c 47.5), THICKNESS = 0.163" ± 0.007".

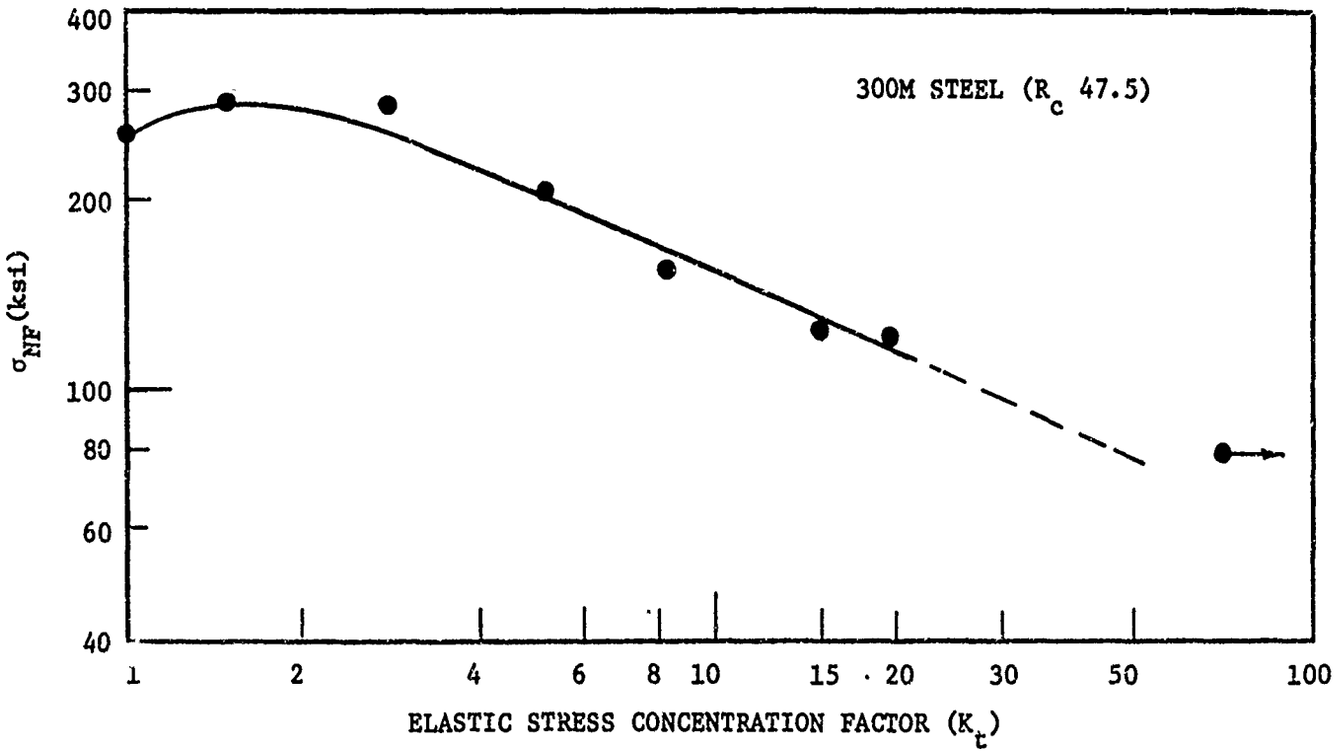

FIGURE 33 EFFECT OF INITIAL STRESS CONCENTRATION FACTOR ON THE NOTCH STRENGTH FOR 300M STEEL (R_c 47.5), THICKNESS = 0.163" ± 0.007".

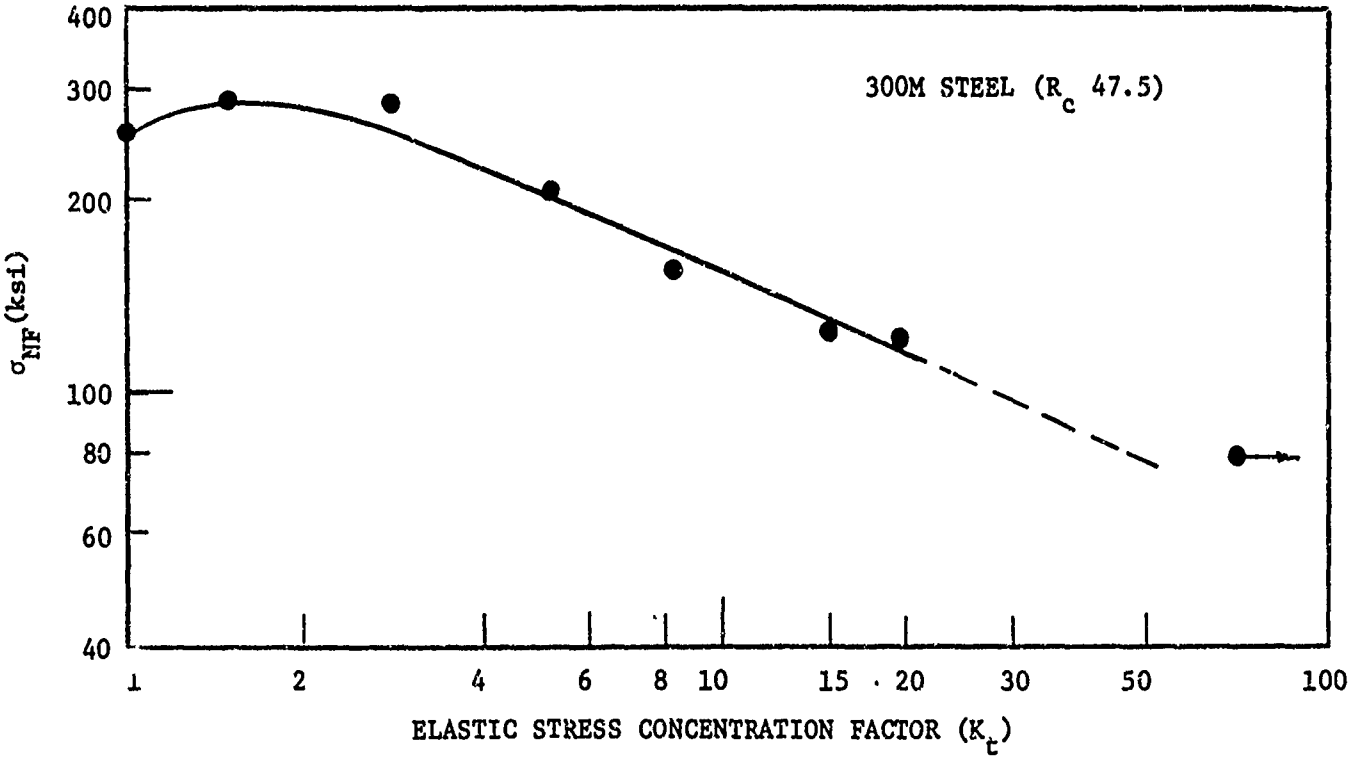

FIGURE 33 EFFECT OF INITIAL STRESS CONCENTRATION FACTOR ON THE NOTCH STRENGTH FOR 300M STEEL (R_c 47.5), THICKNESS = 0.163" ± 0.007".

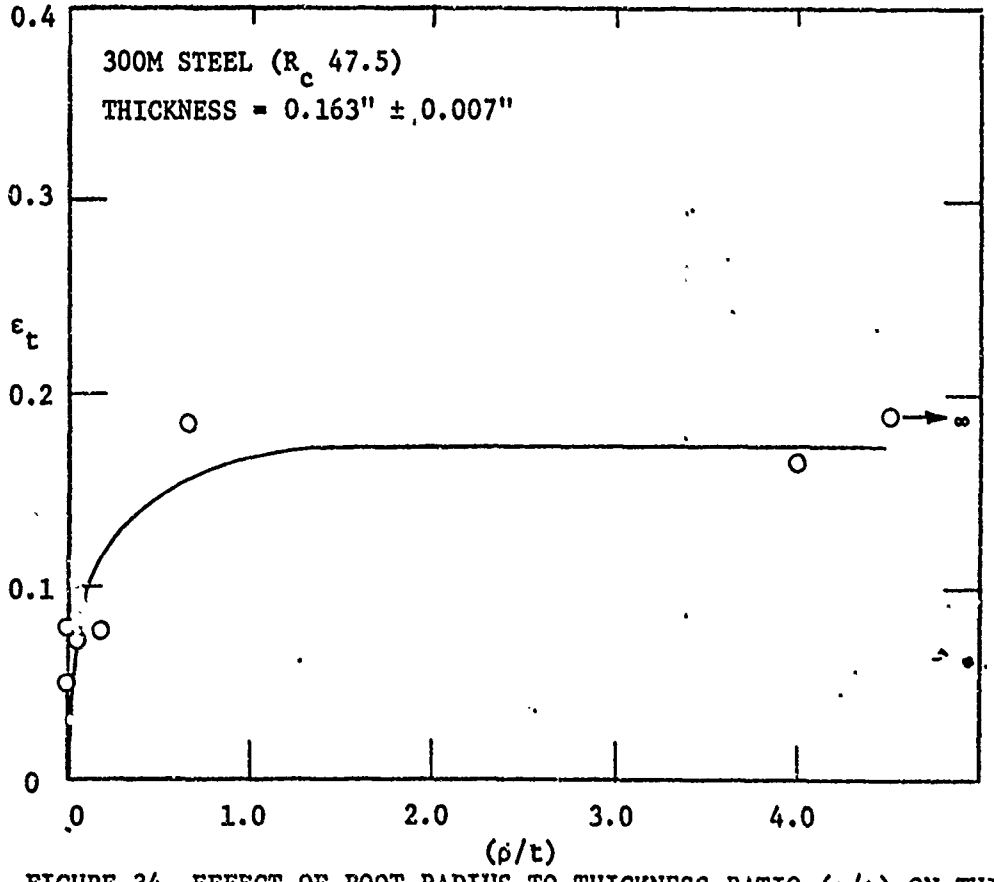

FIGURE 34 EFFECT OF ROOT RADIUS TO THICKNESS RATIO (ρ/t) ON THICKNESS STRAIN (ε_t) AT FRACTURE FOR 300M STEEL (R_c 47.5).

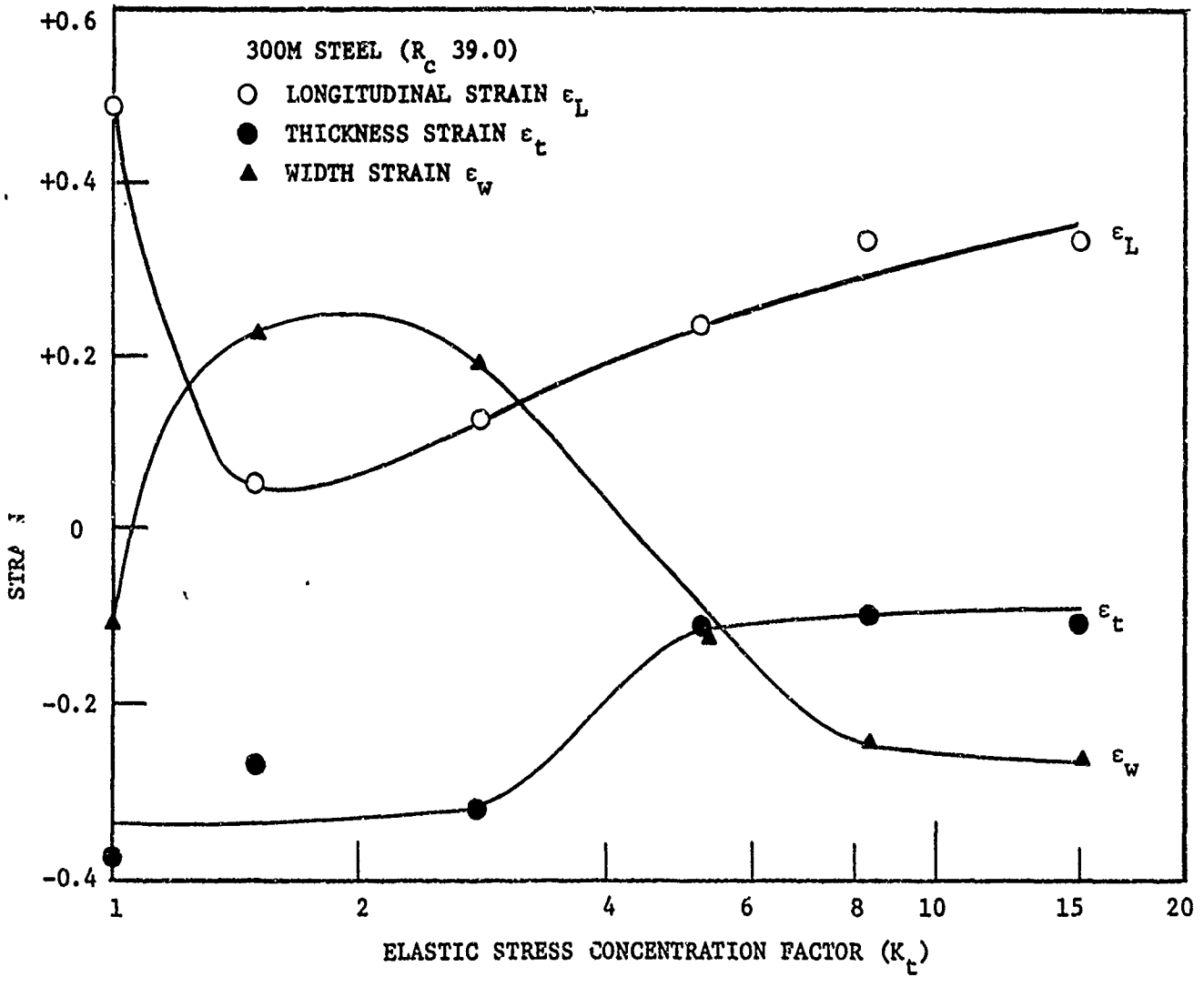

FIGURE 35 FRACTURE STRAINS AS A FUNCTION OF ELASTIC STRESS CONCENTRATION FACTOR FOR 300M STEEL (R_c 39.0), THICKNESS = 0.161" ± 0.005".

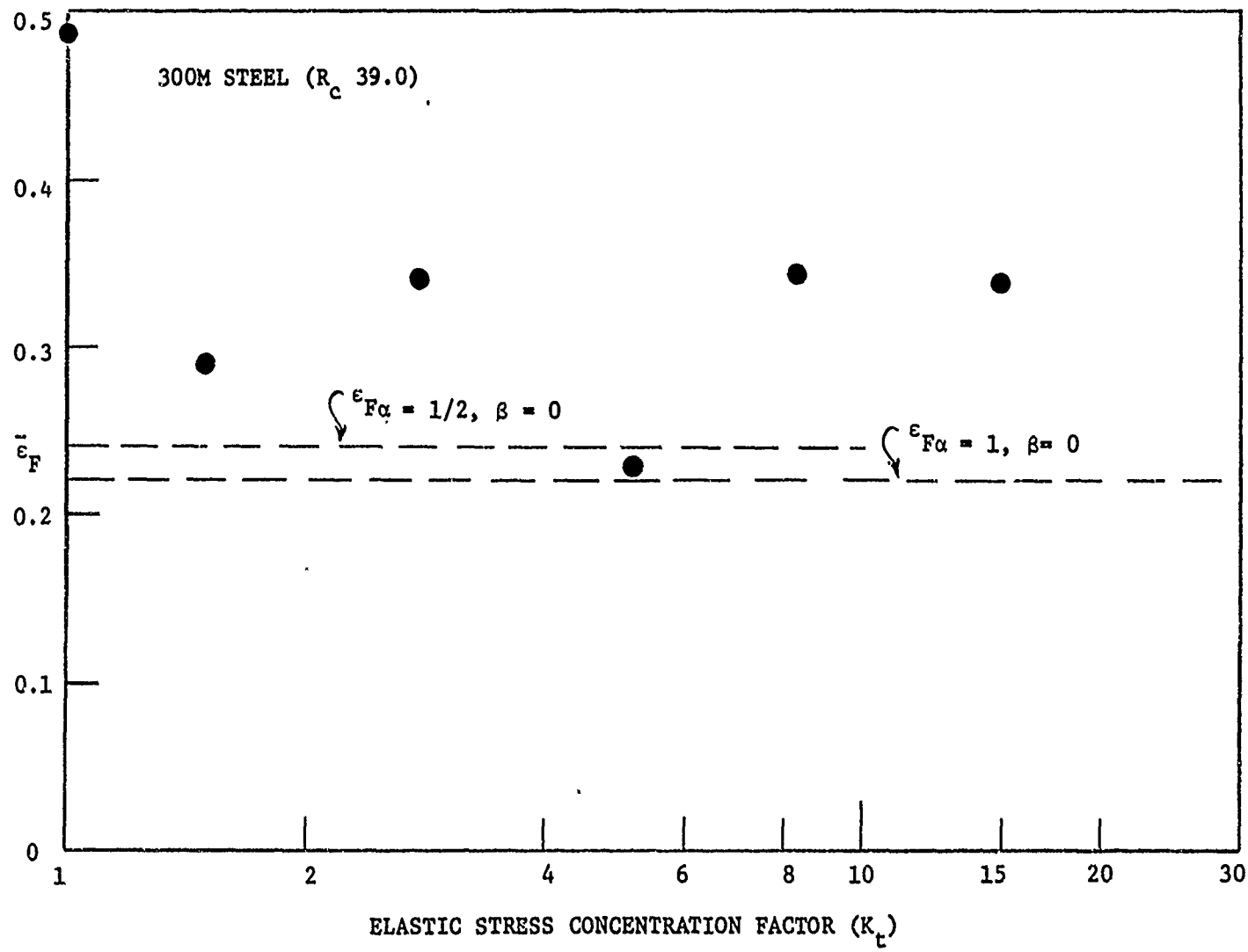

FIGURE 36 EFFECT OF INITIAL STRESS CONCENTRATION FACTOR ON THE EFFECTIVE FRACTURE STRAIN FOR 300M STEEL (R_c 39.0), THICKNESS = 0.161" ± 0.005".

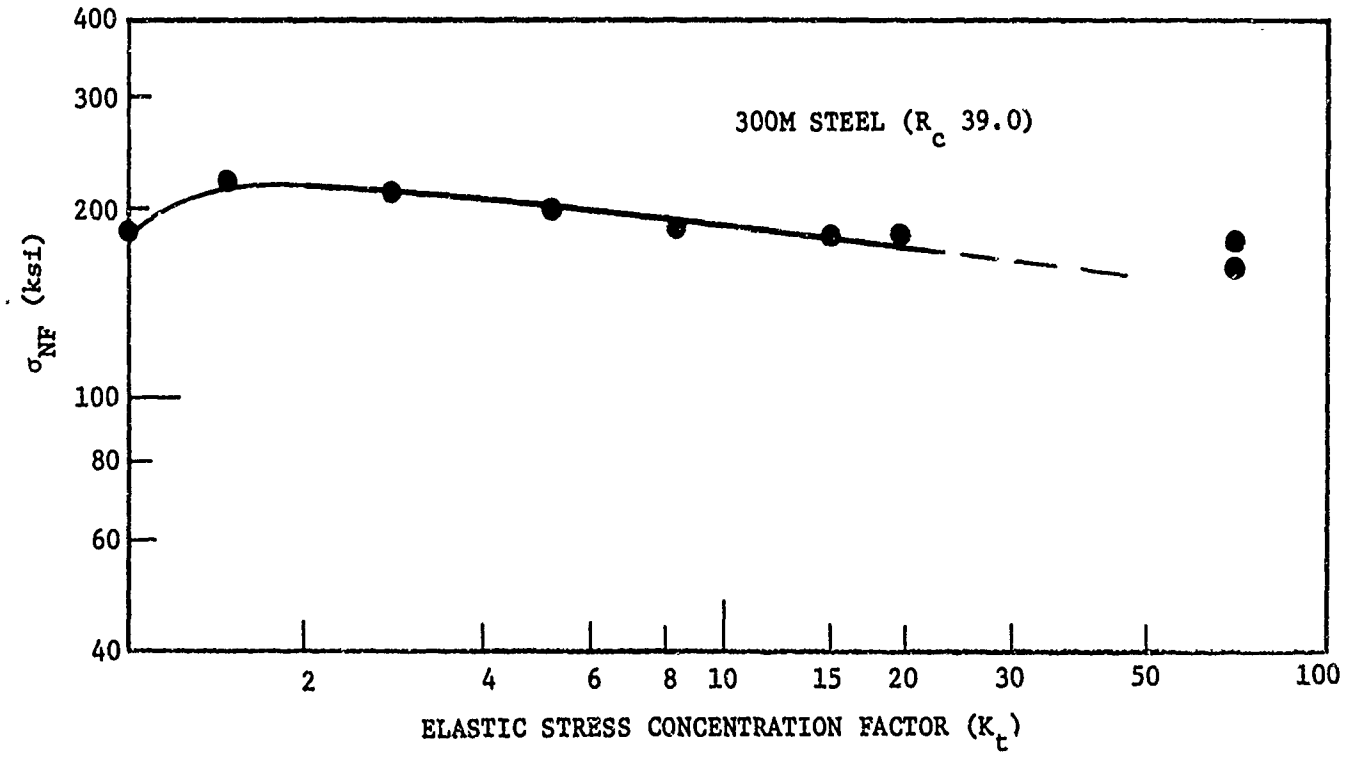

FIGURE 37 EFFECT OF INITIAL STRESS CONCENTRATION FACTOR ON THE NOTCH STRENGTH FOR 300M STEEL (R_c 39.0), THICKNESS = 0.161" ± 0.005".

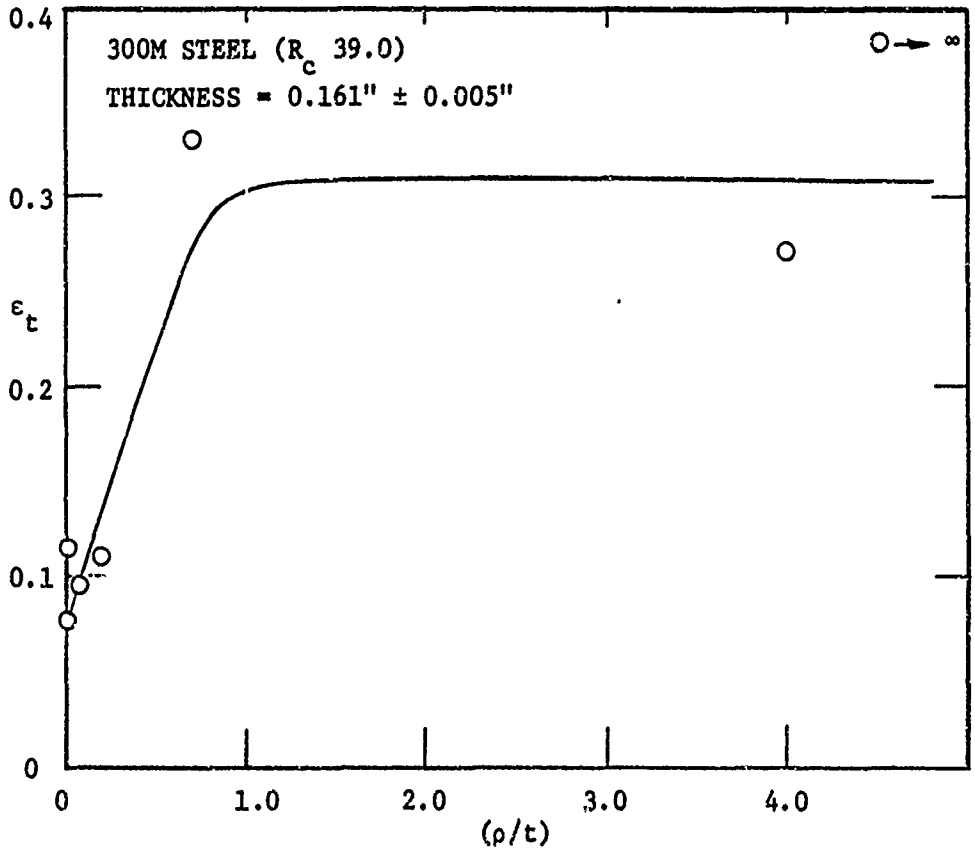

FIGURE 38 EFFECT OF ROOT RADIUS TO THICKNESS RATIO (ρ/t) ON THICKNESS STRAIN (ε_t) AT FRACTURE FOR 300M STEEL (R_c 39.0).

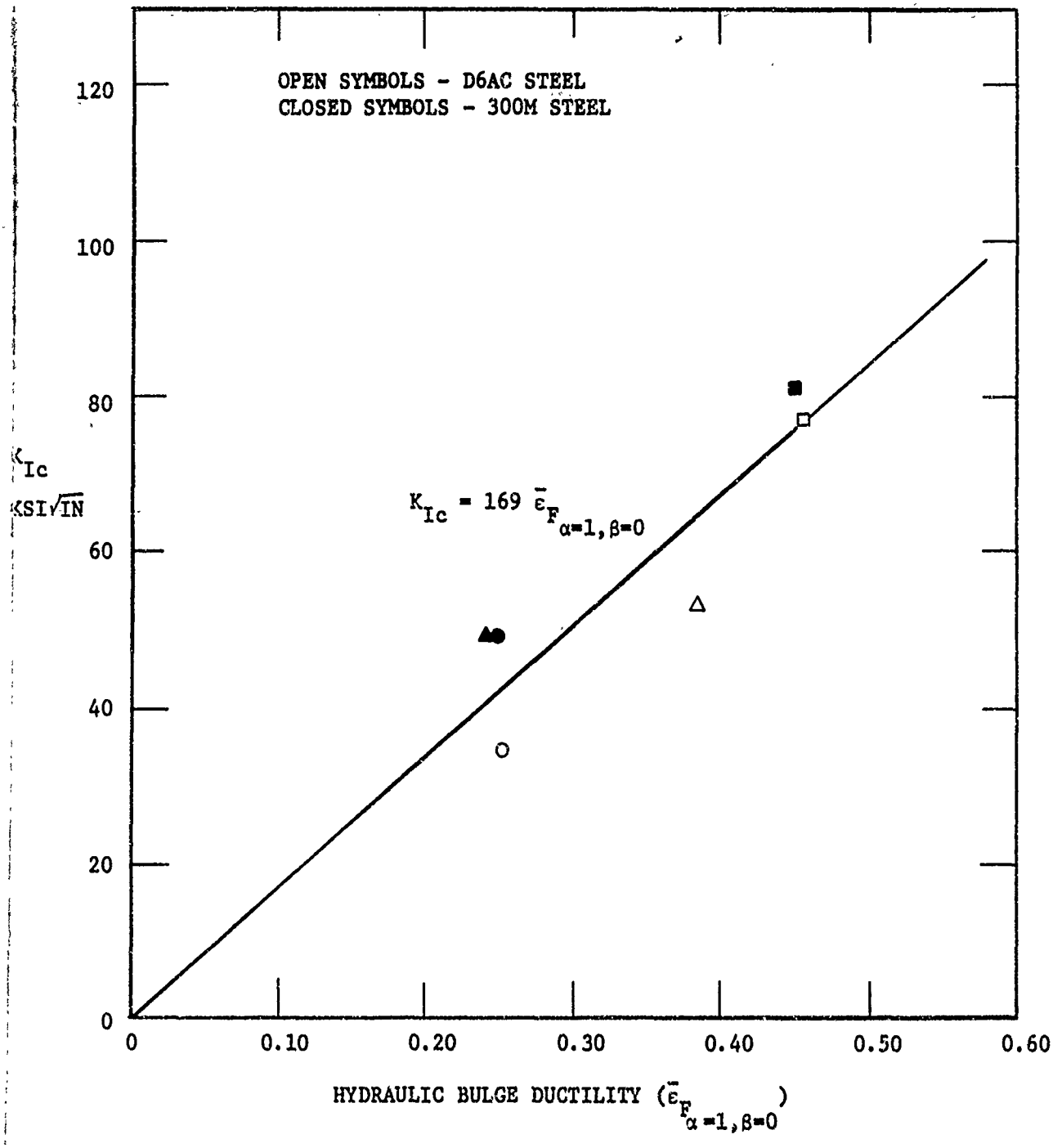

FIGURE 39 PLANE STRAIN FRACTURE TOUGHNESS OBTAINED ON 1" THICK WOL SPECIMENS PLOTTED AGAINST HYDRAULIC BULGE DUCTILITY ON SMOOTHLY GROUND SPECIMENS (RMS - 10; THICKNESS 0.050").

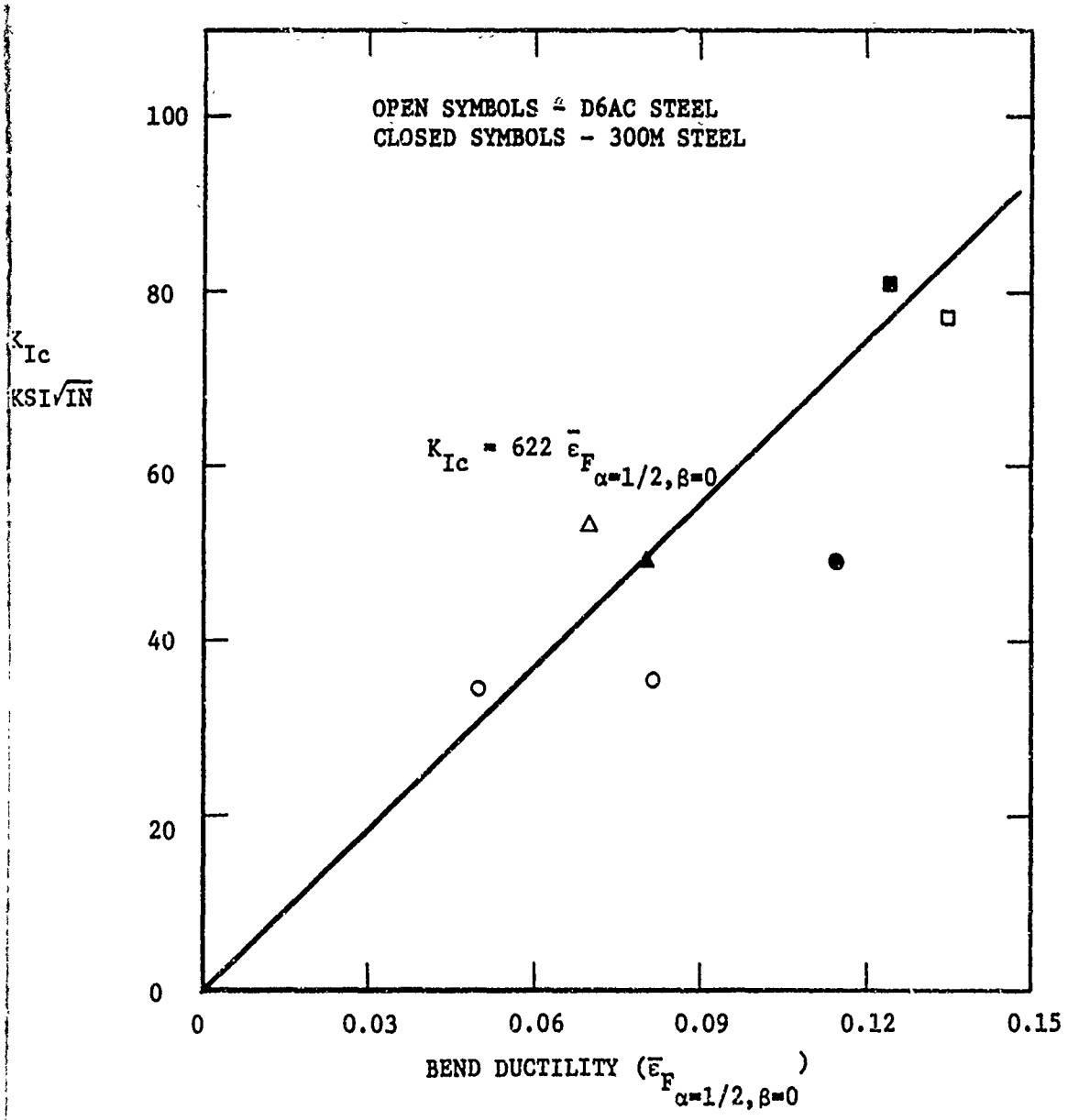

FIGURE 40 PLANE STRAIN FRACTURE TOUGHNESS (K_{Ic}) PLOTTED AGAINST BEND DUCTILITY ($\bar{\varepsilon}_{F_{\alpha=1/2,\beta=0}}$) ON COARSELY GROUND (RMS - 19) SPECIMENS OF THICKNESS = 1.60".

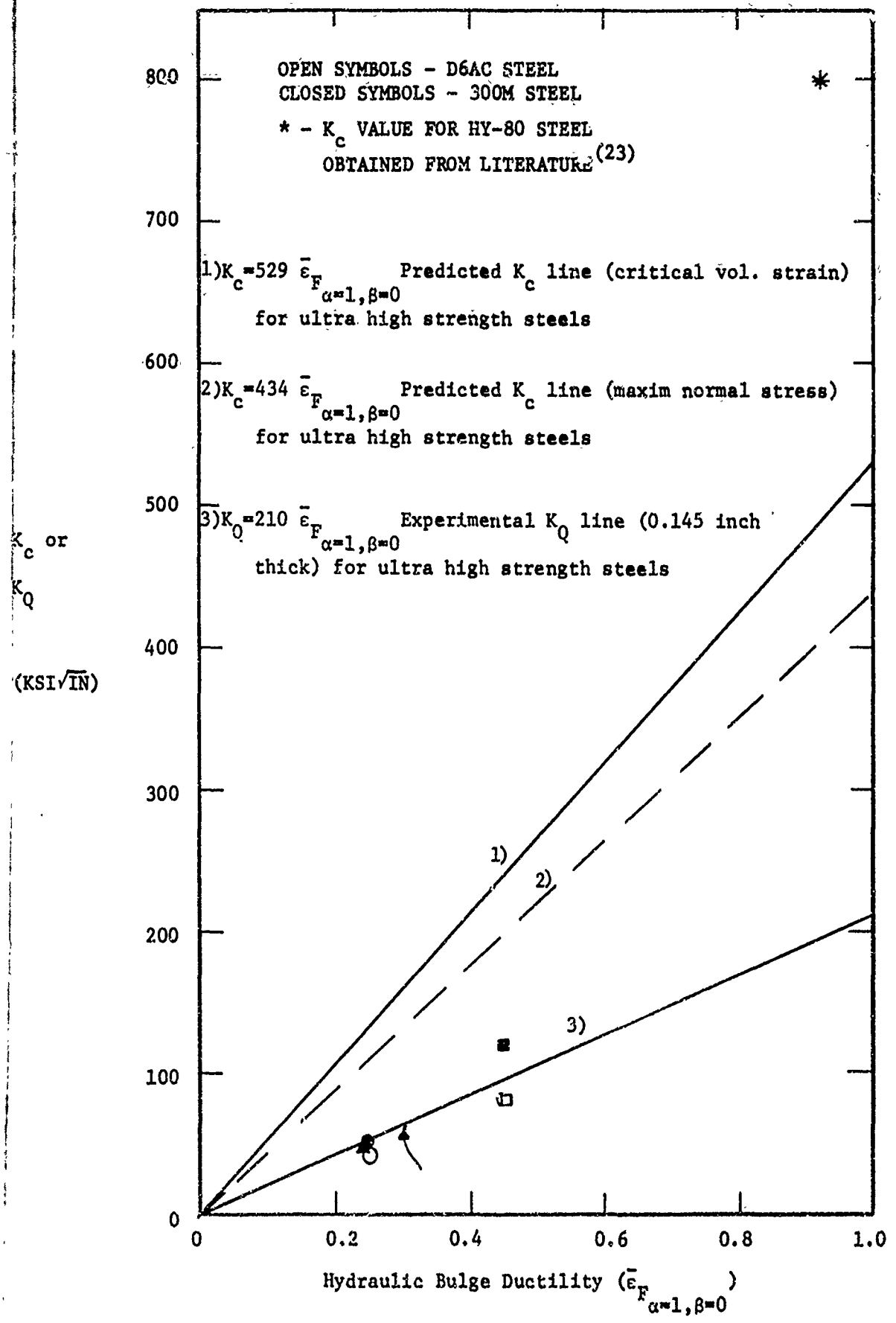

FIGURE 41 APPARENT FRACTURE TOUGHNESS (K_Q) AS A FUNCTION OF HYDRAULIC BULGE DUCTILITY

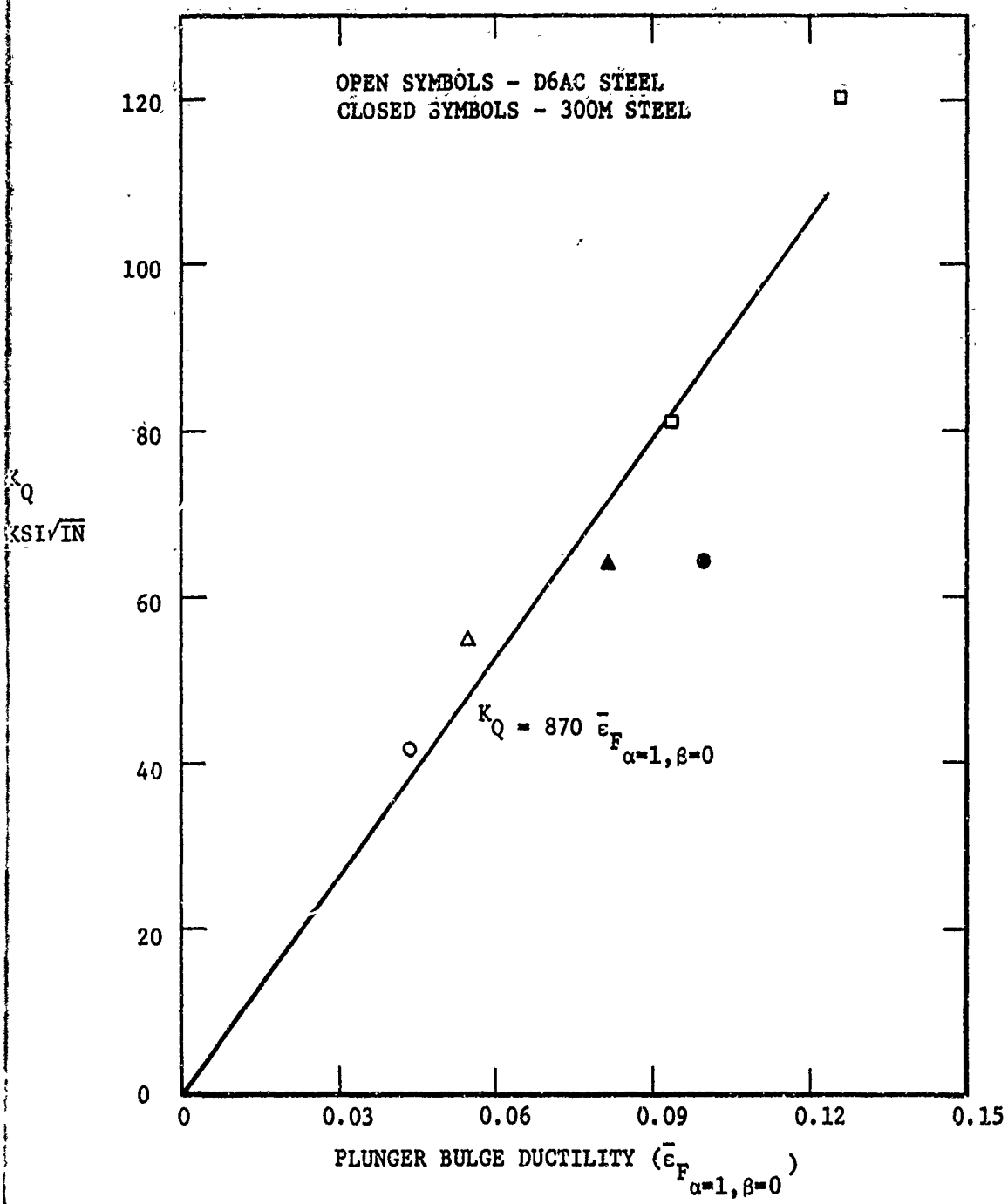

FIGURE 42 APPARENT FRACTURE TOUGHNESS (K_Q) OBTAINED ON 0.145" THICK WOL SPECIMEN VS. PLUNGER BULGE DUCTILITY ($\bar{\varepsilon}_{F_{\alpha=1,\beta=0}}$) ON COARSELY GROUND SPECIMENS (RMS - 19, THICKNESS = 0.150").

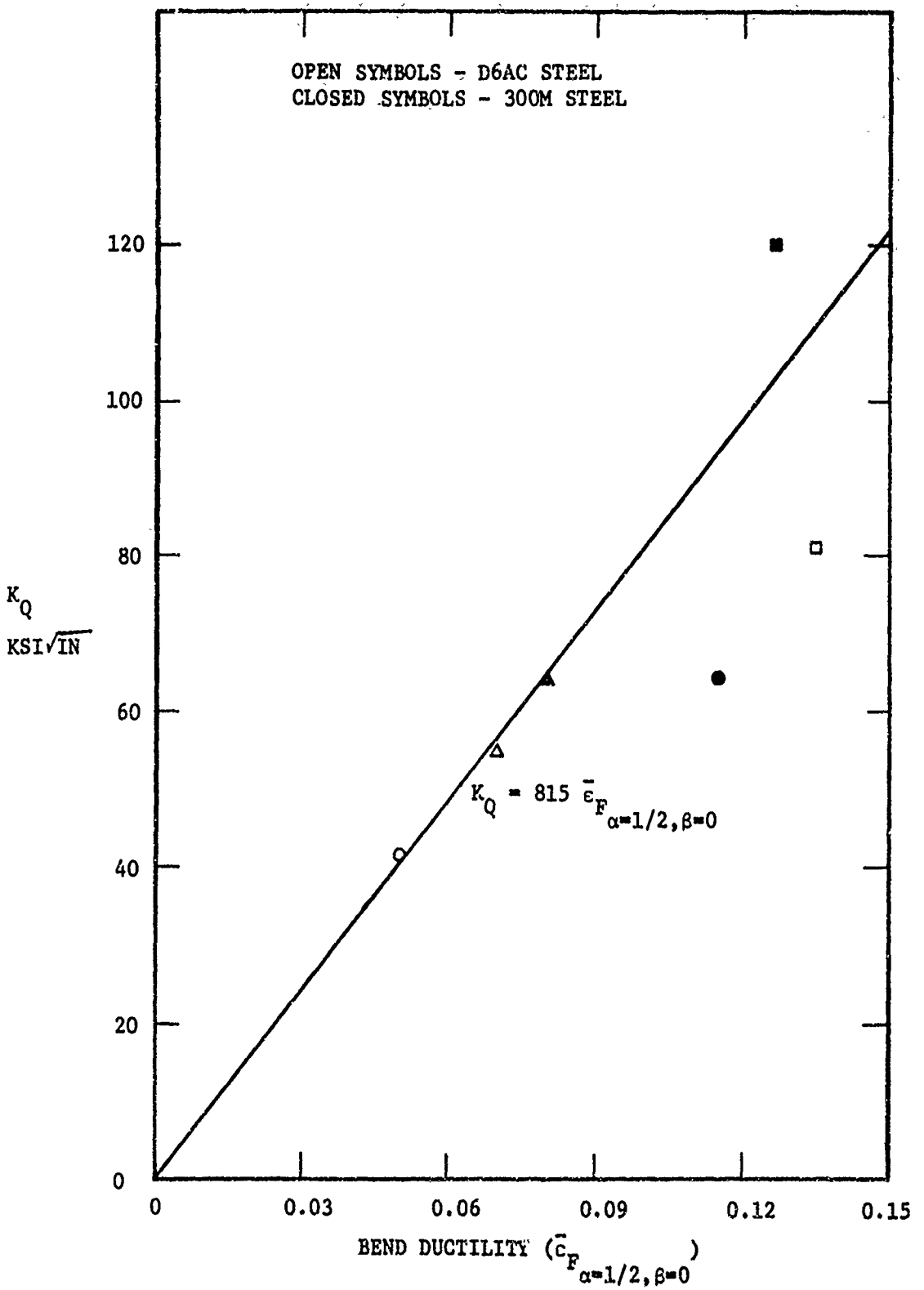

FIGURE 43 APPARENT FRACTURE TOUGHNESS (K_Q) OBTAINED ON 0.145" THICK WOL SPECIMEN PLOTTED AGAINST BEND DUCTILITY ON COARSELY GROUND SPECIMENS (RMS ~~-063~~, THICKNESS = 0.160").